Robust Steady-State Analysis of Power Grid using Equivalent Circuit Formulation with Circuit Simulation Methods

Submitted in partial fulfillment of the requirements for

the degree of

Doctor of Philosophy

in

Department of Electrical and Computer Engineering

Amritanshu Pandey

B.S., Electrical and Electronics Engineering, Visvesvaraya Technological University
M.S., Electrical and Computer Engineering, Carnegie Mellon University

Carnegie Mellon University
Pittsburgh, PA

December 2018

ACKNOWLEDGEMENTS

To my advisors, Larry Pileggi and Gabriela Hug, without their guidance this research would not have materialized and this dissertation would be incomplete.

To my committee members, Granger Morgan and Soummya Kar, for their guidance towards achieving the goals stipulated within this thesis.

To my colleagues, Marko, Martin, David, Aayushya, Dimitrios, Joe and others, for being the most helpful corroborators and for enabling a welcoming and productive working environment.

To my friends, Jolly, Naveen, Akhilesh, Panickos, and many others, for being the most amazing friends and company when the chips were low, and the research was hard.

To my girlfriend, Deirdre, for being by my side throughout the whole journey and for uplifting my spirits when I needed it the most.

Finally, to my wonderful family, Mom, Dad and Anshu, to whom I owe everything I have achieved in my life so far.

Thesis Statement: Develop robust methods to obtain the steady-state operating point of the transmission and distribution power grid independently or jointly using equivalent circuit approach and circuit simulation methods

1. Abstract

A robust framework for steady-state analysis (power flow and three-phase power flow problem) of transmission as well as distribution networks is essential for operation and planning of the electric power grid. The critical nature of this analysis has led to this problem being one of the most actively researched topics in the energy field in the last few decades. This has produced significant advances in the related technologies; however, the present state-of-the-art methods still lack the general robustness needed to securely and reliably operate as well as plan for the ever-changing power grid. The reasons for this are manifold, but the most important ones are: i) lack of general assurance toward convergence of power flow and three-phase power flow problems to the correct physical solution when a good initial state is not available; ii) the use of disparate formulation and modeling frameworks for transmission and distribution steady-state analyses that has led to the two analyses being modeled and simulated separately.

This thesis addresses the existing limitations in steady-state analysis of power grids to enable a more secure and reliable environment for power grid operation and planning. To that effect, we develop a generic framework based on equivalent circuit formulation that can model both the positive sequence network of the transmission grid and the three-phase network of the distribution grid without loss of generality. Furthermore, we demonstrate that when combined with novel as well as adapted circuit simulation techniques, the framework can robustly solve for the steady-state solution for both these network models (positive sequence and three-phase) by constraining the developed models in their physical space independent of the choice of initial conditions. Importantly, the developed framework treats the transmission grid no differently than the distribution grid and, therefore, allows for any further advances in the field to be directly applicable to the analysis of both. One of which is the ability to jointly simulate the positive sequence network of the transmission grid and three-phase network of the distribution grid robustly.

To validate the applicability of our equivalent circuit formulation to realistic industry sized systems as well to demonstrate the robustness of the developed methods, we simulate large positive-sequence and three-phase networks individually and jointly from arbitrary initial conditions and show convergence to correct physical solution. Examples for positive sequence transmission networks include 75k+ nodes US Eastern Interconnection test cases and for three-phase networks include 8k+ nodes taxonomy distribution test cases.

2. Contributions

The primary contributions of this thesis are as follows:

I. *This thesis develops a generic framework based on equivalent circuit formulation that can model the positive sequence transmission network and three-phase distribution network without loss of generality.*

II. *Furthermore, it adapts and further develops novel circuit simulation methods for the field of power system analysis that can ensure robust convergence for positive-sequence power flow and three-phase power flow problems from arbitrary initial conditions.*

III. *Finally, the developed equivalent circuit framework with circuit simulation methods is extended to model the joint transmission and distribution network while ensuring same robust convergence as in the case of power flow and three-phase power flow problems.*

TABLE OF CONTENTS

LIST OF FIGURES

TABLE OF TABLES

3. Introduction and Motivation

An interconnected electric grid is a network of synchronized power providers and consumers that are connected via transmission and distribution lines and operated by one of multiple entities. Secure and reliable operation of this electric grid is of the utmost importance to a country's economy and the well-being of its citizens. In the U.S., the electricity based services are considered as an essential service [1], lack of which can result in significant societal chaos [2]. The grid that has remained mostly untouched since its early inception has begun to experience changes in the last decade or so, some of which include [1]: i) changing generation mix due to electricity generation shift from few large central plants, mostly fossil-fueled, to smaller and often variable renewable generators, ii) changing demand loads in retail electricity markets resulting from demographic and economic changes, iii) integration of smart grid technologies and iv) increasing threats due to adversarial attacks or aging infrastructure. To navigate the grid through these changes while maintaining its reliability and security requires investment toward modern infrastructure, adequate policy and state-of-the-art simulation tools. The underlying work in this thesis will be directed toward developing better power grid simulation tools and analysis methods.

At present, numerous methods exist for simulating and analyzing the electric grid. These can be broadly categorized into one of the following categories: i) steady-state analysis in frequency domain (power flow, three phase power flow, and harmonic analyses), ii) transient and steady-state analysis in time domain, iii) state-estimation, iv) analysis for optimal dispatch of resources, and v) other market dispatch-based analyses. Among these analyses, the two that are primarily used for day-to-day operation and planning of the grid are the steady-state analysis in the frequency domain (power flow and three-phase power flow) to obtain the system frequency voltage and current phasors and the transient analysis in time domain to obtain time domain voltages and currents following a given event. Generally, for system operation and planning, power flow and three-phase power flow runs are first performed on all relevant cases followed by more computational heavy transient analysis for specific cases to gain more insight into the

steady-state results. This pattern of analysis is generally driven by inconsistencies between power flow and transient analysis, wherein steady-state obtained from transient analysis is considered more accurate. This inconsistency between the steady state solution obtained from the transient analysis and the steady-state solution obtained from the power flow analysis is a cause of concern and is conceptually addressed in Appendix B of this thesis. The focus of this thesis, however, is toward developing a better steady-state solver for robust convergence of positive sequence and three-phase power flow problems to the correct physical solution.

The classical power grid has evolved over time such that there existed an invisible divide between the transmission network and distribution network. The flow of power was unidirectional and always moved from the transmission network into the distribution network. This in the past has allowed for the two networks to be studied separately resulting in disparate solution methods and modeling frameworks for analyzing the two. For instance, the steady-state solution of the transmission system is obtained via positive sequence or balanced alternating current (AC) power flow analysis, whereas the steady-state operating point for the distribution system is obtained via three-phase AC power flow analysis. The industry standard for solving the positive sequence power flow problem is the 'PQV' formulation [3], wherein nonlinear power mismatch equations are solved for bus voltage magnitude and angle state variables that further define the steady-state operating point of the system. On the other hand, two distinct analysis methods: i) backward-forward sweep method [4] and ii) current injection method (CIM) [5] are primarily used interchangeably for obtaining the steady-state solution of the three-phase power flow problem. In the grid of tomorrow, however, this invisible divide between the transmission and distribution system is bound to disappear, thereby requiring solution methods and a modeling framework that can model and simulate both the transmission and distribution networks whether independently or jointly. The need for which was unequivocally highlighted by one of the speakers in an ARPA-E workshop to identify paths to large-scale deployment of renewable energy resources: "tools are not graceful in considering penetration levels at which much of the thermal fleet could get de-committed," and that "studies do not co-simulate impact of renewable injection into receiving AC systems" [6]. This thesis will address these concerns by

developing a generic framework for modeling both the transmission network and distribution network that can further simulate them independently or jointly.

In general, all of the existing methods for solving the positive sequence power flow problem and the three-phase power flow problem suffer from lack of robustness [9]-[10] in terms of convergence for the nonlinear problem formulation. The 'PQV' based formulation for the positive sequence power flow problem is known to diverge or converge to non-physical solutions for ill-conditioned [4] and large scale (>50k buses) systems. Similarly, the backward-forward sweep method that was proposed to solve the radial and weakly meshed distribution systems with high R/X ratios [4] has difficulties converging for heavily meshed test cases with more than a single source [11] in the network. On the other hand, the CIM method based on Dommel's work in 1970 [8] has challenges with incorporating multiple PV buses in the system [12]-[13]. Broadly speaking, of the many known challenges in both the power flow and three-phase power flow problem that are contributing toward lack of robustness, the two that are the most detrimental are: i) convergence to non-physical or unacceptable solution [30] and ii) divergence [9].

The factors that are the most fundamental toward making these problems challenging are: i) the use of non-physical macro-models for modeling the power grid components, and ii) in the case of 'PQV' formulation, the use of power mismatch equations with real and reactive power as system state variables to formulate the problem. The non-physical representations of the system equipment may not capture the true behavior of the model in the entire range of system operation. For example, an approximated macro-model for a generator that is represented via positive sequence or three-phase PV model can result in convergence to a low-voltage solution or divergence due to its quadratic voltage characteristics. Similarly, the inherent non-linearities in the 'PQV' formulation almost always cause divergence for large (>50k) and ill-conditioned test cases [35] when solved from an arbitrary set of initial conditions. This lack of a physics-based formulation, along with the methods that can constrain the non-physics abased models in their physical space, is what renders the existing power flow and three-phase power flow problem and solution approaches to be "non-robust."

To develop a robust solver for the steady-state solution of the power grid it is imperative that the solver can efficiently and effectively navigate through these challenges while converging to a solution that is both meaningful and correct. Most importantly, as previously discussed, the developed framework should be able to model both the transmission and distribution network without loss of generality. Intuitionally and physically, both the transmission and distribution electric grid correspond to an electric circuit. Therefore, our approach toward solving the power flow and three-phase power flow problem is to treat them as such and solve both analyses using circuit simulation fundamentals. To achieve this we propose a two pronged approach: i) the use of equivalent circuit formulation with true state variables of currents and voltages [31]-[33] to model both the transmission and distribution power grid networks (Chapter 5), and ii) the use of circuit simulation methods [34]-[35] to ensure robust convergence to correct physical solutions (Chapter 6). Furthermore, the ability to model both transmission and distribution power grids as equivalent circuits allows us to combine the two without loss of generality and to solve the transmission and distribution networks jointly (Chapter 7). In the appendices of this thesis we explore the physics-based approach to modeling the aggregated load in the system and conceptually demonstrate consistent results between the steady-state obtained from transient analysis as well as steady-state obtained from power flow analysis via unification of the two analyses.

LIST OF SYMBOLS

$\mathcal{N}$	Set of buses in the system. Each bus in three-phase power flow problem further consist of three distinct phases.
$\mathcal{G}$	Set of generators in the system.
$\mathcal{L}$	Set of loads in the system.
$\mathcal{T}_X$	Set of transmission lines in the system.
$xfmrs$	Set of transformers in the system.
$\mathcal{Z}$	Set of slack buses in the system.
i, l	$\{1, 2, 3, .. \mathcal{N}\}$
G	$\{1, 2, 3, .. \mathcal{G}\}$
L	$\{1, 2, 3, .. \mathcal{L}\}$
C	$\{R, I\}$
R	Real part of the complex variable.
I	Imaginary part of the complex variable.
k	k^{th} iteration of the Newton-Raphson.
{A, a}	Correspond to phase A.
{B, b}	Correspond to phase B.
{C, c}	Correspond to phase C.
{N, n}	Correspond to phase N.
Ω_{set}	$\{a, b, c, A, B, C\}$
Ω, t	$\in \Omega_{set}$
${P_G}^i + j{Q_G}^i$	Connected complex power generation at bus i.

$P_L{}^i + jQ_L{}^i$	Connected complex power demand at bus i.
$G_{il}^Y + jB_{il}^Y$	Is the bus admittance between buses i and l in the positive sequence Y-matrix.
$P_G{}^{max}, P_G{}^{min}$	Maximum and minimum allowable real power generation for generator G.
$Q_G{}^{max}, Q_G{}^{min}$	Maximum and minimum allowable reactive power generation for generator G.
$\boldsymbol{\kappa}$	Vector of participation factors for generators participating in AGC or droop control.
θ_{il}	Is the voltage angle between buses i and l.
$\tilde{V}_i$	Complex voltage at bus i.
V_{Ri}, V_{Ii}	Real and Imaginary part of the complex voltage at bus i.
I_{Ri}, I_{Ii}	Real and Imaginary part of the complex current flowing in a branch connected to bus i.
$V_{Ri}{}^{\Omega}, V_{Ii}{}^{\Omega}$	Real and Imaginary part of the complex voltage of the phase Ω at bus i.
$\mathcal{O}$	Node in the system with a voltage controlling devices connected to it.
$\mathcal{R}$	Remote node controlled by a voltage controlling device on node $\mathcal{O}$.
$\mathcal{W}$	Controlled node where $\mathcal{W} \in \{\mathcal{O}, \mathcal{R}\}$.
$\left(P_i^{sp} + j\, Q_i^{sp}\right)^{\Omega}$	Specified active and reactive power at bus i for the given phase Ω.
tr	Transformer turns ratio.
Θ	Transformer phase shift.
φ	Firing angle for the FACTS device.
$\{Z_P{}^{\Omega}, I_P{}^{\Omega}, S_P{}^{\Omega}, Z_Q{}^{\Omega}, I_Q{}^{\Omega}, S_Q{}^{\Omega}\}$	ZIP load parameters for the phase Ω.
$\{G^{BIG}, B^{BIG}, \alpha_R^{BIG}, \alpha_I^{BIG}\}$	BIG load model parameters.
$\aleph$	Represents a series element between buses i and l.
sh	Represents a shunt element connected at node i.
$G_{\Omega t}^{\aleph} + jB_{\Omega t}^{\aleph}$	Self and mutual admittance of the line between phases t and Ω.

$G_i^{sh} + jB_i^{sh}$	Shunt admittance connected to node i.
ς	Variable limiting factor.
λ	Homotopy factor for Tx Stepping Method. Lies in the closed set [0, 1].
γ	Scaling factor for Tx Stepping Method.
$\{V_C{}^0, V_C{}^1, V_C{}^2\}$	Represents the zero, positive, and negative sequence voltages for the set C.
$\{I_C{}^0, I_C{}^1, I_C{}^2\}$	Represents the zero, positive, and negative sequence currents for the set C
J	Jacobian of the positive sequence or three-phase power flow solution matrix.
c	Continuous curve for the homotopy methods in the domain of homotopy factor λ.
$\{\boldsymbol{V}_R^{int}, \boldsymbol{V}_I^{int}\}$	Internal nodes real and imaginary voltages vector for the sub-circuit.
$\{\boldsymbol{V}_R^{ext}, \boldsymbol{V}_I^{ext}\}$	External nodes real and imaginary voltages vector for the sub-circuit.
N-2	Loss of two equipment in the system.
N-3	Loss of three equipment in the system.
T	Sub-circuit in the joint T&D system representing the transmission grid.
D_x	Sub-circuit in the joint T&D system representing the distribution grid x amongst the set of distribution grids.
$\mathcal{F}_T$	System equations for the transmission grid within the joint T&D problem.
$\mathcal{F}_{D_x}$	System equations for the distribution grid x within the joint T&D problem.
$\mathcal{F}_C$	System equations for the coupling network between the transmission and distribution grid in the joint T&D problem.

4. Background and Literature Review

4.1 Positive Sequence and Three-Phase Power Flow Formulations

A power grid in its simplest form can be represented by a set of $\mathcal{N}$ buses, where a set of generators $\mathcal{G}$ and load demands $\mathcal{L}$ are subsets of $\mathcal{N}$, which are further connected by a set of line elements, $\mathcal{T}_X$ and a set of transformers xfmrs. Furthermore, there is a set of slack buses represented by $\mathcal{Z}$. In addition to these, the power grid may contain other elements, such as shunts, flexible alternating current transmission system (FACTS), etc. The aim of steady-state analysis of the power grid is to model the fundamental frequency component of the power grid and further solve for the complex voltages at its buses. The high voltage transmission network of the grid generally operates under balanced conditions, and therefore, the steady-state solution of the transmission network is obtained via positive sequence power flow model and analysis. In contrast, the distribution network of the power grid can operate under unbalanced conditions, therefore for it we use three-phase power flow network model and associated analysis to find the steady-state solution. In the following sub-sections, we discuss the current state of the art methods used for steady-state analysis of transmission and distribution networks and highlight their limitations.

4.1.1 'PQV' based Formulation for Positive Sequence Power Flow Problem

The 'PQV' based power flow formulation is the industry standard for solving for the steady-state solution of the high voltage transmission network. In this formulation, a set of $2(\mathcal{N} - |\mathcal{Z}|) - |\mathcal{G}|$ power mismatch equations are solved for unknown complex voltage magnitudes and angles of the system using the Newton Raphson (NR) method. The set of power mismatch equations is defined [3] as follows:

$$P_G{}^i - P_L{}^i = |V_i| \sum_{l=1}^{\mathcal{N}} |V_k| \left(G_{il}^Y \cos\theta_{il} + B_{il}^Y \sin\theta_{il} \right) \quad (1)$$

$$Q_G{}^i - Q_L{}^i = |V_i| \sum_{l=1}^{\mathcal{N}} |V_l| \left(G_{il}^Y \sin\theta_{il} - B_{il}^Y \cos\theta_{il} \right) \quad (2)$$

In order to solve for unknown complex voltages $\tilde{V}_i$ in the system, the real and reactive power mismatch equations given by (1)-(2) are solved for the set of $(\mathcal{N} - |\mathcal{Z}| - |\mathcal{G}|)$ buses in the system, whereas only real mismatch equations (1) are solved for the set of buses with generators $\mathcal{G}$ connected to it.

The 'PQV' formulation is inherently non-linear, since the set of network constraints result in non-linear power mismatch equations independent of physics of the models used. For example, in the 'PQV' formulation, a linear network consisting of linear models for slack bus, transmission lines and shunts would correspond to a non-linear set of power mismatch equations, a feature that can result in convergence difficulties for systems even trivial in size.

4.1.2 Current Injection Method for Three-Phase Power Flow Problem

The current injection method (CIM) for the three-phase power flow problem [5] was proposed to address challenges associated with the 'PQV' formulation and the backward-forward sweep method. In the CIM formulation, the non-linear current mismatch equations for the system buses are solved via the NR method for each individual phase with complex rectangular real and imaginary voltages as the unknown variables. The current mismatch equations for the three-phase power flow problem are defined as follows [5]:

$$\Delta I_{Ri}^{\Omega} = \frac{\left(P_i^{sp}\right)^{\Omega} V_{Ri}^{\Omega} + \left(Q_i^{sp}\right)^{\Omega} V_{Ii}^{\Omega}}{\left(V_{Ri}^{\Omega}\right)^2 + \left(V_{Ii}^{\Omega}\right)^2} - \sum_{l=1}^{\mathcal{N}} \sum_{t \epsilon \Omega_{set}} \left(G_{il}^{\Omega t} V_{Ri}^{t} - B_{il}^{\Omega t} V_{Ii}^{t} \right) \quad (3)$$

$$\Delta I_{Ii}^{\Omega} = \frac{\left(P_i^{sp}\right)^{\Omega} V_{Ii}^{\Omega} - \left(Q_i^{sp}\right)^{\Omega} V_{Ri}^{\Omega}}{\left(V_{Ri}^{\Omega}\right)^2 + \left(V_{Ii}^{\Omega}\right)^2} - \sum_{l=1}^{\mathcal{N}} \sum_{t \epsilon \Omega_{set}} \left(G_{il}^{\Omega t} V_{Ii}^{t} + B_{il}^{\Omega t} V_{Ri}^{t} \right) \quad (4)$$

Although, the CIM method is known to improve the convergence properties for the heavily and weakly meshed three-phase radial distribution systems with high R/X ratio, the method is known to diverge for test-cases with high penetration of PV buses [12]. Traditionally, this was not a problem as the number of PV buses in the distribution system were limited to a small

number; however, with the advent of large-scale installation of distributed energy resources (DERs) and voltage control devices in the distribution system, this is no longer true. Therefore, it is essential that a standard three-phase power flow formulation can robustly handle high penetration of PV buses (any bus with voltage control) in the system.

4.1.3 Backward-Forward Sweep Method

The backward-forward sweep method was initially introduced in [4] to overcome the drawbacks of 'PQV' formulation-based NR method for three-phase radial systems with wide ranging line resistances and reactances. This method starts by breaking the interconnected grid into a radial grid by introducing breakpoints and then solving this radial system efficiently via Kirchhoff's voltage and current laws. To compensate for the currents at the breakpoints, this method introduces current injections at the cut-set nodes. The magnitudes of these currents are calculated by iterative compensation methods [4], [18] that include a backward and a forward sweep step. Although, the method is known to work well with radial systems, it is prone to diverge for test cases that are highly meshed or have multiple sources [11].

4.1.4 Holomorphic embedding load flow method

Holomorphic embedding load flow (HELM) formulation [14] is a direct non-iterative method for solving the power flow problem. The method works by embedding the non-analytic power mismatch equations into the larger analytic set of equations. Convergence of this method is guaranteed [14] by applying an analytic continuation technique to the analytic set of equations. However, this method as originally presented in [14] lacks the ability to model PV buses and works exclusively for systems with PQ buses. Additional work toward extending the HELM formulation to incorporate PV buses is known to suffer from numerical issues [16]-[17]. Furthermore, in practical applications of the HELM method for the power flow problem, singular solution matrix is often encountered, and no theoretical guarantees have yet been provided to counter this challenge, thereby making this solution method non-robust.

4.1.5 Continuation Power Flow Method

The continuation power flow method is another approach used to evaluate the steady-state operating point of the power grid [19]. This algorithm has been primarily used for assessing the

voltage stability of the grid and to trace the maximum available transfer capability curve of the grid. The continuation power flow method involves iteratively evaluating the steady-state operating points of the grid using a two-step predictor and corrector algorithm until the critical operating point is obtained. The algorithm adds an additional state variable: the continuation factor and a corresponding equation to the formulation. In the beginning of this algorithm, conventional NR is used to obtain the base case solution for the analysis. The predictor step is then performed to obtain the new approximated solution for the complex voltages of the system and the continuation parameter variable. A modified NR is then performed to obtain the exact solution from the approximated solution in the corrector step. This iterative process is repeated until the critical point is found. The critical point is the point where the tangent vector for the continuation factor is zero, and it represents an infeasible or collapsed grid state [20]. The analysis methodology is quite useful in assessing the critical point of the electric grid and in general can solve for test grids operating close to the tip of the nose curve. However, the method requires a solved base case to start with, which itself can be quite challenging to solve for in case of hard-to-solve ill-conditioned and large test cases.

4.2 Circuit Simulation Methods

A standard circuit simulator tool (e.g. SPICE) models an integrated circuit using a set of linear and non-linear equations and generally employs the use of the damped Newton-Raphson (NR) method to find the solution to these equations. This iterative NR algorithm is guaranteed to have convergence with quadratic speed, if the following conditions are satisfied [21]:

i. The functions represented by the set of non-linear equations, which in their real domain $\mathbb{R}^n$ must be continuous and smooth.
ii. The solution for the set of non-linear equations from the iterative algorithm must be isolated.
iii. The initial guess for the NR algorithm must be "sufficiently close" to the final solution.

For the purposes of circuit simulation, the first two are usually easily satisfied. Circuit models are generally created such that the underlying functions are continuous and smooth. To satisfy the second condition, non-isolated solutions must be avoided. The source of non-isolated

solutions in the field of circuit simulation can be generally attributed to floating nodes or loops that are formed with components that act as short-circuits at DC condition (for example, voltage sources or inductors). All circuit simulator input files are usually sanitized or pre-processed to flag such network configurations, thereby eliminating the likelihood of non-isolated solutions. The real challenge then lies in finding an initial guess that is "sufficiently close" to the final solution. If the initial guess is not sufficiently close to the final solution, then a large step during an iteration of NR, could easily result in divergence or numerical overflow problems. Often with the use of the limiting methods in Section 4.2.1, some of these problems can be rectified, albeit at the cost of quadratic speed. However, for hard to solve highly non-linear circuit models, limiting methods by themselves are insufficient to ensure convergence. In such cases, homotopy methods such as those described in Section 4.2.2 are generally used to achieve convergence. With homotopy methods, an original problem is broken down into a sequence of sub-problems, wherein the solution to each prior sub-problem is used as the initial guess for subsequent sub-problem. Importantly, the first sub-problem solved within the homotopy algorithm is guaranteed to have an initial guess that is trivial and sufficiently close to the final solution of the modified problem thereby satisfying the third condition for convergence of NR algorithm. In the rest of this section, we will discuss some of the commonly used limiting and homotopy methods in state-of-the-art circuit simulators.

4.2.1 Limiting methods

Limiting methods were first developed in [23]-[24] for simulation of diodes in the early 1970s. The purpose of these methods was to ensure that a large NR step does not lead to numerical overflow problems in the simulator due to the exponential nature of the diode IV curve. The "limiting" was performed on the diode state variables between the $(k+1)^{th}$ and k^{th} iteration of NR to prevent overflow problems. In its simplest form, the implemented logic limited the diode voltage for the $(k+1)^{th}$ NR iteration to $\hat{V}_{k+1}$ via expressions developed as a function of thermal voltage (V_t). The choice of limiting factors of $2V_t$ and $10V_t$ in the original SPICE tool was made from empirical observation [24], and is shown below:

Condition	Action
$\lvert V_{k+1} - V_k \rvert \leq 2V_t$	$\hat{V}_{k+1} = V_{k+1}$
$V_{k+1} > V_{CRIT}$	$\hat{V}_{k+1} = V_{k+1}$
$V_{k+1} < V_k \,\&\, 10V_t < V_k$	$\hat{V}_{k+1} = V_{k+1} - 2V_t$
$V_k < V_{k+1} \,\&\, 10V_t < V_{k+1}$	$\hat{V}_{k+1} = \max(10V_t,\, V_k + 2V_t)$

Another limiting technique for NR algorithm for diodes that is based upon alternating bases was proposed by Colon and implemented by Kao [22]. This algorithm was further modified by Nagel. In this algorithm, a current iteration is performed during NR instead of voltage iteration, if the diode conductance for the new iterate has a slope greater than a pre-specified slope. The slope itself is directly related to the voltage across the diode, and therefore a critical voltage (V_{CRIT}) can be pre-defined and used as a boundary condition. Nagel [24] found that a near optimal value of V_{CRIT} is obtained when the voltage has minimum radius of convergence, given as:

$$V_{CRIT} = V_t \, ln\left(\frac{V_t}{\sqrt{2I_s}}\right) \tag{5}$$

where I_s is the diode saturation current. This algorithm has the following logic [22]:

Condition	Action
$V_{k+1} \leq V_{CRIT}$	$\hat{V}_{k+1} = V_{k+1}$
$V_{k+1} > V_{CRIT}$	$\hat{V}_{k+1} = V_{k+1} + V_t \ln\left(\frac{V_{k+1} - V_k}{V_t} + 1.0\right)$

4.2.2 Homotopy Methods

Homotopy methods are generally applied when limiting methods fail to ensure convergence. Many such homotopy methods are included in the state-of-the-art circuit simulators, amongst which, the two that are most commonly used are described below.

4.2.2.1 Gmin stepping

Gmin stepping is a combined algorithm and implementation itself comes from a combined logic of multiple sources [28]. The method requires the addition of a variable conductance to each node in the system and can be easily explained by the following sequence of steps:

i. To solve for the DC solution of an integrated circuit, first a large conductance (Gmin) is connected from every node in the system to ground. This essentially "swamps" any larger resistances in the system and ensures that the circuit solution at 0^{th} iteration has circuit node voltages very close to the value of zero. The solution to this modified system is trivial and can be found by solving the NR loop with initial system voltages set to 0.

ii. The value of Gmin is then gradually stepped down in subsequent sub-problems until a value close to zero for Gmin is achieved. The initial condition to each subsequent sub-problem is obtained from the final solution of the prior sub-problem thereby resulting in an ever-so slight change in the solution between subsequent sub-problems.

iii. The final solution obtained at Gmin value of zero is the DC solution of the original circuit.

4.2.2.2 Source Stepping

An alternate homotopy technique that can be applied to circuits that have independent sources is called source stepping. The algorithm for source stepping is described in the following steps:

i. Initially all the independent sources in the systems are turned off, thereby resulting in a trivial solution for the modified problem, wherein all the system voltage and current magnitudes are zero.

ii. The independent sources are then gradually turned back on to their original values in small incremental steps resulting in a sequence of sub-problems. As in the case of Gmin stepping, the initial condition for each subsequent sub-problem is obtained from the final solution of the prior sub-problem.

iii. The final solution, which is the DC solution for the circuit, is obtained when all independent sources in the system are scaled all the way up to their original value.

Unfortunately, this method is known to not work well with all kinds of circuit simulation problems. Simulation of a digital circuit is an example for that, wherein the turn-on of a digital transistor circuit due to a small change in voltage can cause a sudden change in circuit state, thereby resulting in convergence issues [28].

Other heuristics used to ensure robust convergence of circuit simulations are well documented in [21]-[27].

5. Equivalent Circuit Approach

We proposed the equivalent circuit approach [31]-[35] for steady-state analysis of the power grid to tackle the challenges exhibited by the existing formulations. This approach for generalized modeling of the power system in steady-state (i.e. power flow and three-phase power flow) represents both the transmission and distribution power grid in terms of equivalent circuit elements without loss of generality. It was shown that each of the power system components (including constant power models, i.e. PQ and PV buses) can be directly mapped to an equivalent circuit model based on the underlying relationship between current and voltage state variables. Importantly, this formulation can represent any physics based load model or measurement based semi-empirical models as a sub-circuit, as shown in [42]-[45], and these models can be combined hierarchically with other circuit abstractions to build larger aggregated models. In addition, by modeling both the transmission and distribution system equivalently using circuit fundamentals, the equivalent circuit approach allows for the joint simulation of transmission and distribution systems, a framework intractable with existing solution methods due to the use of disparate formulations and models for analysis of transmission and distribution systems. In the following sub-sections, we derive the equivalent circuit models for the most common network elements used in the positive sequence power flow and three-phase power flow problem. Then, in Section 5.5, we develop equivalent circuit models from physics based fundamental principles using the three-phase induction motor (IM) as an example. Appendix A introduces a new empirical load model for aggregated load in the grid that can capture the true sensitivity of the modeled load and can be fitted with available measurement data.

5.1 Split-Circuit Formulation due to Non-Analyticity of Power Flow Equations

In the equivalent circuit approach, we represent the equivalent circuit models for different power grid components in the network using the current and voltage state variables. For positive sequence power flow and three-phase power flow analyses this translates to linear and non-linear functions of complex voltage and complex current state variables.

The grid components that are represented by linear functions of complex voltages and complex currents are directly mapped into an equivalent circuit using basic circuit elements such as the conductance, susceptance, independent and controlled sources. However, in case of non-linear representations of grid components, the equivalent circuit models are constructed by first linearizing the set of non-linear equations using Taylor's expansion and then representing them using a fundamental set of circuit elements. Importantly, Taylor expansion of these non-linear representations require the computation of their first-order derivative that is not possible for complex terms with conjugate operator, such as the ones observed in PV and PQ node fundamental constraints. This is due to the non-analyticity of these terms, because of which, they are not differentiable. Therefore, to circumvent this challenge of non-analyticity, the derived equivalent circuit models for power flow and three-phase power flow problem are split into two coupled circuits: one real, and one imaginary [31], both of which are analytic and differentiable.

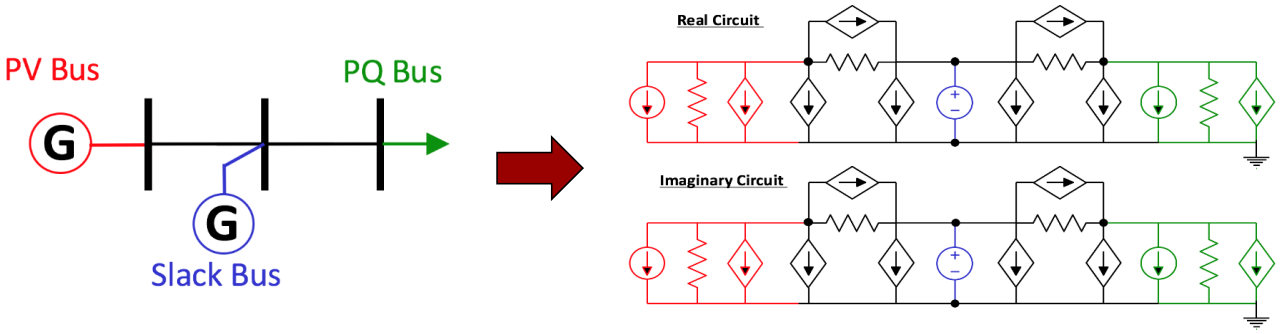

Figure 5-1: Simple three-bus power flow network and its corresponding equivalent circuit.

For example, consider a simple three-bus power flow network given in the left of the Figure 5-1. To represent the equivalent circuit model for this network, we derive the corresponding real and imaginary equivalent circuits, as shown in the right hand of Figure 5-1. In the following subsections, we will derive the real and imaginary equivalent circuit models for the most common power flow and three-phase power flow models, a methodology that can be easily extended to derive an equivalent circuit for any future grid component.

5.2 Equivalent Circuit Models for the Positive Sequence Power Flow Problem

5.2.1 PV Bus

The PV bus model in the positive sequence power flow problem is used to represent the aggregated characteristics of a generator that is required to hold its real power and voltage magnitude constant, as described here in terms of rectangular current-voltage state variables:

$$P_G = V_{RG}I_{RG} + V_{IG}I_{IG} \tag{6}$$

$$|V_G|^2 = V_{RG}^2 + V_{IG}^2 \tag{7}$$

In order to derive the equivalent circuit model representing the PV bus behavior described by (6)-(7), we have a choice to model the PV node as a complex voltage source (as functions of complex current) [31] or a complex current source (as functions of complex voltage) [33]. The equations that represent the generator PV bus as a set of complex voltages sources are given by:

$$V_{RG} = \frac{P_G I_{RG} \pm I_{IG}\sqrt{V_G^2(I_{RG}^2 + I_{IG}^2) - P_G^2}}{I_{RG}^2 + I_{IG}^2} \tag{8}$$

$$V_{IG} = \frac{P_G I_{IG} \pm I_{RG}\sqrt{V_G^2(I_{RG}^2 + I_{IG}^2) - P_G^2}}{I_{RG}^2 + I_{IG}^2} \tag{9}$$

This model for PV nodes is known to have convergence issues [33] due to the existence of the square root term in equations (8)-(9) that can result in non-real values for derived complex voltage sources, if a negative term within the square root term is encountered. To address this problem, we instead model the PV node as complex current sources to mimic the characteristic behavior of equations (6)-(7). This offers superior convergence when applying NR iterations to the resulting equation system [33].

The split real and imaginary equations for complex current sources for a PV node are given by:

$$I_{RG} = \frac{P_G V_{RG} + Q_G V_{IG}}{{V_{RG}}^2 + {V_{IG}}^2} \tag{10}$$

$$I_{IG} = \frac{P_G V_{IG} - Q_G V_{RG}}{{V_{RG}}^2 + {V_{IG}}^2} \tag{11}$$

In addition to producing real power constrained generator currents, the PV node also controls the voltage magnitude either at its own node or any other remote node in the system if its reactive power output is within the limits. We represent this constraint by a control circuit, as shown in the following subsection. The reactive power Q_G of the generator is controllable and acts as the additional unknown variable for the additional constraint that is introduced due to voltage control.

To derive the equivalent circuit of the PV node, the first order terms of the Taylor expansions for (10)-(11) are used to linearize the functions, as shown in Figure 5-2. Linearization of the real generator current results in the following terms:

$$\begin{aligned} I_{RG}^{k+1} = {} & \frac{\partial I_{RG}}{\partial Q_G}\Big|_{Q_G^k, V_{RG}^k, V_{IG}^k}\left(Q_G^{k+1}\right) + \frac{\partial I_{RG}}{\partial V_{RG}}\Big|_{Q_G^k, V_{RG}^k, V_{IG}^k}\left(V_{RG}^{k+1}\right) + \frac{\partial I_{RG}}{\partial V_{IG}}\Big|_{Q_G^k, V_{RG}^k, V_{IG}^k}\left(V_{IG}^{k+1}\right) + I_{RG}^k \\ & - \frac{\partial I_{RG}}{\partial Q_G}\Big|_{Q_G^k, V_{RG}^k, V_{IG}^k}\left(Q_G^k\right) - \frac{\partial I_{RG}}{\partial V_{RG}}\Big|_{Q_G^k, V_{RG}^k, V_{IG}^k}\left(V_{RG}^k\right) - \frac{\partial I_{RG}}{\partial V_{IG}}\Big|_{Q_G^k, V_{RG}^k, V_{IG}^k}\left(V_{IG}^k\right) \end{aligned} \tag{12}$$

Similarly, linearization by Taylor's expansion of imaginary current results in:

$$\begin{aligned} I_{IG}^{k+1} = {} & \frac{\partial I_{IG}}{\partial Q_G}\Big|_{Q_G^k, V_{RG}^k, V_{IG}^k}\left(Q_G^{k+1}\right) + \frac{\partial I_{IG}}{\partial V_{RG}}\Big|_{Q_G^k, V_{RG}^k, V_{IG}^k}\left(V_{RG}^{k+1}\right) + \frac{\partial I_{IG}}{\partial V_{IG}}\Big|_{Q_G^k, V_{RG}^k, V_{IG}^k}\left(V_{IG}^{k+1}\right) + I_{IG}^k \\ & - \frac{\partial I_{IG}}{\partial Q_G}\Big|_{Q_G^k, V_{RG}^k, V_{IG}^k}\left(Q_G^k\right) - \frac{\partial I_{IG}}{\partial V_{RG}}\Big|_{Q_G^k, V_{RG}^k, V_{IG}^k}\left(V_{RG}^k\right) - \frac{\partial I_{IG}}{\partial V_{IG}}\Big|_{Q_G^k, V_{RG}^k, V_{IG}^k}\left(V_{IG}^k\right) \end{aligned} \tag{13}$$

The terms in (12) represent the basic elements of the real circuit of PV node. The first term in (12) represents a current source that is a function of the reactive power; the second term represents a conductance, since the real current is proportional to the real voltage; the third term represents a voltage-controlled current source, since the real current is proportional to the imaginary voltage. The remaining terms are all dependent on known values from the previous iteration, so they can be lumped together and represented as an independent current source.

Similarly, the terms in (13) represent the basic circuit elements for the imaginary circuit of the PV node. The first term in (13) represents a current source that is a function of reactive power; the second term represents a voltage-controlled current source, since the imaginary current is proportional to the real voltage; the third term represents a conductance, since the imaginary current is proportional to the imaginary voltage. The remaining terms are all dependent on known values from the previous iteration, so they can be lumped together and be represented as an independent current source as in the case of real circuit.

Figure 5-2 represents the derived real and imaginary circuits for complex current source representing the PV node.

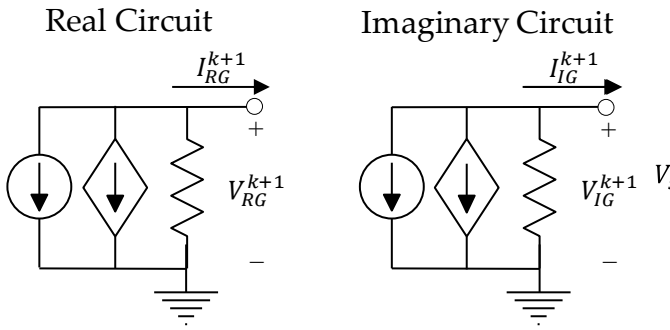

Figure 5-2: Equivalent Circuit Model for PV generator model.

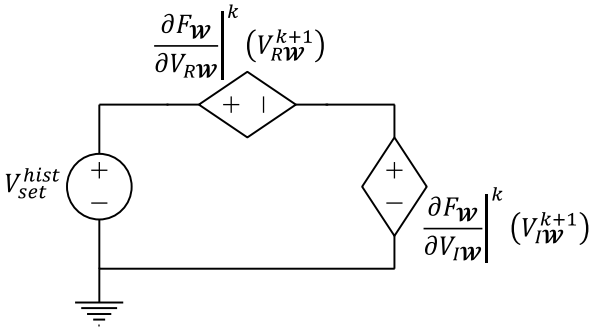

Figure 5-3: Voltage magnitude constraint control equivalent circuit.

5.2.2 Voltage Regulation of the Bus

Numerous power grid elements such as generators, FACTS devices, transformers, shunts, etc., can control a voltage magnitude at a given node in the system. Moreover, they can control the voltage magnitude at either their own node ($\mathcal{O}$) or a remote node ($\mathcal{R}$) in the system. In the equivalent circuit formulation, the control of the voltage magnitude by a control circuit (Figure 5-3) is governed by:

$$F_{\mathcal{W}} \equiv V_{set}^2 - V_{R\mathcal{W}}^2 - V_{I\mathcal{W}}^2 = 0, where\ \mathcal{W} \in \mathcal{O}, \mathcal{R} \tag{14}$$

The circuit in Figure 5-3 is derived from the linearized version of (14). It is stamped into the matrix equations for each node $\mathcal{W}$ in the system whose voltage is being controlled such that there

exists at least one path between the node $\mathcal{W}$ and the equipment's node $\mathcal{O}$ that is controlling it. The additional unknown variable for this additional constraint is dependent on the power system device that is controlling the voltage magnitude. For example, the additional unknown variable for a generator is its reactive power Q_G, whereas in the case of transformers, it is the transformer turns ratio tr, and for FACTS devices it is the firing angle φ. The previous section showed how the additional unknown variable for PV buses is integrated in its respective equivalent circuit.

5.2.2.1 Reactive power limits of a PV generator model

The PV model for the generator derived in Section 5.2.1 does not account for reactive power limits for the modeled voltage control equipment. The general practice in the industry and academia today is to apply the reactive power limits via the use of discontinuous piecewise linear models (PV-PQ switching). In this approach, the voltage control equipment has two discrete modes of operation: i) voltage control mode – reactive power of the voltage equipment is within its limits and the active set of equations include (14) ii) set reactive power mode – reactive power is either set to its maximum or minimum value and the active set of constraints include (15)-(16).

$$if\ \hat{Q}_G > Q_{MAX}\ then, Q_G = Q_{MAX} \tag{15}$$

$$if\ \hat{Q}_G < Q_{MIN}\ then, Q_G = Q_{MIN} \tag{16}$$

To apply reactive power limits for the PV model in the power flow analyses, the model is switched between the voltage control mode and set reactive power mode in the outer loop of the NR iterations depending on the obtained value of reactive power ($\hat{Q}_G$) in the inner loop of the NR algorithm. This methodology generally tends to work well for small cases. However, a necessary condition for convergence of system with discontinuous piecewise models is that only one element/model is switched to different piecewise linear segment at a time [37]-[38], an intractable approach while solving a larger system wherein a significant number of voltage control equipment violate their limits. Therefore, due to this practical consideration, the existing state-of-the-art tools limit a larger number of generators at once. This approach can result in oscillations during NR that could further prevent convergence of the overall system. The following example demonstrates this behavior.

In this example, positive-sequence power flow simulation is run on a test case representing a real electric network in Africa [39]. Upon convergence of the inner NR loop, several generators violated their limits. Upon applying PV-PQ switching in the outer loop oscillatory behavior is observed as seen in the Figure 5-4. The vertical axis of the figure shows the number of generators that are limited in the outer loop of NR iterations, and the horizontal axis represents the outer loop count for the power flow analyses. As seen in the figure, due to the observed oscillatory behavior, convergence is prevented in this test case.

To address this limitation wherein oscillatory behavior is observed during PV-PQ switching, we propose two distinct approaches:

i. Setting a pre-determined parameter that is the maximum allowable count of generator switching (between PV and PQ mode), after which each generator is set permanently to its Q limit value that it encountered last.

ii. The use of a continuous and twice differentiable model for the generator voltage control.

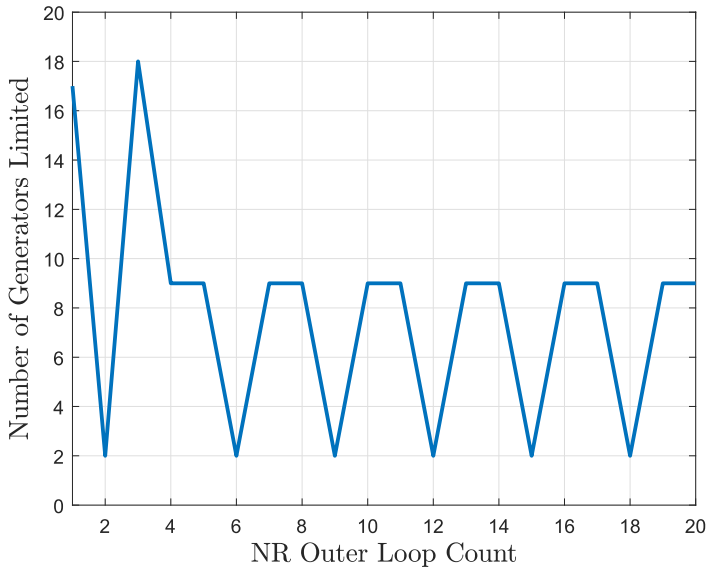

Figure 5-4: Oscillations observed during PV-PQ switching in the outer loop of NR.

The first approach is briefly discussed prior to introducing the continuous twice differentiable generator model. In this approach, a fixed pre-determined parameter (integer number) is inputted by the user that is applied in the algorithm to prevent the generator oscillations between

different discontinuous piecewise segments. The algorithm is implemented to count the number of times each generator back-offs during the simulation. In case this number is greater than the specified parameter, the generator is no longer allowed to back-off and its reactive power Q_G is limited to either Q_{MAX} or Q_{MIN} for rest of the simulation, hence preventing any further oscillations between different segments. Even though this approach has been shown to prevent oscillations in many test instances, convergence is not always guaranteed. This is primarily due to the shrinking of the solution space once the generator is permanently limited, which can often lead to divergence due to the lack of solution in the reduced solution space. Furthermore, this can cause non-physical behavior of the generator model resulting in a final solution that contains a scenario where either:

i. A generator's reactive power Q_G is set to its lower reactive power limit (Q_{MIN}) while the magnitude of voltage at the controlled node is lower than the set voltage, or
ii. A generator's reactive power Q_G is set to its higher reactive power limit (Q_{MAX}) while the magnitude of the voltage at the controlled node is higher than the set voltage.

Hence, to prevent the generator oscillations during PV-PQ switching while ensuring that the physical behavior of the generator is preserved, we propose the use of the following continuous generator model.

5.2.3 Continuous Model for a Generator/PV Bus

5.2.3.1 General Introduction

To address the limitations of the discontinuous piecewise generator model, we propose a continuous and twice differentiable generator model [36]. In this model, we model the generator voltage constraint using a non-linear sigmoid function that can control the voltage of the controlled node when the reactive power of the generator is within its limits and can limit the generator reactive power when one of its limits are violated. Importantly this model is continuous and twice differentiable and does not require discontinuous switching between piece-wise sections thereby preventing oscillations that otherwise can be detrimental for system convergence. Importantly, the proposed continuous model allows for the use of robust methods for NR

convergence such as homotopy methods (as discussed later in the thesis) that require the set of network models to be continuous.

5.2.3.2 Description of Models

The proposed continuous model for the PV node models its complex currents as a function of complex voltages, as in the case of the discontinuous piecewise model for the PV node as shown in (10)-(11). However, this model replaces the voltage constraint given by (14) with a sigmoid function given in (17). Importantly, the model equations for the proposed model are both continuous and twice differentiable and include the reactive power limits for the generator inherently.

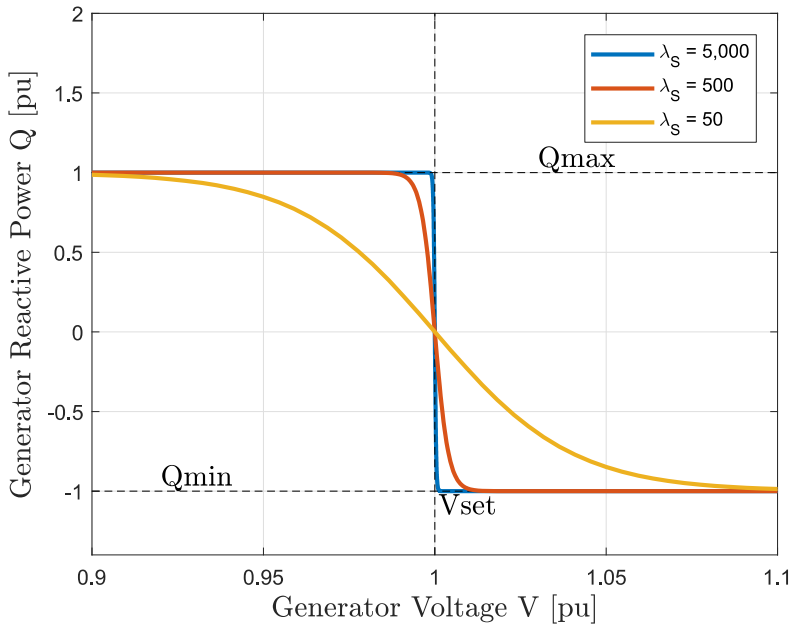

Figure 5-5: Voltage constraint behavior for continuous generator model.

$$Q_G = \frac{Q_{MAX} - Q_{MIN}}{1 + \exp(\lambda_S * \left[\sqrt{V_{RW}^2 + V_{IW}^2} - V_{set}\right]} + Q_{MIN} \tag{17}$$

The sigmoid function in (17) mimics the behavior of the PV node during both the "voltage control behavior" mode and "set reactive power behavior" mode. In case, the reactive power needed to control the voltage of the controlled node is within its limits, the model operates in the steep slope part of the curve in Figure 5-5 thereby maintaining the controlled node voltage to its

set value. In case, the reactive power needed to control the controlled node's voltage is outside its limits, the model saturates the reactive power output thereby no longer controlling the controlled node's voltage. Importantly, the smoothing parameter (λ_S) in (17) controls the slope of the generator model voltage characteristics as shown in Figure 5-5. A higher value for this parameter tends to better mimic the behavior of the piecewise discontinuous generator model at the cost of more rigid non-linear behavior. In contrast, reducing the magnitude of this parameter relaxes the function non-linearities while approximating the voltage control behavior of the existing generator model. Due to the highly non-linear nature of this behavior, convergence difficulties can be observed when this model is used. Therefore, in the following section we discuss techniques that are used to achieve robust convergence for the network equations with the use of a proposed continuous generator model.

5.2.3.3 Aid to Convergence

We propose two homotopy based approaches to achieve robust convergence with systems containing the continuous generator model. Homotopy methods for general application to robust convergence of power flow and three-phase power flow analysis are discussed in depth in Section 6.2. However, due to the applicability of these methods to continuous generator model convergence, they are briefly discussed here:

5.2.3.3.1 Relaxation of generator convergence parameter to enable robust convergence

To ensure the robust convergence for the continuous generator model, in the first approach, we embed a generator convergence parameter λ_G in the continuous generator model i.e.:

$$Q_G = \frac{\lambda_G(Q_{MAX} - Q_{MIN})}{1 + exp(\lambda_S * \left[\sqrt{V_{RW}^2 + V_{IW}^2} - V_{set}\right]} + \lambda_G Q_{MIN} \tag{18}$$

To use the properties of homotopy methods to achieve robust convergence, we first need to obtain the value of λ_G that will result in a trivial solution for the generator continuous model. This is achieved by calculating the initial value of generator convergence parameter ${\lambda_G}^{init}$ via solving the inner loop of the power flow problem with generator models that have unbounded reactive power limits and choosing its value such that:

$$\lambda_G^{\,init} = \begin{cases} \frac{Q_G}{Q_{MAX}}, & if\ Q_G > Q_{MAX} \\ \frac{Q_G}{Q_{MIN}}, & if\ Q_G < Q_{MIN} \\ 1, & otherwise \end{cases} \tag{19}$$

Once we have obtained an initial value ($\lambda_G^{\,init}$) for the parameter that results in the trivial solution for the continuous generator model, we vary the parameter in small increments until the original problem is solved. As always with the use of homotopy methods, the final solution of the previous sub-problem is chosen as the initial guess for each subsequent sub-problem.

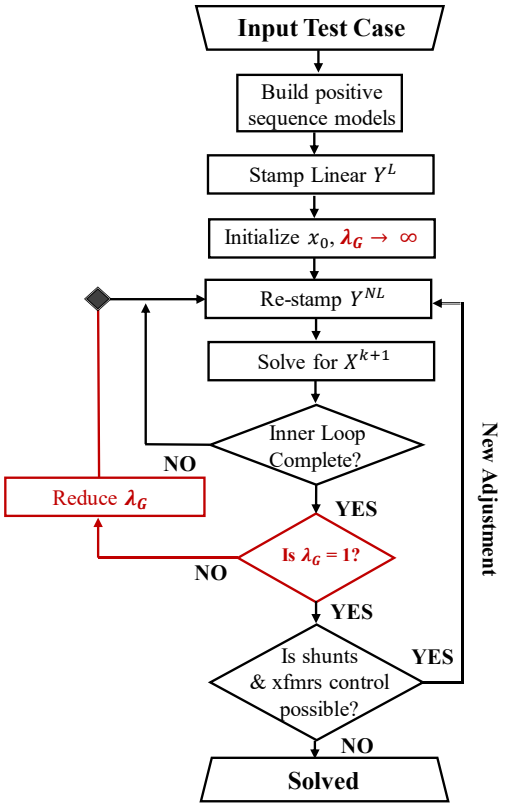

Algorithm 5-1: Flowchart for dynamic handling of generator convergence parameter for better convergence

Algorithm 5-1 describes the general flow of this homotopy method. First, for all generators in the network, generator convergence parameter $\lambda_G^{\,init}$ is initialized via (19). Following which, for each successful convergence of the inner loop of NR, the generator convergence parameter is incrementally varied until the value of unity is achieved for all $\boldsymbol{\lambda_G}$. The range of generator

convergence parameter λ_G is given by $[1, \infty)$. Figure 5-6 graphically demonstrates this methodology.

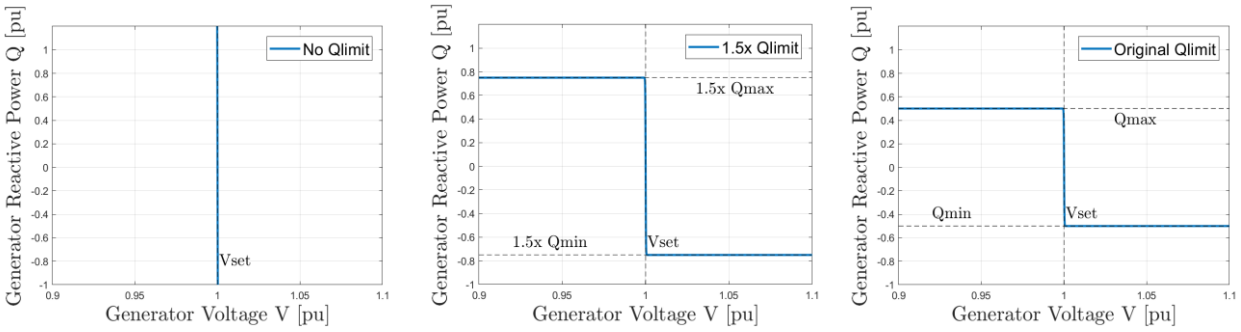

Figure 5-6: Generator characteristics as a function of generator convergence parameter

5.2.3.3.2 Relaxation of generator smoothing parameter for achieving robust convergence

In this approach, generator smoothness parameter (λ_S) in (17) is adjusted if convergence difficulties are encountered due to the rigid non-linearities in the continuous model. The highly non-linear nature of the continuous generator model voltage constraint in the region around Q_{MAX} and Q_{MIN} is due to the steep change in the gradient of the function. To relax these non-linearities to enable smoother convergence requires adjustment of the generator smoothness factor, as shown in Figure 5-7.

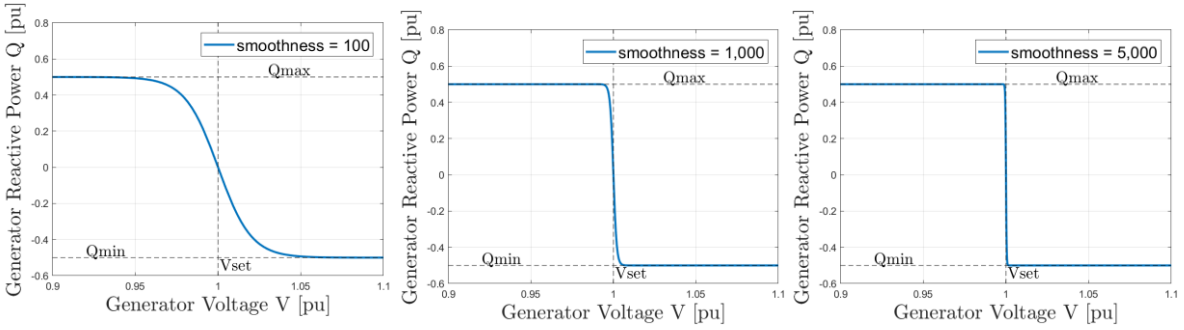

Figure 5-7: Generator characteristics as a function of generator smoothness parameter

Reducing the magnitude of the generator smoothness parameter relaxes the non-linearities in generator model, whereas increasing the magnitude mimics the piecewise behavior of conventional generator model. Therefore, if convergence difficulties are encountered in the inner loop of NR, then the generator smoothness parameter is first relaxed until convergence for the continuous model is achieved (representing the trivial problem within the homotopy method).

The parameter is then gradually scaled back up until the original model is solved as in the case of any homotopy method. The Algorithm 5-2 depicts the flow of this approach.

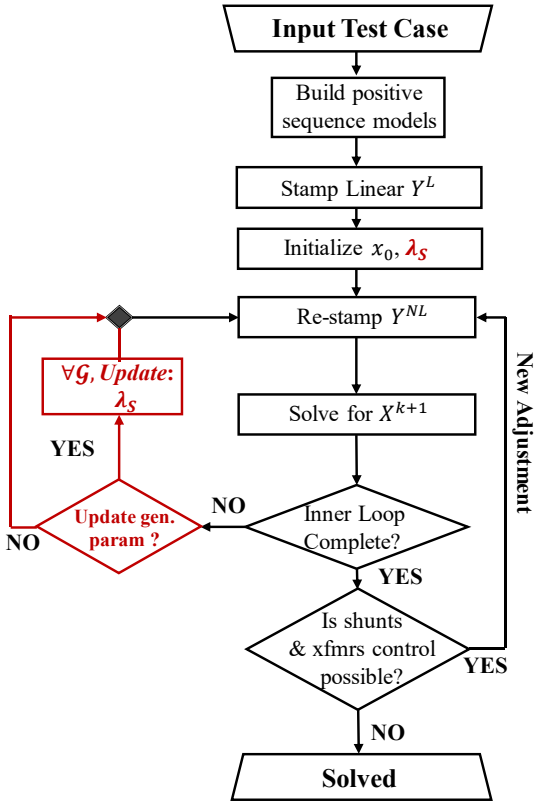

Algorithm 5-2: Flowchart for dynamic handling of generator smoothness parameter for better convergence.

5.2.3.4 Results for the Continuous Generator

5.2.3.4.1 Experiment 1

The purpose of this experiment is to demonstrate that the use of the continuous generator model can eliminate the limitations of the piecewise discontinuous generator model as shown in Section 5.2.2.1. In this experiment, we consider the test grid for a realistic grid in Africa that was previously discussed in Section 5.2.2.1. This case when solved with the discontinuous piecewise generator model resulted in oscillations during PV-PQ switching in the outer loop of the power flow solver as shown in Figure 5-4 and hence, the solution for the test case could not be obtained.

However, with the use of a continuous generator model along with methods that aids its convergence, oscillations are easily prevented with successful convergence for the example test case.

5.2.4 Slack Bus

Slack bus model is used in power flow analysis for two primary purposes. First, it provides the reference angle for the power grid circuit and second, it absorbs or produces any slack (power losses and load-generation mismatch in the system) in the system. In its most basic form, the model is the easiest bus type to model. In the real circuit, it appears as an independent voltage source of value $|V_i| \cos\theta_i$, and in the imaginary circuit it appears as a voltage source of value $|V_i| \sin\theta_i$. When the phase θ is 0° the imaginary component appears as a short to ground.

In real life, however, no single generator covers the complete slack in the system. Generally, all the generators change their real-power set-points based on the primary droop control and furthermore a subset of them adjust their set-points based on the secondary control i.e. automatic generation control (AGC) signal. Therefore, it is important that the steady-state analysis, which is trying to mimic the true behavior of the grid during normal or contingency operation, is able to model the distributed slack behavior of the grid. We incorporate this approach within our formulation using continuous analytical models for droop control as well as for AGC [36]. Although, droop control and AGC represent two distinct phenomena within the grid operation, their models for power flow problem can be achieved via same set of equations. We achieve this by adding an additional variable delta P (ΔP_G) to generators that are participating in either droop control or AGC. These variables in turn share the slack in the grid based on the pre-defined vector of participation factors $\boldsymbol{\kappa}$, which in turn can be pre-calculated based on either the size of the generator or the inertia of the machine. The equations for the distributed slack operation are as follows:

$$P_{slack} + \Delta P_{slack} = V_{slack}^{R} I_{slack}^{R} + V_{slack}^{I} I_{slack}^{I} \tag{20}$$

$$\boldsymbol{\Delta P_G} = \boldsymbol{\kappa^T \Delta P_{slack}} \; \forall \boldsymbol{G} \in \{AGC/droop\} \tag{21}$$

$$\boldsymbol{P_G^{MIN}} < \boldsymbol{P_G} + \boldsymbol{\Delta P_G} < \boldsymbol{P_G^{MAX}} \tag{22}$$

where $\boldsymbol{\Delta P_{slack}}$ is a diagonal matrix with each element as ΔP_{slack} and $\boldsymbol{\Delta P_G}$ is the vector of additional power produced by the generators participating in AGC or droop control.

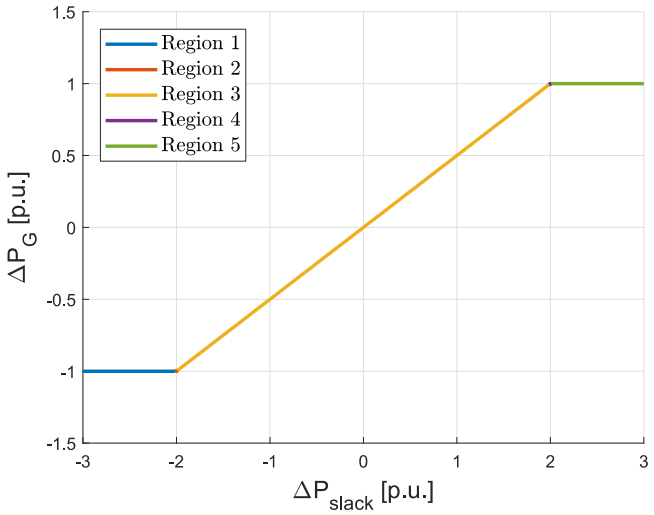

Figure 5-8: Continuous analytical model for modeling the AGC and droop control of the generator based on participation factor.

We represent the behavior given by (21) and (22) in our approach with the use of continuous analytical generator models for AGC or droop control as shown in Figure 5-8. The model consists of a set of functions that together consist of three linear segments (Region 1, 3, and 5 in the Figure 5-8) patched with two quadratic segments (Region 2 and 4 in the Figure 5-8) to produce a net continuous differentiable function [36]. With the use of this model within our formulation, all or selected sub-set of the participating generators contribute toward the slack in the system until they hit their minimum or maximum limit. Importantly, the model is differentiable and continuous and hence can be directly included implicitly within the inner loop of NR solver thus utilizing all the circuit heuristics developed within this thesis to ensure robust convergence. This is a significant improvement over the existing methodologies that are used to model the AGC in the power flow tools that implement this feature using outer loop around the NR solver with discontinuous piecewise models.

To demonstrate our approach for AGC and droop control we run a simple experiment on a sample 23-node (savnw) system. We first run the base case (pre-contingency) without AGC or droop control enabled and document the real power generation for different generators. We then perform a N-1 contingency on the base case by taking off-line a generator on bus 211 and further document the updated real power generation for different generators: i) with AGC and droop control enabled ii) without AGC and droop control enabled. As tabulated in Table 5-1, when the

generator contingency is performed with AGC disabled, the slack generator picks up all the real power generation mismatch due to the loss of generator on bus 211. However, in the case with AGC enabled, the real power generation is distributed amongst different generators (in AGC) based on the participation factors until they hit their limits, upon which the participating factors are re-distributed automatically, and remaining generators share the remaining slack.

TABLE 5-1: RESULTS TO DEMONSTRATE AGC FUNCTIONALITY USING CONTINUOUS ANALYTICAL MODEL.

Generator ID	P_G^{MAX} [MW]	P_G^{MIN} [MW]	κ	Real Power Generation [MW]		
				Pre-contingency	Post-contingency	
				AGC-Disabled	AGC-Enabled	AGC-Disabled
101	810	0	0.23	750	810	750
102	810	0	0.23	750	810	750
206	900	0	0.25	800	900	800
211*	616	0	0.18	600	0*	0*
3011	900	0	0.08	257.74	635.22	864.39
3018	117	0	0.03	100	117	100

*Generator taken off-line during a contingency

5.2.5 PQ Bus

Like the PV bus, the constant power node (PQ bus) is also represented as an equivalent circuit via either a complex voltage source or a complex current source. It has been empirically determined that superior convergence is observed when the load bus is modeled as a complex current source. The two fundamental equations that represent the behavior of the PQ load model, are given by:

$$P_L = V_{RL}I_{RL} + V_{IL}I_{IL} \tag{23}$$

$$Q_L = V_{RL}I_{IL} - V_{IL}I_{RL} \tag{24}$$

The terms in equation (23)-(24) are re-arranged to derive the complex current sources of the PQ node as a function of complex voltage state variables:

$$I_{RL} = \frac{P_L V_{RL} + Q_L V_{IL}}{V_{RL}^2 + V_{IL}^2} \tag{25}$$

$$I_{IL} = \frac{P_L V_{IL} - Q_L V_{RL}}{V_{RL}^2 + V_{IL}^2} \tag{26}$$

Linearizing the load model in (25) and (26) as shown in (27)-(28) via Taylor expansion results in three elements in parallel for both real and imaginary circuits: a conductance, a voltage-controlled current source, and an independent current source.

$$\begin{aligned} I_{RL}^{k+1} = {} & \frac{\partial I_{RL}}{\partial V_{RL}}\Big|_{Q_L^k, V_{RL}^k, V_{IL}^k}\left(V_{RL}^{k+1}\right) + \frac{\partial I_{RL}}{\partial V_{IL}}\Big|_{Q_L^k, V_{RL}^k, V_{IL}^k}\left(V_{IL}^{k+1}\right) + I_{RL}^k - \frac{\partial I_{RL}}{\partial V_{RL}}\Big|_{Q_L^k, V_{RL}^k, V_{IL}^k}\left(V_{RL}^k\right) \\ & - \frac{\partial I_{RL}}{\partial V_{IL}}\Big|_{Q_L^k, V_{RL}^k, V_{IL}^k}\left(V_{IL}^k\right) \end{aligned} \tag{27}$$

$$\begin{aligned} I_{IL}^{k+1} = {} & \frac{\partial I_{IL}}{\partial V_{RL}}\Big|_{Q_L^k, V_{RL}^k, V_{IL}^k}\left(V_{RL}^{k+1}\right) + \frac{\partial I_{IL}}{\partial V_{IL}}\Big|_{Q_L^k, V_{RL}^k, V_{IL}^k}\left(V_{IL}^{k+1}\right) + I_{IL}^k - \frac{\partial I_{IL}}{\partial V_{RL}}\Big|_{Q_L^k, V_{RL}^k, V_{IL}^k}\left(V_{RL}^k\right) \\ & - \frac{\partial I_{IL}}{\partial V_{IL}}\Big|_{Q_L^k, V_{RL}^k, V_{IL}^k}\left(V_{IL}^k\right) \end{aligned} \tag{28}$$

The linearized elements in (27)-(28) are represented in Figure 5-9 to represent the split equivalent circuit for the PQ load model.

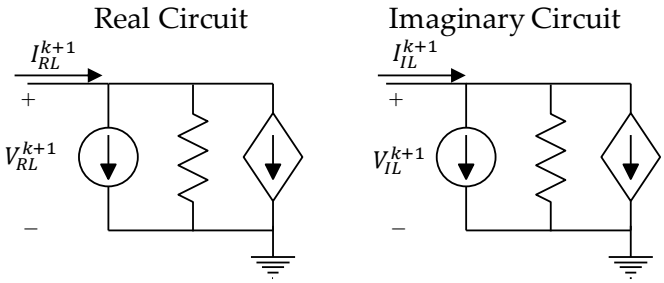

Figure 5-9: Equivalent split-circuit PQ load model.

5.2.6 ZIP Model

The currents consumed by the PQ load model are insensitive to voltage magnitude at its terminal. This can result in inaccurate results for the power flow analysis where the system solution has either visibly high or low voltages. Therefore, a more comprehensive load model such as the ZIP load model is needed to capture the voltage sensitive nature of the aggregated load. The ZIP load model models the aggregated load in the system as a mix of constant

impedance, constant current, and constant power load models that can be mathematically represented as follows:

$$P_i^{ZIP} = Z_P(|V_i|)^2 + I_P(|V_i|) + S_P \tag{29}$$

$$Q_i^{ZIP} = Z_Q(|V_i|)^2 + I_Q(|V_i|) + S_Q \tag{30}$$

In the equivalent circuit approach, the equations for the ZIP load model can be re-written as:

$$I_{Ri}^{ZIP} = Z_P V_{Ri} - Z_Q V_{Ii} + \frac{S_P V_{Ri} + S_Q V_{Ii}}{(V_{Ri})^2 + (V_{Ii})^2} + \left(\sqrt{{I_P}^2 + {I_Q}^2}\right).cos\left(I_{pf} + \delta_i\right) \tag{31}$$

$$I_{Ii}^{ZIP} = Z_P V_{Ii} + Z_Q V_{Ri} + \frac{S_P V_{Ii} - S_Q V_{Ri}}{(V_{Ri})^2 + (V_{Ii})^2} + \left(\sqrt{{I_P}^2 + {I_Q}^2}\right).sin\left(I_{pf} + \delta_i\right) \tag{32}$$

where:

$$I_{pf} = tan^{-1}\left(\frac{I_Q}{I_P}\right) \tag{33}$$

$$\delta_i = tan^{-1}\left(\frac{V_{Ii}}{V_{Ri}}\right) \tag{34}$$

For the load model given in (31) through (34), the constant impedance part of the load is linear, whereas the constant current and constant power part of the aggregated load is nonlinear. Linearizing the set of equations using Taylor expansion results in the following expressions:

$$I_{Ri}^{ZIP\,k+1} = I_{Ri}^{ZIP\,k} + \left(\frac{\partial I_{Ri}^{ZIP}}{\partial V_{Ri}}\bigg|_{V_{Ri}^k, V_{Ii}^k}\right)\left({V_{Ri}}^{k+1} - {V_{Ri}}^{k}\right) + \left(\frac{\partial I_{Ri}^{ZIP}}{\partial V_{Ii}}\bigg|_{V_{Ri}^k, V_{Ii}^k}\right)\left({V_{Ii}}^{k+1} - {V_{Ii}}^{k}\right) \tag{35}$$

$$I_{Ii}^{ZIP\,k+1} = I_{Ii}^{ZIP\,k} + \left(\frac{\partial I_{Ii}^{ZIP}}{\partial V_{Ri}}\bigg|_{V_{Ri}^k, V_{Ii}^k}\right)\left({V_{Ri}}^{k+1} - {V_{Ri}}^{k}\right) + \left(\frac{\partial I_{Ii}^{ZIP}}{\partial V_{Ii}}\bigg|_{V_{Ri}^k, V_{Ii}^k}\right)\left({V_{Ii}}^{k+1} - {V_{Ii}}^{k}\right) \tag{36}$$

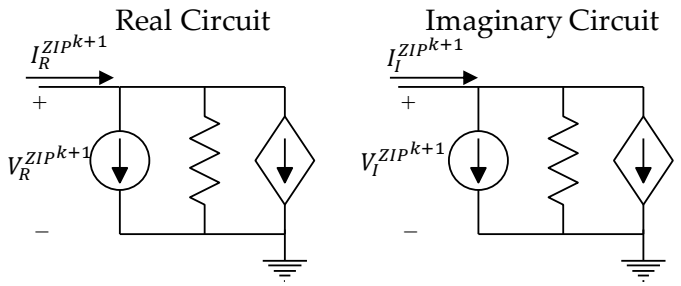

Figure 5-10: Real and Imaginary Equivalent Circuit for the ZIP load model.

The linearized set of equations can then be mapped into the equivalent circuit and is shown in Figure 5-10.

5.2.7 BIG Model

The BIG aggregated load model introduced in [44]-[46] (Figure 5-11) was shown to more accurately capture the true load behavior when compared against the traditional non-linear PQ load model, and was demonstrated as comparable to the more comprehensive non-linear ZIP load model. Importantly, the BIG load model can be easily fitted with real-time measurement data and is linear in our equivalent circuit formulation while capturing the true sensitivities of the aggregated load. Hence it results in linear equality constraints for the load bus in the positive sequence power-flow analysis. This load model is defined by a combination of constant current source ($\alpha_R^{BIG} + j\alpha_I^{BIG}$), a conductance ($G^{BIG}$) and a susceptance ($B^{BIG}$) whose real and imaginary currents are given by:

$$I_R^{BIG} + jI_I^{BIG} = \alpha_R^{BIG} + j\alpha_I^{BIG} + \left(V_R^{BIG} + jV_I^{BIG}\right)(G^{BIG} + B^{BIG}) \tag{37}$$

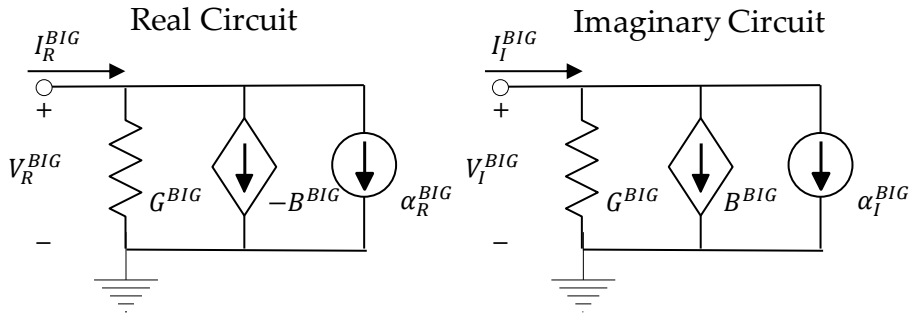

Figure 5-11: Equivalent circuit of a BIG load model.

The appendix A of this thesis delves deeper into the proposed BIG load model and discusses its advantages over other existing aggregated load models in detail. It also refers to machine learning methods that have been developed within our group to fit the BIG load model to capture the true sensitivities of the load currents.

5.2.8 Transformer

Transformers are an integral part of the electric grid and are used to step-up or step-down the grid voltages. In addition to this, some transformers contain a built-in phase shifter and have a capability to introduce phase shifts between the buses to which they are connected. We derive the equivalent circuit of the transformer with the transformer impedance modeled on the secondary of the transformer as shown in Figure 5-12.

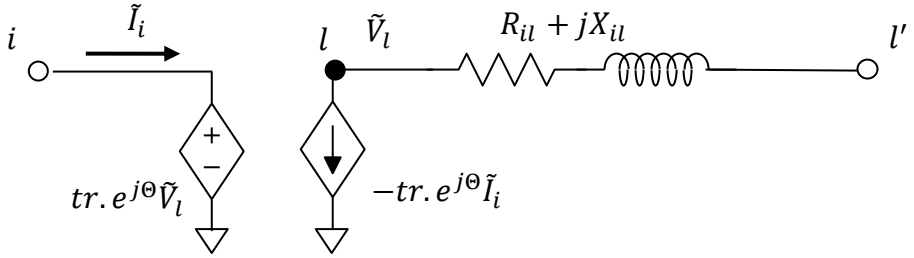

Figure 5-12: Equivalent circuit for a transformer.

To derive the split circuit equivalent model of the transformer, we begin by relating the primary and secondary voltages ($\tilde{V}_i$ and $\tilde{V}_l$) by the turns ratio tr and the phase angle Θ:

$$\frac{\tilde{V}_i}{\tilde{V}_l} = tr.e^{j\Theta} \rightarrow \frac{V_R^i + jV_I^i}{V_R^l + jV_I^l} = tr(cos\,\Theta + j\,sin\,\Theta) \tag{38}$$

Representing the primary transformer voltages as functions of secondary transformer voltages by splitting them into real and imaginary parts result in:

$$V_R^i = tr\left(V_R^l \cos\Theta - V_I^l \sin\Theta\right) \tag{39}$$

$$V_I^i = tr\left(V_I^l \cos\Theta + V_R^l \sin\Theta\right) \tag{40}$$

The first term of (39) represents a voltage-controlled voltage source, where the controlling voltage is the secondary side voltage in the real circuit. The second term is a voltage-controlled

voltage source, but here the controlling voltage is the secondary side voltage in the imaginary circuit. The equation (40) represents similar terms. These terms can be used to represent the primary side of transformer equivalent circuit as shown in Figure 5-13.

Similarly, the real and imaginary equivalent circuit for the secondary of the transformer can be developed by the primary and secondary current relationship. The primary and secondary complex currents ($\tilde{I}_i$ and $\tilde{I}_l$) in terms of the turns ratio are given by:

$$\frac{\tilde{I}_l}{\tilde{I}_i} = -tr.e^{-j\theta} \rightarrow \frac{I_R^l + jI_I^l}{I_R^i + jI_I^i} = -tr(cos\,\Theta - j\,sin\,\Theta) \tag{41}$$

We derive the currents for the secondary side of the transformer as a function of primary side currents and finally split them into respective real and imaginary terms:

$$I_R^l = -tr\left(I_R^i \cos\Theta + I_I^i \sin\Theta\right) \tag{42}$$

$$I_I^l = -tr\left(I_I^i \cos\Theta - I_R^i \sin\Theta\right) \tag{43}$$

The first term of (42) represents a current-controlled current source, where the controlling current is the current which flows through the primary side in the real circuit. The second term represents a current-controlled current source, but here the controlling current is the current which flows through the primary side in the imaginary circuit. The equation (43) represents similar terms. These terms can be used to represent the secondary side of transformer equivalent circuit as shown in Figure 5-13 for the phase shifter value of 0.

The leakage term of the transformer $Z_{il} = R_{il} + jX_{il}$ is modeled on the secondary side. We model it using same approach as that of the transmission line given in Section 5.2.9 resulting in the following real and imaginary terms:

$$I_R^l = V_R^{l'l} G_{il} - V_I^{l'l} B_{il} \tag{44}$$

$$I_I^l = V_I^{l'l} G_{il} + V_R^{l'l} B_{il} \tag{45}$$

The first term of (44) is a conductance and the second term is a voltage-controlled current source; likewise for equation (45). A full equivalent circuit model for the transformer for phase shifter magnitude of 0° is shown in Figure 5-13.

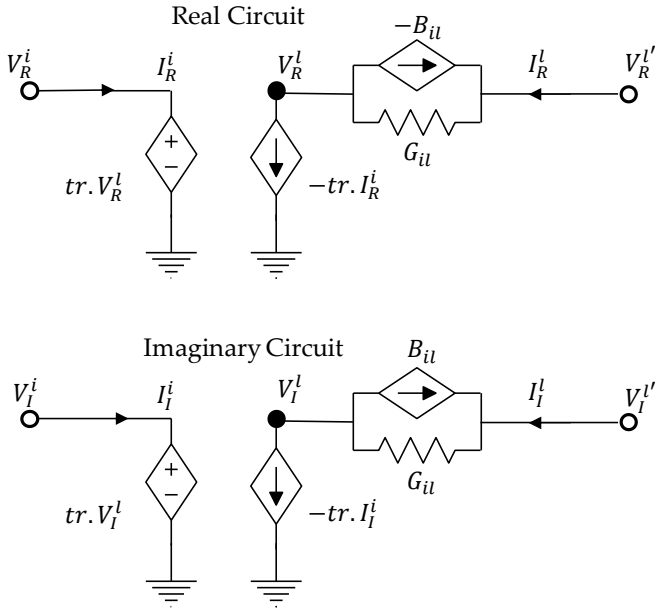

Figure 5-13: Real and Imaginary Circuit for a Transformer Model.

5.2.8.1 Control of transformer taps

Transformers with controllable taps can control the voltage at either its own node or another node in the system given by $\mathcal{W}$. In the existing methodology, transformers taps are generally adjusted in the outer loop of the solver based on the system voltages obtained in the inner loop NR solution. However, this technique suffers from oscillations and convergence to non-physical solutions as described in the case of generators in Section 5.2.2.1. Therefore, to overcome these challenges, we propose the use of a continuous transformer model for the control of transformer taps in the system.

In this continuous twice differential transformer model, a sigmoid curve is used to describe the relationship between the transformer turns ratio and the voltage at the controlled node. Within its limits, the transformer taps adjust its value to control the controlled node's voltage. However, if the transformer taps hit its limit, the turns ratio value saturates and no longer controls the controlled node voltage.

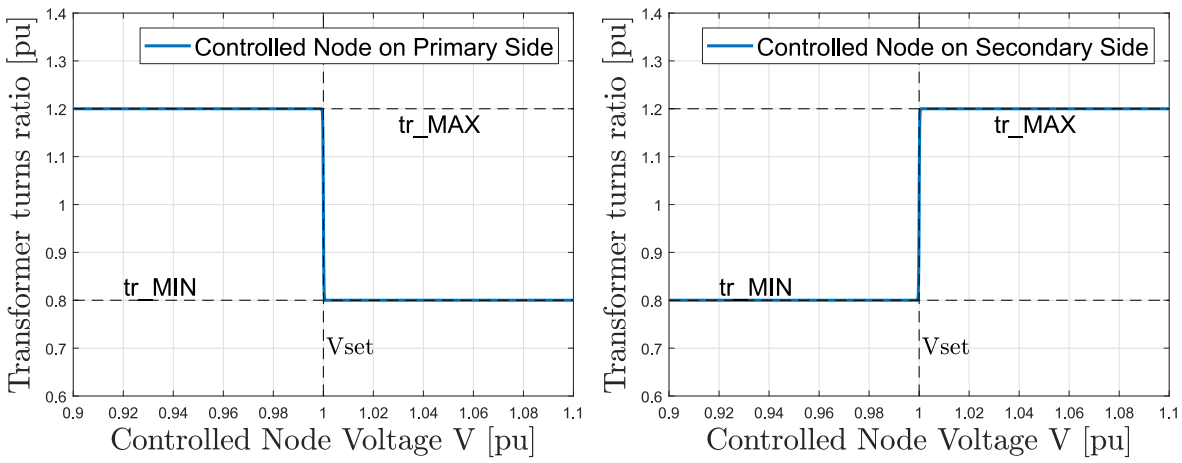

Figure 5-14: Continuous transformer tap control schematic.

Unlike the generator continuous model in Section 5.2.3, in the transformer continuous model a set of sigmoid curves are used to control the voltage of the controlled node $\mathcal{W}$ as a function of turns ratio depending on the relative location of the controlled bus as shown in Figure 5-14. For instance, consider a bus connected to the primary side of the transformer whose voltage is being controlled. If the observed voltages on the controlled bus are lower than the set voltage, then the primary taps are increased to adjust the voltage toward the set voltage whereas if the observed voltages are higher than the set value then the primary taps are reduced to adjust the voltage. On the other hand, if the controlled bus $\mathcal{W}$ is on the secondary side of the transformer, then the primary taps are reduced to increase the voltage of the controlled bus $\mathcal{W}$ and increased to the reduce the voltage of the controlled bus on the secondary side. The voltage constraint characteristics for the controlled node $\mathcal{W}$ whose relative location is on the primary side of the transformer is:

$$tr = \frac{tr_{MAX} - tr_{MIN}}{1 + \exp(\lambda_S * \left[\sqrt{V_{R\mathcal{W}}^2 + V_{I\mathcal{W}}^2} - V_{set}\right]} + tr_{MIN} \tag{46}$$

In case the controlled node $\mathcal{W}$'s relative location is on the secondary side of the transformer, then the voltage constraint characteristics are given by:

$$tr = \frac{tr_{MIN} - tr_{MAX}}{1 + \exp(\lambda_S * \left[\sqrt{V_{RW}^2 + V_{IW}^2} - V_{set}\right]} + tr_{MAX} \quad (47)$$

In the continuous model for the transformer voltage control, the turns ratio parameter (tr) is an unknown variable (with continuous range) and requires additional stamps in the system Jacobian for incorporating the sensitivities of transformer currents to transformer turns ratio. Importantly, the voltage and current equations are no longer linear functions of unknown variables, and therefore, are linearized prior to being stamped in the Jacobian matrix.

Importantly, the actual tap adjustment in the transformer is discrete, therefore, once the inner loop of NR is completed with the continuous model, the taps are snapped to their closest discrete value to obtain the final solution. In practice, it is rare that the snapping back action could result in system to diverge. However, theoretically it is possible due to two reasons:

i. The modified system state due to the change in transformer tap magnitude from its continuous to discrete value could result in an infeasible network.
ii. The set of non-linear equations representing the modified system state may diverge with prior solution as the initial condition.

In our solver, we make use of continuation (like methodology in Section 5.2.3.3.1) and optimization-based methods [63] to address this rare occurring concern. In case the system is infeasible due to the change in transformer tap magnitude from its continuous to discrete value, the optimization-based methods can identify the system infeasibility and accordingly adjust the discrete elements values such that the system is feasible. In case, the divergence is due to the lack of good initial conditions for the snapped system state, continuation methods can be used to gradually modify the discrete elements parameters from their continuous value to discrete value until convergence is achieved.

5.2.9 Transmission Line

Positive-sequence power flow tends to use a simplified pi-model for the transmission line. The model is shown in Figure 5-15. In this model, both the series and the shunt impedances are approximated by a simplified lumped pi-model, which further is a linear model with branch

currents as linear functions of from and to node voltages. We derive the split circuits for this model trivially using Kirchhoff's current law. In this derivation, for the sake of simplicity, the real and imaginary series and the shunt current terms for the transmission line are derived separately and then later combined to represent the whole model.

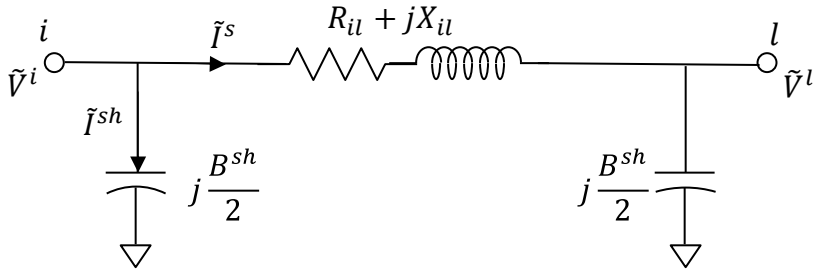

Figure 5-15: Equivalent circuit of a pi-model of the transmission line.

The series complex current for the transmission line between nodes i and l can be calculated from Ohm's law:

$$I_R^s + jI_I^s = \frac{V_R^{il} + jV_I^{il}}{R_{il} + jX_{il}} \tag{48}$$

The real and imaginary terms of (48) can be split into their respective equations:

$$I_R^s = V_R^{il}\frac{R_{il}}{R_{il}^2 + jX_{il}^2} + V_I^{il}\frac{X_{il}}{R_{il}^2 + jX_{il}^2} \tag{49}$$

$$I_I^s = V_I^{il}\frac{R_{il}}{R_{il}^2 + jX_{il}^2} - V_R^{il}\frac{X_{il}}{R_{il}^2 + jX_{il}^2} \tag{50}$$

Finally, the conductance (G_{il}) and susceptance (B_{il}) values can be used to simplify the derived terms, which can then be mapped into the equivalent circuit.

$$I_R^s = V_R^{il}G_{il} - V_I^{il}B_{il} \tag{51}$$

$$I_I^s = V_I^{il}G_{il} + V_R^{il}B_{il} \tag{52}$$

Like series terms, the shunt terms for the line model can be calculated via Ohm's law, that can then be split into their real and imaginary terms as given in (54)-(55). The series and shunt terms can then be combined and mapped into their equivalent circuits as shown in Figure 5-16.

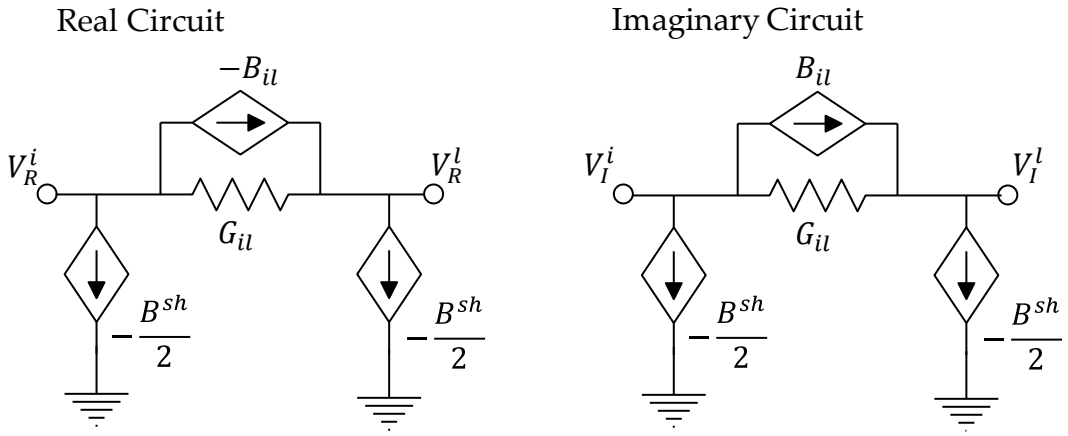

Figure 5-16: Real and Imaginary Circuit for the pi-model of Transmission Line.

$$I_R^{sh} + jI_I^{sh} = (V_R^i + jV_I^i)j\frac{B^{sh}}{2} \tag{53}$$

$$I_R^{sh} = -V_I^i\frac{B^{sh}}{2} \tag{54}$$

$$I_I^{sh} = V_R^i\frac{B^{sh}}{2} \tag{55}$$

5.2.10 Preliminary Result for Positive Sequence Power Flow

The purpose of this experiment is to validate the equivalent circuit approach for positive sequence power flow. To do so we simulate multiple cases from the flat start and document the results in Table 5-2. We report the case as converged if the solution obtained from our framework can be plugged into a commercial solver to result in the same solution. Additionally, we also document the number of iterations it took for the case to converge.

TABLE 5-2: PRELIMINARY RESULTS FOR POSITIVE SEQUENCE POWER FLOW WITH EQUIVALENT CIRCUIT APPROACH

Case Name	Number of Nodes	Reference	Iteration Count	Solution
case14	14	IEEE	4	Converged
case118	118	IEEE	5	Converged

case145	145	IEEE	14	Converged
SouthCarolina500	500	ACTIVSg500	4	Converged
Texas2000_June2016	2000	ICSEG	5	Converged
case1354pegase	1354	PEGASE	5	Converged
Case13659pegase	13659	PEGASE	xx	Diverged
bench	1648	PSSE benchmark	7	Converged
bench2	7917	PSSE benchmark	xx	Diverged

Results in Table 5-2 demonstrate that the equivalent circuit approach can solve the positive sequence power problem for most of the test cases from flat start. However, as expected some of the cases diverge when simulated from the flat start. Therefore, in the rest of this thesis, we will develop methods that can ensure convergence for hard-to-solve ill conditioned and large test cases from arbitrary initial conditions. First, however, we extend the equivalent circuit formulation framework used here for positive-sequence power grid models to three-phase power grid models.

5.3 Equivalent Circuit Models for Three-Phase Power Flow Problem

Now we develop equivalent circuit models for some of the most commonly used elements in the distribution grid for three-phase power flow analysis.

5.3.1 Slack Bus

In the distribution system analysis, the transmission edge of the grid is usually modeled as an infinite bus, which is represented via a substation or infinite bus that generally feeds into but rarely absorbs power from the distribution system. Each phase of the infinite or the slack bus can be represented in the real circuit as an independent voltage source of value $|V_i^{\Omega}| cos(\theta_i^{\Omega})$, and in the imaginary circuit (imaginary portion of the split circuit) as an independent voltage source of value $|V_i^{\Omega}| sin(\theta_i^{\Omega})$. It should be noted that if the slack bus is connected in a wye configuration, its magnitude represents the line-to-neutral voltage, whereas if connected in delta configuration, it will represent the line-to-line voltage. The complete split circuit model for a 3-phase slack bus connected in grounded wye configuration is shown in Figure 5-17. Importantly, it should be noted that in future with presence of multiple large generation resources within the distributed grid, it is likely that the distribution grid will contribute toward slack power during primary and secondary control as in the case of transmission grid. This can be easily incorporated into our

framework using distributed slack framework following the methodology stipulated in Section 5.2.4.

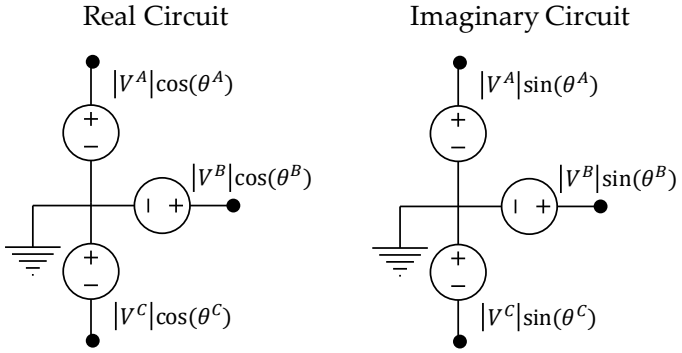

Figure 5-17: Real and Imaginary circuits for Slack bus in three-phase power flow problem.

5.3.2 ZIP Load Model

Amongst all of the existing aggregated load models in distribution system analysis, the ZIP load model is the most comprehensive. It models the aggregated load in the system as a mix of constant impedance, constant current, and constant power load models, which can be mathematically represented for each phase as follows:

$$\left(P_i^{ZIP}\right)^{\Omega} = Z_P{}^{\Omega}\left(\left|V_i{}^{\Omega}\right|\right)^2 + I_P{}^{\Omega}\left(\left|V_i{}^{\Omega}\right|\right) + S_P{}^{\Omega} \tag{56}$$

$$\left(Q_i^{ZIP}\right)^{\Omega} = Z_Q{}^{\Omega}\left(\left|V_i{}^{\Omega}\right|\right)^2 + I_Q{}^{\Omega}\left(\left|V_i{}^{\Omega}\right|\right) + S_Q{}^{\Omega} \tag{57}$$

In the equivalent circuit approach, the equations for the ZIP load model can be re-written as:

$$\left(I_{Ri}^{ZIP}\right)^{\Omega} = Z_P{}^{\Omega}V_{Ri}{}^{\Omega} - Z_Q{}^{\Omega}V_{Ii}{}^{\Omega} + \frac{S_P{}^{\Omega}V_{Ri}{}^{\Omega} + S_Q{}^{\Omega}V_{Ii}{}^{\Omega}}{\left(V_{Ri}^{\Omega}\right)^2 + \left(V_{Ii}^{\Omega}\right)^2} + \left(\sqrt{I_P^{\Omega 2} + I_Q^{\Omega 2}}\right).cos\left(I_{pf}^{\Omega} + \delta_i{}^{\Omega}\right) \tag{58}$$

$$\left(I_{Ii}^{ZIP}\right)^{\Omega} = Z_P{}^{\Omega}V_{Ii}{}^{\Omega} + Z_Q{}^{\Omega}V_{Ri}{}^{\Omega} + \frac{S_P{}^{\Omega}V_{Ii}{}^{\Omega} - S_Q{}^{\Omega}V_{Ri}{}^{\Omega}}{\left(V_{Ri}^{\Omega}\right)^2 + \left(V_{Ii}^{\Omega}\right)^2} + \left(\sqrt{I_P^{\Omega 2} + I_Q^{\Omega 2}}\right).sin\left(I_{pf}^{\Omega} + \delta_i{}^{\Omega}\right) \tag{59}$$

where:

$$I_{pf}^{\Omega} = \tan^{-1}\left(\frac{{I_Q}^{\Omega}}{{I_P}^{\Omega}}\right) \tag{60}$$

$$\delta_i{}^{\Omega} = \tan^{-1}\left(\frac{{V_{Ii}}^{\Omega}}{{V_{Ri}}^{\Omega}}\right) \tag{61}$$

For the load model given in (58) through (61), the constant impedance part of the load is linear, whereas the constant current and constant power part of the aggregated load is nonlinear. Linearizing the set of equations using Taylor expansion results in the following expression for each phase Ω in Ω_{set}:

$$\begin{aligned}\left(I_{Ri}^{ZIP}\right)^{\Omega k+1} = \left(I_{Ri}^{ZIP}\right)^{\Omega k} &+ \left(\left.\frac{\partial I_{Ri}^{ZIP}}{\partial V_{Ri}}\right|_{V_{Ri}^k, V_{Ii}^k}\right)^{\Omega}\left({V_{Ri}}^{\Omega k+1} - {V_{Ri}}^{\Omega k}\right) \\ &+ \left(\left.\frac{\partial I_{Ri}^{ZIP}}{\partial V_{Ii}}\right|_{V_{Ri}^k, V_{Ii}^k}\right)^{\Omega}\left({V_{Ii}}^{\Omega k+1} - {V_{Ii}}^{\Omega k}\right)\end{aligned} \tag{62}$$

$$\begin{aligned}\left(I_{Ii}^{ZIP}\right)^{\Omega k+1} = \left(I_{Ii}^{ZIP}\right)^{\Omega k} &+ \left(\left.\frac{\partial I_{Ri}^{ZIP}}{\partial V_{Ri}}\right|_{V_{Ri}^k, V_{Ii}^k}\right)^{\Omega}\left({V_{Ri}}^{\Omega k+1} - {V_{Ri}}^{\Omega k}\right) \\ &+ \left(\left.\frac{\partial I_{Ii}^{ZIP}}{\partial V_{Ii}}\right|_{V_{Ri}^k, V_{Ii}^k}\right)^{\Omega}\left({V_{Ii}}^{\Omega k+1} - {V_{Ii}}^{\Omega k}\right)\end{aligned} \tag{63}$$

The linearized set of equations can then be mapped into the equivalent three-phase model of the ZIP load either in wye (Y) or delta (D) formation, as shown in Figure 5-18.

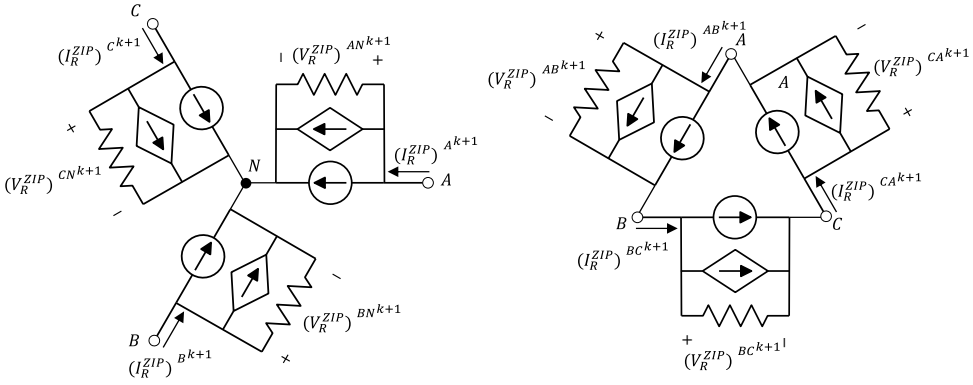

Figure 5-18: Real circuit for a) wye connected ZIP Load Model (on left) b) delta (D) connected ZIP load model (on right).

It is important to note that the ZIP model results in non-linear network constraints for both the 'PQV' and CIM formulations, which further adds to already existing non-linearities in the formulation. We propose to replace the non-linear ZIP model with a linear three-phase BIG model that provides comparable accuracy.

5.3.3 Three-phase BIG load model

The proposed linear positive sequence BIG load model in Section 5.2.7 is further extended to a linear three-phase aggregated load model that can be connected in either wye or delta connection as in the case of the ZIP load model. Refer to Appendix A for more detailed explanation of the BIG load model.

5.3.4 Transmission Line

The three main types of transmission lines in the distribution grid are the overhead line, underground cable, and the triplex cable. The overhead line generally consists of a 4-wire configuration with three phase conductors and one neutral conductor. The concentric underground cable, on the other hand, consists of a 7-wire configuration with three phase conductors, along with corresponding neutral conductors and an additional neutral conductor. The triplex cable consists of three wires with two hot conductors and one neutral conductor.

The impedance matrix for the overhead, underground and triplex lines are of the order 4x4, 7x7, and 3x3, respectively. However, with the use of Kron's reduction [32], we can eliminate neutral wires from the models resulting in 3x3, 3x3 and 2x2 impedance matrices for overhead lines, underground cables and triplex cables, respectively. Finally, admittance matrix ($\tilde{Y}_{line}$) for the line model can then be calculated by finding the inverse of the impedance matrix (Z_{line}):

$$\tilde{Y}_{line} = Z_{line}^{-1} \tag{64}$$

With the calculated admittance matrix, the transmission line branch currents can be represented by Ohm's Law, where $\tilde{V}_{Aa}$, $\tilde{V}_{Bb}$ and $\tilde{V}_{Cc}$ are the voltage drops across the lines:

$$\begin{bmatrix} \tilde{I}_A \\ \tilde{I}_B \\ \tilde{I}_C \end{bmatrix} = \begin{bmatrix} \tilde{Y}_{aa} & \tilde{Y}_{ab} & \tilde{Y}_{ac} \\ \tilde{Y}_{ba} & \tilde{Y}_{bb} & \tilde{Y}_{bc} \\ \tilde{Y}_{ca} & \tilde{Y}_{cb} & \tilde{Y}_{cc} \end{bmatrix} \begin{bmatrix} \tilde{V}_{Aa} \\ \tilde{V}_{Bb} \\ \tilde{V}_{Cc} \end{bmatrix} \tag{65}$$

Since the series admittances $G_{il}^{\aleph} + jB_{il}^{\aleph}$ of the branches have both real and imaginary components, the system from (65) can be split as:

$$\begin{bmatrix} I_R^A \\ I_I^A \\ I_R^B \\ I_I^B \\ I_R^C \\ I_I^C \end{bmatrix} = \begin{bmatrix} G_{aa}^{\aleph} & -B_{aa}^{\aleph} & G_{ab}^{\aleph} & -B_{ab}^{\aleph} & G_{ac}^{\aleph} & -B_{ac}^{\aleph} \\ B_{aa}^{\aleph} & G_{aa}^{\aleph} & B_{ab}^{\aleph} & G_{ab}^{\aleph} & B_{ac}^{\aleph} & G_{ac}^{\aleph} \\ G_{ba}^{\aleph} & -B_{ba}^{\aleph} & G_{bb}^{\aleph} & -B_{bb}^{\aleph} & G_{bc}^{\aleph} & -B_{bc}^{\aleph} \\ B_{ba}^{\aleph} & G_{ba}^{\aleph} & B_{bb}^{\aleph} & G_{bb}^{\aleph} & B_{bc}^{\aleph} & G_{bc}^{\aleph} \\ G_{ca}^{\aleph} & -B_{ca}^{\aleph} & G_{cb}^{\aleph} & -B_{cb}^{\aleph} & G_{cc}^{\aleph} & -B_{cc}^{\aleph} \\ B_{ca}^{\aleph} & G_{ca}^{\aleph} & B_{cb}^{\aleph} & G_{cb}^{\aleph} & B_{cc}^{\aleph} & G_{cc}^{\aleph} \end{bmatrix} \begin{bmatrix} V_R^{Aa} \\ V_I^{Aa} \\ V_R^{Bb} \\ V_I^{Bb} \\ V_R^{Cc} \\ V_I^{Cc} \end{bmatrix} \tag{66}$$

Using the same approach, the transmission line shunt currents can be derived, where $\tilde{V}_A$, $\tilde{V}_B$ and $\tilde{V}_C$ are the line-to-ground nodal voltages. Since the admittance of the shunt elements in the pi-model is purely imaginary ($\tilde{Y}_i^{sh} = jB_i^{sh}$), we derive the following set of equations from Ohm's law:

$$\begin{bmatrix} {I_R^A}^{sh} \\ {I_I^A}^{sh} \\ {I_R^B}^{sh} \\ {I_I^B}^{sh} \\ {I_R^C}^{sh} \\ {I_I^C}^{sh} \end{bmatrix} = \begin{bmatrix} 0 & -B_{aa}^{sh} & 0 & -B_{ab}^{sh} & 0 & -B_{ac}^{sh} \\ B_{aa}^{sh} & 0 & B_{ab}^{sh} & 0 & B_{ac}^{sh} & 0 \\ 0 & -B_{ba}^{sh} & 0 & -B_{bb}^{sh} & 0 & -B_{bc}^{sh} \\ B_{ba}^{sh} & 0 & B_{bb}^{sh} & 0 & B_{bc}^{sh} & 0 \\ 0 & -B_{ca}^{sh} & 0 & -B_{cb}^{sh} & 0 & -B_{cc}^{sh} \\ B_{ca}^{sh} & 0 & B_{cb}^{sh} & 0 & B_{cc}^{sh} & 0 \end{bmatrix} \begin{bmatrix} V_R^A \\ V_I^A \\ V_R^B \\ V_I^B \\ V_R^C \\ V_I^C \end{bmatrix} \tag{67}$$

Equations (66) and (67) for the transmission line are then mapped into an equivalent circuit given by linear resistors and voltage-controlled current sources. Figure 5-19 shows the real sub-circuit for one of the phases of a transmission line.

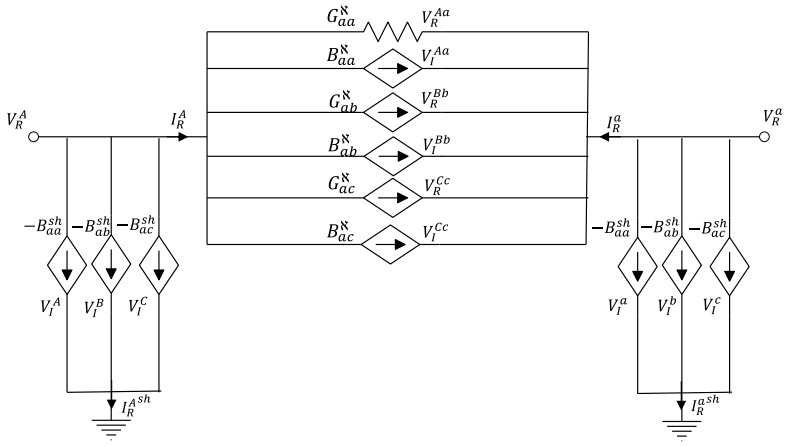

Figure 5-19: Real circuit of a transmission line (Phase A).

5.3.5 Three-Phase Transformers

Three-phase transformers are used in the distribution grid to transform the voltages from transmission level to sub-transmission level and to divide three-phase circuits into single-phase circuits. Different configurations for the three-phase transformers are possible in the distribution system, some of which include:

i. Grounded wye – grounded wye (grY – grY)
ii. Delta – delta (D – D)
iii. Wye – delta (wye – D)
iv. Grounded wye – delta (grY – D)
v. Delta – wye (D – wye)
vi. Open wye – open delta

In the next subsection we will derive the model for the grounded wye – grounded wye three-phase transformer configuration. Following the same methodology, equivalent circuits for the other transformer configurations can also be derived.

Grounded wye – grounded wye (grY – grY) Configuration

In the grounded wye – grounded wye configuration of the three-phase transformer, the relationship between the primary and secondary currents ($\tilde{I}_{pri}^{\Omega}$, $\tilde{I}_{sec}^{\Omega}$) and voltages ($\tilde{V}_{pri}^{\Omega}$, $\tilde{V}_{sec}^{\Omega}$) for each individual phase is as follows:

$$\tilde{V}_{pri}^{\Omega} = tr\tilde{V}_{sec}^{\Omega} e^{j\Theta^{\Omega}} \tag{68}$$

$$\tilde{I}_{sec}^{\Omega} = -tr\tilde{I}_{pri}^{\Omega} e^{-j\Theta^{\Omega}} \tag{69}$$

Splitting of these current and voltage equations into real and imaginary terms results in the following equations:

$$V_{R\,pri}^{\Omega} = tr\left(V_{R\,sec}^{\Omega} cos\Theta^{\Omega} - V_{I\,sec}^{\Omega} sin\Theta^{\Omega}\right) \tag{70}$$

$$V_{I\,pri}^{\Omega} = tr\left(V_{R\,sec}^{\Omega} sin\Theta^{\Omega} + V_{I\,sec}^{\Omega} cos\Theta^{\Omega}\right) \tag{71}$$

$$I_{R\,sec}^{\Omega} = -tr\left(I_{R\,pri}^{\Omega} cos\Theta^{\Omega} + I_{I\,sec}^{\Omega} sin\Theta^{\Omega}\right) \tag{72}$$

$$I_{I\,sec}^{\Omega} = -tr\left(-I_{R\,pri}^{\Omega} sin\Theta^{\Omega} + I_{I\,sec}^{\Omega} cos\Theta^{\Omega}\right) \tag{73}$$

The equations (70) through (73) can be further mapped into the equivalent circuit model of the transformer by using controlled voltage and current sources. Furthermore, the transformer losses for each phase are modeled on the secondary of the transformer. The split equations for the transformer loss terms for each phase are given by the following set of equations:

$$\tilde{I}_{R}^{\Omega} = G_{loss}\tilde{V}_{R}^{\Omega\Omega'} - B_{loss}\tilde{V}_{I}^{\Omega\Omega'} \tag{74}$$

$$\tilde{I}_{I}^{\Omega} = G_{loss}\tilde{V}_{I}^{\Omega\Omega'} + B_{loss}\tilde{V}_{R}^{\Omega\Omega'} \tag{75}$$

Figure 5-20 shows the real circuit for the grounded wye – grounded wye transformer with zero phase shift.

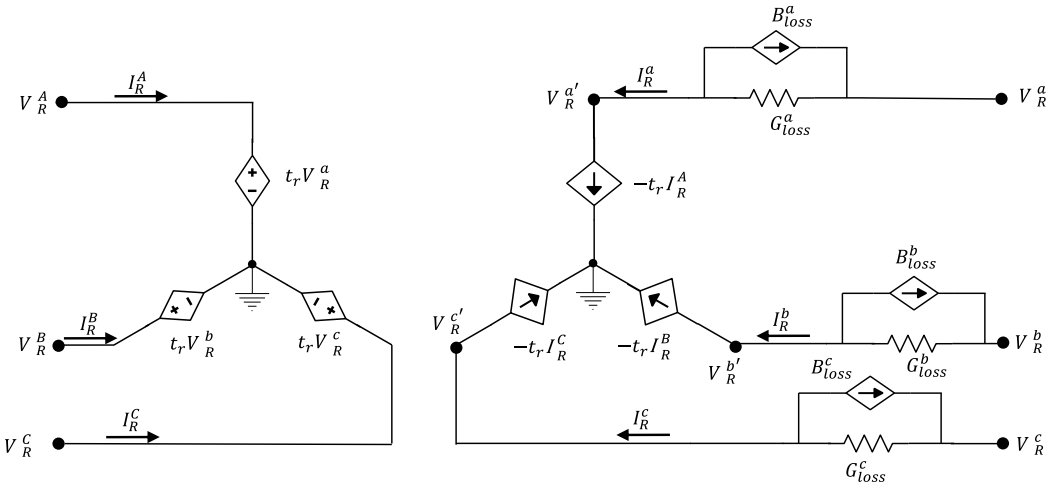

Figure 5-20: Real circuit for the grounded wye – grounded wye transformer with no phase shift.

Importantly, the three-phase transformer model has the ability to control the voltage either at the primary or secondary side for individual phases via the control of its turns ratio. The model of three-phase transformer can do so via a discontinuous piecewise model in the outer loop or via a continuous transformer tap model extended from one shown in Section 5.2.8.1 for a positive-sequence model of the transformer.

5.4 Preliminary results for Three-phase power flow

In this section, we will demonstrate preliminary results for the three-phase power flow solver using the equivalent circuit approach. For the purposes of this experiment we choose a standard 4-bus test case [29].

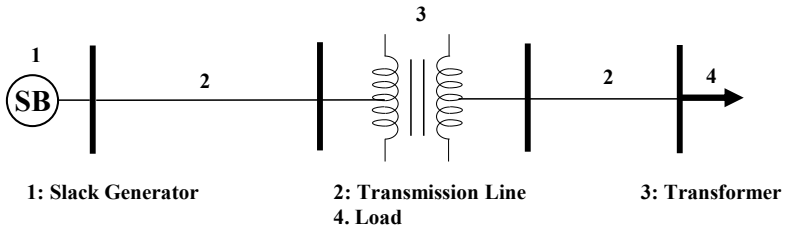

Figure 5-21: Standard 4-Bus Test Case System.

The schematic of the standard 4-bus test case is shown in Figure 5-21. The preliminary results for this test case are shown for different transformer configurations in Table 5-3. The tabulated

results represent the phase voltages for the load bus in Figure 5-21, which compare well against the results obtained from the standard reference [29].

TABLE 5-3: SUGAR THREE-PHASE RESULTS FOR 4-BUS TEST CASE

Configuration	Balanced				Unbalanced			
	SUGAR 3-Phase [V∠°]		Results in [29] [V∠°]		SUGAR 3-Phase [V∠°]		Results in [29] [V∠°]	
Step-down grY-grY	V_A:	1918∠-9.1	V_A:	1918∠-9.1	V_A:	2175∠-4.1	V_A:	2175∠-4.1
	V_B:	2061∠-128.3	V_B:	2061∠-128.3	V_B:	1930∠-126.8	V_B:	1930∠-126.8
	V_C:	1981∠110.9	V_C:	1981∠110.9	V_C:	1833∠102.8	V_C:	1833∠102.8
Step-down D-D	V_{AB}:	3442∠22.3	V_{AB}:	3442∠22.3	V_{AB}:	3431∠24.3	V_{AB}:	3431∠24.3
	V_{BC}:	3497∠-99.4	V_{BC}:	3497∠-99.4	V_{BC}:	3647∠-100.4	V_{BC}:	3647∠-100.4
	V_{CA}:	3384∠140.7	V_{CA}:	3384∠140.7	V_{CA}:	3294∠138.6	V_{CA}:	3294∠138.6
Step-down Y-D	V_{AB}:	3437∠-7.8	V_A:	3437∠-7.8	V_{AB}:	3425∠-5.8	V_A:	3425∠-5.8
	V_{BC}:	3497∠-129.3	V_B:	3497∠-129.3	V_{BC}:	3646∠-130.3	V_B:	3646∠-130.3
	V_{CA}:	3388∠110.6	V_C:	3388∠110.6	V_{CA}:	3298∠108.6	V_C:	3298∠108.6
Step-up grY-grY	V_A:	13630∠-3.5	V_{AB}:	13631∠-3.5	V_A:	13814∠-2.2	V_{AB}:	13815∠-2.2
	V_B:	13681∠-123.5	V_{BC}:	13682∠-123.5	V_B:	13613∠-123.4	V_{BC}:	13614∠-123.4
	V_C:	13665∠116.5	V_{CA}:	13661∠116.5	V_C:	13618∠114.9	V_{CA}:	13615∠114.9
Step-up D-D	V_{AB}:	23658∠26.6	V_{AB}:	23657∠26.6	V_{AB}:	23611∠27.2	V_{AB}:	23610∠27.2
	V_{BC}:	23688∠-93.5	V_{BC}:	23688∠-93.5	V_{BC}:	24015∠-93.7	V_{BC}:	24015∠-93.7
	V_{CA}:	23625∠146.5	V_{CA}:	23625∠146.5	V_{CA}:	23492∠145.9	V_{CA}:	23492∠145.9
Step-up Y-D	V_{AB}:	23682∠56.6	V_{AB}:	23681∠56.6	V_{AB}:	23638∠57.1	V_{AB}:	23637∠57.1
	V_{BC}:	23664∠-63.6	V_{BC}:	23664∠-63.6	V_{BC}:	23995∠-63.8	V_{BC}:	23995∠-63.8
	V_{CA}:	23626∠176.5	V_{CA}:	23625∠176.5	V_{CA}:	23496∠175.9	V_{CA}:	23495∠175.9

Similar to the case of the preliminary results for the positive-sequence power flow in Section 5.2.10, we validate the equivalent circuit models for three-phase power flow elements. We compare the results obtained for the 4-bus test case with our tool against those reported in the literature. The results obtained from our tool match well with those reported in the literature thereby validating the models.

However, in general, representing of the grid elements as equivalent circuit models by itself cannot ensure convergence for three-phase power flow test cases from arbitrary initial conditions. Therefore, the following chapters in the thesis will develop models and techniques that can ensure convergence to the correct physical solution for any three-phase test case from arbitrary initial conditions.

5.5 Physics Based Models

We have previously shown in [42] that any physics-based device model can be directly mapped into an equivalent circuit to be used in both the steady-state analysis (discussed here) as well as the transient analysis (see Appendix B). In general, physics-based models developed from fundamental principles are used for time-domain transient analysis [50]. However, in both the power flow and the three-phase power flow analyses, simplified, aggregated models are used often, resulting in less accurate and inconsistent results. Understandably, it is often necessary to use simplified aggregated models due to the lack of data pertaining to individual grid elements. However, this is not always the case, and more accurate estimation of the grid operating state with true voltage sensitivities can be obtained by using physics-based models in the power flow and three-phase power flow analyses.

Existing frameworks often cannot directly incorporate physics-based models based on the current and voltage state variables into the problem formulation. In contrast, our equivalent circuit formulation can directly incorporate any physics-based model based on the current and voltage variables into the problem statement without loss of generality. To demonstrate this further, using an example of an induction motor, we derive an equivalent circuit model of the same from fundamental principles that is further used in power flow analysis. In Appendix B, we show that the same model can be used for time-domain transient analysis to result in consistent solution with the ones obtained in power flow and three-phase power flow analyses.

5.5.1 Physics based model for Induction Motor (IM)

Electric motors comprise roughly 45% of the total global electricity consumption [51], the majority of which can be attributed to IMs. Importantly, modeling these IMs in detail based on the true physics of the device can significantly improve the characterization of aggregated load in the grid. Often IMs are represented in the network model via PQ load or ZIP load models or are aggregated with other loads in the system that are further represented by the same. More advanced models for IMs that are based on the true physics of the device have been known to be used in three-phase power flow analysis [52]. However, these in-depth models tend to assume fixed speed operation (hence ignoring speed-flux non-linearities) thereby not capturing the true

characteristics of the IM. In this section we develop a physics-based model for IM that can be used in both the power flow and three-phase power flow analyses. Prior to deriving the model of IM, we briefly discuss DQ transformation required for further derivations.

5.5.1.1 Direct-Quadrature (DQ) Transformation

The flux generated by the three-phase IM in ABC frame has time varying coefficients in its voltage terms due to the sinusoidal nature of the mutual inductance. This makes the analysis of three phase IM cumbersome in the ABC reference frame. However, this undesirable feature can be eliminated by use of the DQ transformation. DQ transformation can be performed in one of the three reference frames: i) synchronous reference frame; ii) stationary reference frame; and iii) rotating reference frame.

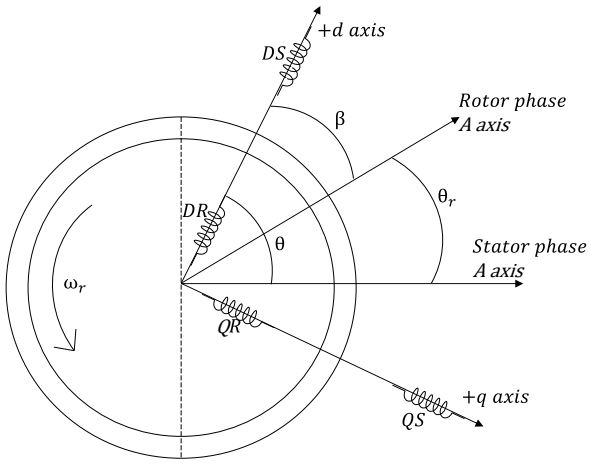

Figure 5-22: Superimposition of DQ-axis on 3-phase induction motor.

The final response of the IM is independent of the chosen reference frame. However, each of the reference frames has its own advantages and disadvantages depending on the problem that is being investigated [53]. For the purposes of this derivation, we make use of the synchronously rotating reference frame where DQ transformation matrix P_θ for the stator variables is as follows:

$$[P_\theta] = \frac{2}{3}\begin{bmatrix} 0.5 & 0.5 & 0.5 \\ cos(\theta) & cos(\theta-\lambda) & cos(\theta+\lambda) \\ sin(\theta) & sin(\theta-\lambda) & sin(\theta+\lambda) \end{bmatrix} \quad (76)$$

and,

$$[F_{0dq}] = [P_\theta].[F_{abc}] \tag{77}$$

where function F can represent either currents or voltages.

For rotor variable transformation, θ is replaced with β in the equations above. For synchronous reference frame, the machine angle and speed variables are defined as follows:

$$\omega = p\theta = \omega_s \tag{78}$$

$$\beta = \theta - \theta_r = \theta_s - \theta_r \tag{79}$$

where p is the differential operator. ω_s and ω_r are the synchronous and rotor speed of the motor, respectively, and θ_s and θ_r are the stator and rotor position, respectively.

5.5.1.2 Motor Equations in Transient Domain

As we have transformed the three-phase parameters of IM into the DQ-frame, we can further derive the model of an IM. The set of electrical equations that define the true behavior of the IM in time-domain are as follows [50]:

$$v_{ds} = R_s I_{ds} + p\psi_{ds} - \psi_{qs} p\theta \tag{80}$$

$$v_{qs} = R_s I_{qs} + p\psi_{qs} + \psi_{ds} p\theta \tag{81}$$

$$v_{dr} = R_r I_{dr} + p\psi_{dr} - \psi_{qr} p\beta \tag{82}$$

$$v_{qr} = R_r I_{qr} + p\psi_{qr} + \psi_{dr} p\beta \tag{83}$$

The flux linkages of the IM are represented by the symbol ψ and are calculated using the following formulas:

$$\psi_{ds} = (L_{ls} + L_m) I_{ds} + L_m I_{dr} \tag{84}$$

$$\psi_{dr} = (L_{ls} + L_m) I_{dr} + L_m I_{ds} \tag{85}$$

$$\psi_{qs} = (L_{ls} + L_m) I_{qs} + L_m I_{qr} \tag{86}$$

$$\psi_{qr} = (L_{ls} + L_m)I_{qr} + L_m I_{qs} \tag{87}$$

where L_{ls} and L_{lr} represent the leakage-inductance of stator circuit and rotor circuit, respectively. L_m is the mutual inductance between the rotor and stator circuits. R_s and R_r are the stator and rotor resistance, respectively. The non-linearity in the electrical part of the IM is due to the speed voltage terms.

In addition to the equations above, the mechanical part of the IM is defined by a single differential equation [50]:

$$p\omega_r = \frac{(T_e - T_L - D\omega_r)}{J} \tag{88}$$

where

$$T_e = \frac{3}{4} L_m poles\left(I_{dr}I_{qs} - I_{qr}I_{ds}\right) \tag{89}$$

and T_e is the electrical torque of the IM in N.m and J is the motor net inertia in kg.m^2. $poles$ represents the number of poles in the induction motor. The load torque (T_L) is generally described with a polynomial function of rotor speed.

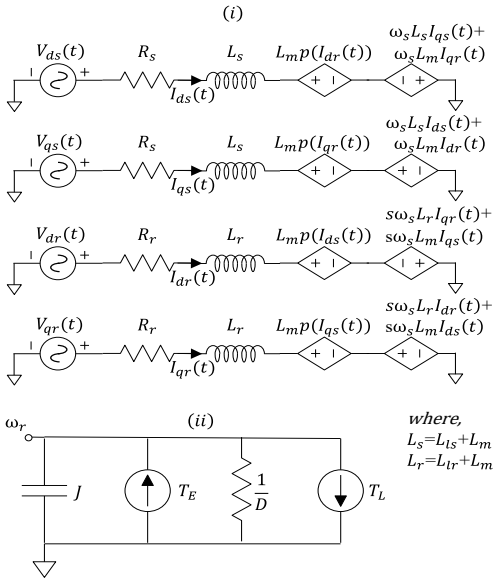

Figure 5-23: Equivalent circuit for 3-phase induction motor: (i) Electrical circuit; and (ii) Mechanical Circuit.

The equations derived above map the time-domain behavior of a balanced three-phase squirrel cage IM into the mathematical form. This mathematical set of equations can be directly mapped into an equivalent circuit following the methods in [43], and is shown in Figure 5-23.

5.5.2 Steady-State Fundamental Frequency Model

To further use this model for positive sequence and three-phase power flow analysis, we zero out the time-derivative terms. Due to the use of the DQ-transformation, once the time-domain terms are nulled, we obtain a steady-state model in source frequency. Furthermore, an additional equation can be incorporated for three-phase power flow analysis to consider zero sequence terms in the case of unbalance voltages at the motor terminals. If the motor were to have negative torque it would have to be separately calculated and added to (89).

To validate the IM model, we make use of a 20 hp, 460 volts three-phase single squirrel cage induction motor. The motor data is given in Table 5-4.

TABLE 5-4: THREE-PHASE SQUIRREL CAGE INDUCTION MOTOR PARAMETERS

V_{LL} (Volts)	f (Hz)	R_s (Ω)	R_r (Ω)	L_{ls} and L_{lr} (mH)
460	0.2761	0.2761	0.1645	2.191
L_m (mH)	poles	J (kg.m^2)	D (N.m.s)	T_L (N.m)
76.14	2	0.1	0.01771	10

For the validation, the IM model is connected to a slack bus via a transmission line. The IM is then simulated at mechanical load of 10 N.m at rated source voltage in pu. The results are documented in Table 5-5 and are converted to SI units from pu to compare with the steady-state results obtained from MATLAB SimscapePowerSystems for the same test case. The results are a exact match thereby validating the model.

TABLE 5-5: IM RESULTS IN EQUIVALENT CIRCUIT FRAMEWORK FOR STEADY-STATE (POWER FLOW) AND TIME-DOMAIN TRANSIENT ANALYSIS

Parameter	Unit	Equivalent Circuit Framework	SimScapePowerSystems
Rotor Speed	rad.s^{-1}	375.01	375.01
Electric Torque	N.m	16.64	16.64

Parameter	Unit	Equivalent Circuit Framework	SimScapePowerSystems
Stator direct-axis current	Amps	-11.36	-11.36
Stator quadrature-axis current	Amps	13.09	13.09
Rotor direct-axis current	Amps	11.56	11.56
Rotor quadrature-axis current	Amps	-0.49	-0.49

6. Circuit Simulation Methods for Power System Analyses

Decades of research in circuit simulation have demonstrated that circuit simulation methods can be applied for determining the DC state of highly non-linear circuits using NR. These techniques have been shown to make NR robust and practical for large-scale circuit problems [43], even those consisting of billions of nodes. Most notable is the ability to guarantee convergence to the correct physical solution (i.e. global convergence) and the capability of finding multiple operating points [48]. We propose analogous techniques for ensuring convergence to the correct physical solution for the power flow problem [34]-[35]. In this section, we provide a short overview of these techniques that can be applied to both positive sequence power flow and three-phase power flow problems without loss of generality. Note that throughout this section, the symbol superscript Ω in the mathematical expressions represents a phase from the set Ω_{set} of three *phases a, b* and *c* for the three-phase problem and represents the *positive sequence* (p) component for the power flow problem.

6.1 Limiting Methods

6.1.1 Variable Limiting

The solution space of the system node voltages in a power flow problem is well defined. While solving the power flow problem, a large NR step may step out of this solution space and result in either divergence or convergence to a non-physical solution. It is, therefore, important to limit the NR step before an invalid step out of the solution space is made. In [34] we proposed variable limiting to achieve the postulated goal. In this technique, the state variables that are most sensitive to initial guesses are damped when the NR algorithm takes a large step out of the pre-defined solution space. Note, however, that *not all* of the system variables are damped for the variable limiting technique, as is done for traditional damped NR. Circuit simulation research has shown that damping most sensitive variables provides superior convergence compared to damped NR in general [43].

In the power flow and three-phase problem, the voltages on the PV node are highly sensitive to the reactive power (Q_G) value at that node. In the equivalent circuit formulation of the power flow and three-phase power flow problem each PV node augments the solution space by additional unknown variable Q_G for which initial guess must be assigned. However, unlike the node voltages, it is very hard to choose the appropriate initial guess for these Q_G variables, as they exhibit a large solution space. Therefore, with an arbitrary choice of these initial values, the power flow or three-phase power flow problem may diverge or converge to the wrong solution.

To tackle this problem the voltages at the PV node are damped during the NR iterations whenever they make a large step out of the pre-defined solution space. Figure 6-1 can be used to demonstrate this graphically. The plot in Figure 6-1 shows results for a 2869 PEGASE bus test system that was represented in equivalent circuit formulation and simulations were run on it for six different initial guesses for unspecified Q_G. The maximum bus voltage from the solution of the power flow problem for each initial guess was then plotted for two scenarios: without and with variable limiting technique enabled. The plots in the figure show that when variable limiting is not enabled, the voltage solution diverges to very high magnitudes (up to 10^4) and may not converge even in 100 iterations. However, when the variable limiting option is enabled, divergence is not observed, and the bounded bus voltages result in fast convergence.

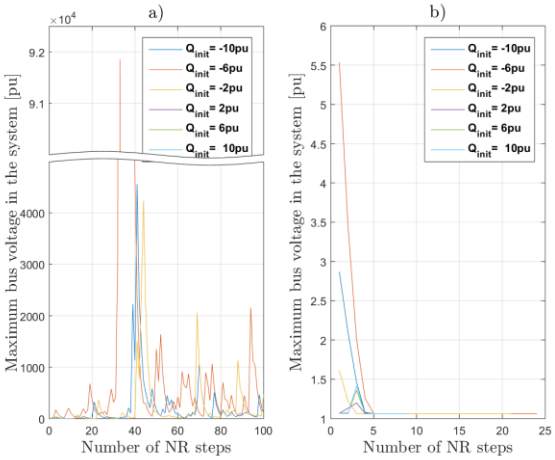

Figure 6-1: Voltage profile for maximum bus voltage in 2869 Bus System: a) w/o Variable Limiting b) with Variable Limiting.

To apply variable limiting in our prototype simulator, the mathematical expressions for the PV nodes in the system are modified as follows:

$$I_{CG}^{\Omega\ k+1} = \varsigma \frac{\partial I_{CG}^{\Omega}}{\partial V_{RG}^{\Omega}} \underbrace{\left(V_{RG}^{\Omega\ k+1} - V_{RG}^{\Omega\ k}\right)}_{\Delta V_{RG}^{\Omega}} + I_{CG}^{\Omega\ k} + + \varsigma \frac{\partial I_{CG}^{\Omega}}{\partial V_{IG}^{\Omega}} \underbrace{\left(V_{IG}^{\Omega\ k+1} - V_{IG}^{\Omega\ k}\right)}_{\Delta V_{IG}^{\Omega}} + \frac{\partial I_{CG}^{\Omega}}{\partial Q_{G}^{\Omega}} \left(Q_{G}^{\Omega\ k+1} - Q_{G}^{\Omega\ k}\right) \tag{90}$$

where, $0 \leq \varsigma \leq 1$. The magnitude of ς is dynamically varied through heuristics such that convergence to the correct physical solution is achieved in the most efficient manner. The heuristics depend on the largest delta voltage ($\Delta V_{RG}^{\Omega},\ \Delta V_{IG}^{\Omega}$) step during subsequent NR iterations. If during subsequent NR iterations, a large step ($\Delta V_{RG}^{\Omega},\ \Delta V_{IG}^{\Omega}$) is encountered, then the factor ς is decreased. The factor ς is scaled back up if consecutive NR steps result in monotonically decreasing absolute values for the largest error.

6.1.2 Voltage Limiting

An equally simple, yet effective, technique is to limit the absolute value of the delta step that the real and imaginary voltage vectors can make during each NR iteration. This is analogous to the voltage limiting technique used for diodes in circuit simulation, wherein the maximum allowable voltage step during NR is limited to twice the thermal voltage of the diode [43]. Similarly, for the power flow and three-phase power flow analyses, a hard limit is enforced on the normalized real and imaginary voltages in the system. The mathematical implementation of voltage limiting in our formulation is as follows:

$$\left(V_C^{\Omega}\right)^{k+1} = \min_{V_C^{min}} \max_{V_C^{max}} \left(\left(V_C^{\Omega}\right)^{k} + \delta_S \min\left(\left|\Delta\left(V_C^{\Omega}\right)^{k}\right|, \Delta V_C^{max}\right)\right)$$

$$\min_{V_C^{min}} \max_{V_C^{max}} = \begin{cases} V_c^{max}, & if\ x > V_c^{max} \\ V_c^{min}, & if\ x < V_c^{min} \\ x, & otherwise \end{cases} \tag{91}$$

and $\delta_S = sign\left(\Delta\left(V_C^{\Omega}\right)^{\mathrm{k}}\right)$ and $C \in \{R, I\}$ represents the placeholder for real and imaginary parts.

6.1.3 Limiting Methods for other System Variables

Similar to limiting of voltages during power flow and three-phase power flow problem, other system variables are also limited to constrain the behavior of the network components in their physical space. In general, a good limiting technique is one that can exploit knowledge of system physics to well-define a narrow normal operating range within which the variable can be constrained. However, this is not always possible. For instance, the generator reactive power variable Q_G can have a wide range for its operating setpoint depending on the size of the generator. In such scenarios, the variables are limited by first mapping them into another variable for which we can define a better operating range. In case of generators, reactive power Q_G variables are limited by first mapping the $Q_G{}'$s into calculated currents $I_C^{\Omega} + \Delta\left(I_C^{\Omega}\right)^{k+1}$ at $(k+1)^{th}$ NR step, and then finding the new $Q_G{}^{k+1}$ from the inverse function (f^{-1}) of limited currents $\left(I_C^{\Omega} + \overline{\Delta\left(I_C^{\Omega}\right)^{k+1}}\right)$. Similar approaches can also be used to limit other system variables in future.

6.2 Homotopy Methods

Limiting methods may fail to ensure convergence for certain ill-conditioned and large test systems when solved from an arbitrary set of initial guesses. To ensure convergence for these network models to the correct physical solutions independent of the choice of initial conditions, we propose the use of homotopy methods.

6.2.1 Background

Homotopy methods are not new to the field of power system simulation. Homotopy methods in the past have been used to study the voltage collapse of a given network or to determine the maximum available transfer capability [19]-[20]. They have also been researched for locating all solutions to a power flow problem [41], [55]. However, their use for enabling convergence for hard to solve positive sequence and three-phase power flow problems has been limited. Of the proposed methods for providing better convergence [9], [40] most have suffered from convergence to low voltage solutions or divergence. On the other hand, some of them have been developed for formulations that do not apply to both positive sequence as well as three-phase

power flow [56] problems. Furthermore, none of the previously proposed homotopy methods are known to scale up to test systems that are of the size of the European or the US grids, and in general they are not extendable to the three-phase power flow problem.

6.2.2 General Introduction

In the homotopy approach, the original problem is replaced with a set of sub-problems that are sequentially solved. The set of sub-problems exhibit certain properties, namely, the first sub-problem has a trivial solution and each subsequent sub-problem has a solution very close to the solution of the prior sub-problem. Mathematically this can be described via the following expression:

$$\mathcal{H}(x,\lambda) = (1-\lambda)\mathrm{F}(x) + \lambda\mathcal{G}(x) \tag{92}$$

where $\lambda \in [0,1]$.

The method begins by replacing the original problem $\mathrm{F}(x) = 0$ with $\mathcal{H}(x,\ \lambda) = 0$. The equation set $\mathcal{G}(x)$ is a representation of the system that has a trivial solution. The homotopy factor λ has the value of 1 for the first sub-problem, and therefore, the initial solution for $\mathcal{H}(x,\ \lambda)$ is equal to the trivial solution of $\mathcal{G}(x)$. For the final sub-problem that corresponds to the original problem, the homotopy factor λ has the value of zero. To generate sequential sub-problems, the homotopy factor is dynamically decreased in small steps until it has reached the value of zero.

In the following sections, we discuss two homotopy methods that are specifically developed for the power flow and three-phase power flow analyses i.e. Tx stepping and dynamic power stepping method.

6.2.3 Tx Stepping

We propose a new homotopy approach, "Tx Stepping," that is specifically invented for the non-linearities observed in the power flow and three-phase power flow problems.

6.2.3.1 General Approach

In Tx stepping method, the series elements in the system (transmission lines, transformers etc.) are first "virtually" shorted to solve the initial problem that has a trivial solution. Specifically, a

large conductance ($\gg G_{il}$) and a large susceptance ($\gg B_{il}$) are added in parallel to each transmission line and transformer model in the system. In case of three-phase power flow, a large self-impedance ($\gg Y_{\Omega\Omega}^{il}$) is added in parallel to each phase of the transmission line and transformer model. Furthermore, the shunts in the system, are open-circuited by modifying the original shunt conductance and susceptance values. Importantly, the solution to this initial problem results in high system voltages (magnitudes), as they are essentially driven by the slack bus complex voltages and the PV bus voltage magnitudes due to the low voltage drops in the lines and transformers (as expected with virtually shorted systems). Similarly, the solution for the bus voltage angles lies within an ϵ-small radius around the slack bus angle. Subsequently, like other continuation methods, the formulated system problem is then gradually relaxed to represent the original system by taking small increment steps of the homotopy factor (λ) until convergence to the solution of the original problem is achieved. Mathematically, the line and transformer impedances during homotopy for the power flow is expressed by:

$$\forall il \in \mathcal{T}_X, xfmrs: \hat{G}_{il} + j\hat{B}_{il} = (G_{il} + jB_{il})(1 + \lambda\gamma) \tag{93}$$

and for the three-phase problem:

$$\begin{bmatrix} \hat{Y}_{aa}^{il} & \hat{Y}_{ab}^{il} & \hat{Y}_{ac}^{il} \\ \hat{Y}_{ba}^{il} & \hat{Y}_{bb}^{il} & \hat{Y}_{bc}^{il} \\ \hat{Y}_{ca}^{il} & \hat{Y}_{cb}^{il} & \hat{Y}_{cc}^{il} \end{bmatrix} = \begin{bmatrix} \mathrm{Y}_{aa}^{il}(1+\gamma\lambda) & \mathrm{Y}_{ab}^{il} & \mathrm{Y}_{ac}^{il} \\ \mathrm{Y}_{ba}^{il} & \mathrm{Y}_{bb}^{il}(1+\gamma\lambda) & \mathrm{Y}_{bc}^{il} \\ \mathrm{Y}_{ca}^{il} & \mathrm{Y}_{cb}^{il} & \mathrm{Y}_{cc}^{il}(1+\gamma\lambda) \end{bmatrix} \tag{94}$$

where, G_{il}, B_{il}, and ${Y_{\Omega\Omega}}^{il}$ are the original system impedances and $\hat{G}_{il}, \hat{B}_{il}$, and ${\hat{Y}_{\Omega\Omega}}^{il}$ are the system impedances used while iterating from the trivial problem to the original problem. The parameter γ is used as a scaling factor for the conductances and susceptances. If the homotopy factor (λ) takes the value of one, the system has a trivial solution and if it takes the value zero, the original system is represented.

Along with ensuring convergence for a problem, Tx stepping can avoid the undesirable low voltage solutions for the positive sequence power flow and three-phase power flow problem since the initial problem results in a solution with high system voltages, and each subsequent step of

the homotopy approach continues and deviates ever so slightly from this initial solution, thereby guaranteeing convergence to the high voltage solution for the original problem.

6.2.3.2 Handling of Transformer Phase Shifters and Taps

To "virtually short" a power system, we must also account for transformer taps tr^{Ω} and phase shifting angles θ^{Ω}. In a "virtually" shorted condition, all the nodes in the system must have complex voltages that are near the slack bus or PV bus complex voltages, which can be intuitively defined by a small epsilon norm ball around these voltages. Therefore, to achieve the following form, we must modify the transformer taps and phase shifter angles such that at $\lambda = 1$, their turns ratios and phase shift angles correspond to a magnitude of 1 pu and 0°, respectively. Subsequently, the homotopy factor λ is varied such that the original problem is solved with original transformer tap and phase shifter settings. This can be mathematically expressed as follows:

$$\forall i \in xfmrs : \hat{tr}_i^{\Omega} = tr_i^{\Omega} + \lambda\left(1 - tr_i^{\Omega}\right) \tag{95}$$

$$\forall i \in xfmrs : \hat{\theta}_i^{\Omega} = \theta_i^{\Omega} - \lambda\theta_i^{\Omega} \tag{96}$$

6.2.3.3 Handling of Voltage Control for Remote Buses

To achieve a trivial solution during the first step of Tx stepping it is essential that we also handle remote voltage control appropriately. Remote voltage control refers to a device on node $\mathcal{O}$ in the system controlling the voltage of another node $\mathcal{W}$ in the system. This behavior is highly non-linear and if not handled correctly can result in divergence or convergence to a low voltage solution. Existing commercial tools for power flow and three-phase power flow analyses have difficulties dealing with this problem and suffer from lack of robust convergence when modeling remote voltage control in general. With Tx stepping we can handle this problem efficiently and effectively. We first incorporate a "virtually short path" between the controlling node ($\mathcal{O}$) and the controlled node ($\mathcal{W}$) at $\lambda = 1$, such that the device at the controlling node can easily supply the current needed for node $\mathcal{W}$ to control its voltage. Then following the homotopy progression, we gradually relax the system such that the additional line connecting the controlling node ($\mathcal{O}$) and controlled node ($\mathcal{W}$) is open at $\lambda = 0$.

6.2.3.4 Implementation of Tx Stepping in Equivalent Circuit Formulation

Unlike traditional implementations of homotopy methods, in equivalent circuit formulation we do not directly modify the non-linear set of mathematical equations, but instead embed a homotopy factor in each of the equivalent circuit models for the power grid components. In doing so we allow for incorporation of any power system equipment into the Tx stepping approach within the equivalent circuit formulation framework, without loss of generality. Furthermore, we ensure, that the physics of the system is preserved while modifying it for the homotopy method. Figure 6-2 and Figure 6-3 demonstrates how the homotopy factor is embedded into the equivalent circuit of the transmission line and transformer, respectively.

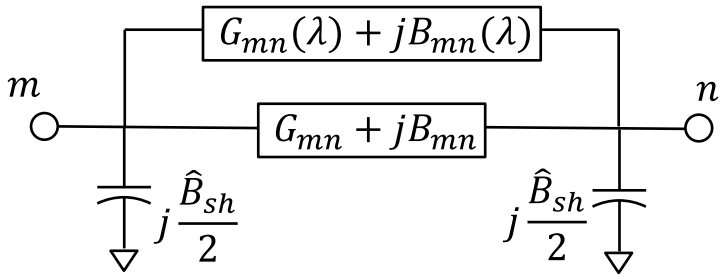

Figure 6-2: Homotopy factor embedded in transmission line equivalent circuit.

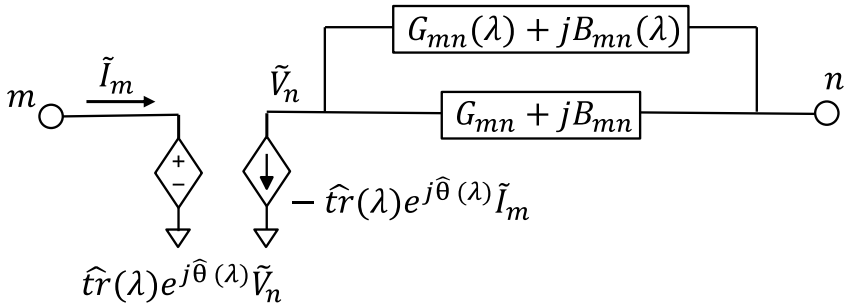

Figure 6-3: Homotopy factor embedded in transformer equivalent circuit.

6.2.3.5 Notes on convergence

The proposed Tx stepping method is within the subset of homotopy methods and to ensure convergence (i.e. be globally convergent) for any homotopy method the following conditions must be met [62]:

i. Defined path for the homotopy method i.e. $c(\lambda) \in \mathcal{H}^{-1}(0)$ with $(x, \lambda) \in range(c)$ must be smooth and should exist.

ii. If a curve c exists, then it should intersect the final solution at $\lambda = 0$.

The first condition can be met through implicit function theorem and requires that the Jacobian ($\mathcal{H}'(\lambda)$) of the homotopy function is of full rank for all values of λ along the curve. In the power flow or three-phase flow problem this corresponds to the Jacobian (J) matrix of the network constraints that in the case of equivalent circuit formulation are the Kirchhoff's current laws. Based on domain knowledge of power systems, it is understood that the network Jacobian matrix is singular if the system is operating at its limits (tip of the nose curve) [49] or beyond (infeasible system). This is an unlikely case from the physics perspective for any well-conditioned system over the range of λ, and therefore, the Jacobian (J) is generally full rank over the complete range of λ. In rare cases, the network Jacobian ($\mathcal{H}'(\lambda)$) defined for λ value on the curve (i.e. $c(\lambda),\ \lambda \in [1, 0]$) can be singular. This is either because the system in infeasible such that no further power transfer is possible or that the system is highly ill-conditioned and is operating at the tip of the nose curve. For such infeasible or highly ill-conditioned networks, it is possible that a rank deficient Jacobian may be encountered along the homotopy curve. To achieve robust convergence for such networks that are either infeasible or highly ill-conditioned, optimization-based methods [63] or techniques for structural perturbations are used [64]. An example of the optimization-based method is addition of current sources to all system nodes during Tx-stepping while minimizing their value [63], whereas an example for structural perturbation includes adding and removing transmission lines to the network dynamically during the homotopy path. In the optimization-based method shown in [63], the network is guaranteed to have a feasible solution for some value of complex current sources, thereby asserting the existence of a full rank Jacobian matrix. Similarly, a full rank Jacobian matrix can also be ensured for ill-conditioned systems by structurally relaxing the weak part of the grid by adding more lines at the start and gradually removing them for the original problem.

The second condition is more easily met and is linked to existence theorems in non-linear analyses [62]. If some boundary condition exists that prevents the curve from extending to infinity prior to intersecting the solution at $\lambda = 0$, then this condition is met. In our formulation, different limiting techniques ensure that the solution at any point on the curve c does not diverge and extend to infinity.

6.2.4 Dynamic Power Stepping

Another homotopy technique that can ensure robust convergence for systems that have a low percentage of constant voltage nodes in the system is the dynamic power stepping method. Existing distribution systems and small transmission systems tend to belong to this class of systems and, therefore, dynamic power stepping can be applied to robustly obtain the steady-solution by solving either the power flow or the three-phase power flow problem. This method has been described for the positive-sequence power flow and three-phase power flow problem in [34], [65] and is analogous to the source stepping and Gmin stepping approaches in standard circuit simulation solvers.

In the dynamic power stepping method, the system loads and generation are scaled back by a factor of β until the convergence is achieved. If these loads and generations are scaled down all the way to zero, then the constraints for the PQ buses in the system result in linear network constraints. Similarly, current source non-linearities of the PV buses that are due to the constant real power are also eliminated. Therefore, by applying the power stepping factor, the non-linearities in the system are greatly eased and convergence is easily achieved. Upon convergence, the factor is gradually scaled back up to unity to solve the original problem. In this method, as in all continuation methods, the solution from the prior step is used as the initial condition for the next step. The mathematical representation of dynamic power stepping for the three-phase power flow and positive sequence power flow problem is as follows:

$$\forall G \in PV: \hat{P}_G^{\Omega} = \beta P_G^{\Omega} \tag{97}$$

$$\forall L \in PQ: \hat{P}_L^{\Omega} = \beta P_L^{\Omega} \; and \; \hat{Q}_L^{\Omega} = \beta Q_L^{\Omega} \tag{98}$$

where, *PQ* are all load nodes and *PV* are all generator nodes.

6.3 Algorithm

In this sub-section we describe the algorithm for the equivalent circuit framework when used in conjunction with circuit simulation methods. The algorithm is implemented in our tool: SUGAR (Simulation with Unified Grid Analyses and Renewables) and can be used to solve any

positive-sequence power flow problem or three-phase power flow problem without the loss of generality.

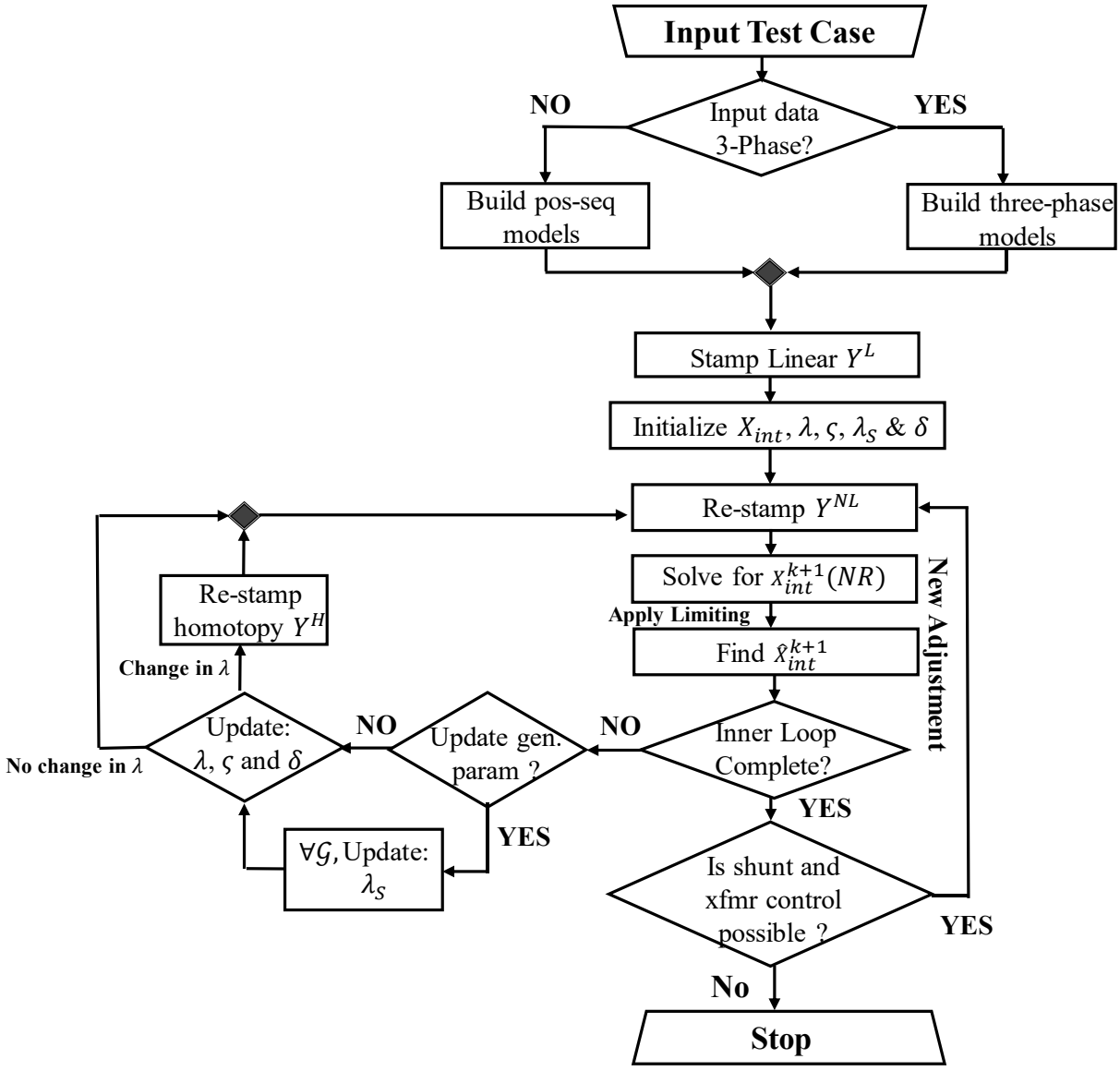

Algorithm 6-1: SUGAR algorithm for solving positive sequence and three-phase power flow problems.

The described Algorithm 6-1 shows the recipe for solving the positive-sequence as well as three-phase power flow problem in the equivalent circuit approach with the use of circuit simulation methods. The developed solver begins with parsing the input file and gauging if the input data are for the positive sequence or three-phase power flow problem. Based on the type of data (i.e. power flow or three-phase power flow data), it starts with building the system models.

An empty Jacobian matrix structure is initialized based on the size of the system and non-changing linear models (Y^L, J^L) are first stamped in it. These stamps remain constant throughout the NR iterations. Input state variables and other continuation parameters ($x_0, \delta, \zeta, \ \lambda, \ \lambda_s$) are then initialized following which the non-linear models are stamped (Y^{NL}, J^{NL}) and NR is applied with limiting methods enabled to calculate the next iterate for the voltages, the generator reactive powers and any other continuous control variables ($\hat{X}^{k+1}$). In the solver, from the practical point of view, the available initial conditions in the input file are first used as the initial conditions. The use of the proposed limiting methods generally solves the system within 7 to 10 iterations with these initial conditions. However, in cases where the system is ill-conditioned or lacking a good initial guess, the solver begins to gradually increase the homotopy factor (λ) until a trivial solution is found (this method does not require a good initial guess as homotopy methods have trivial solution for the first step). Once trivial solution is found, homotopy factors and other continuation factors for generators are dynamically updated (in this case decreased), and homotopy models (Y^H, J^H) are stamped or re-stamped to ensure convergence to the correct physical solution for the original problem at ($\lambda = 0$). Upon convergence of the inner loop, remaining controllable switched shunts and transformer taps are adjusted and the inner loop is repeated until the final solution is achieved. In cases, where continuous models are used for the control of discrete shunts and discrete transformer taps, a final loop is implemented to snap them to their closest discrete values.

6.4 Results

In this section we will report the results obtained via the use of the equivalent circuit framework with the use of circuit simulation methods. To run the test cases and validate our approach, we integrated these methods into our tool SUGAR. The results from SUGAR will demonstrate the ability of our framework to solve ill-conditioned, large real-life, and in general hard-to-solve positive-sequence and three-phase power flow test cases from arbitrary initial conditions. The following result section is divided into positive-sequence power flow results sub-section and three-phase power flow results sub-section.

6.4.1 Positive Sequence Power Flow Results

Following few sub-sections discuss results from the positive sequence power flow analysis. The set of results include ill-conditioned and hard to solve test cases as well as large test cases. However, first we demonstrate the efficacy of circuit simulation methods.

6.4.1.1 Efficacy of Circuit Simulation Methods

We use the first set of results to demonstrate that the use of circuit simulation methods developed within this section can significantly improve the robustness of convergence within the equivalent circuit framework. The section shows how the results obtained in the equivalent circuit framework with the use of circuit simulation methods fare against those obtained in the equivalent circuit framework without the use of circuit simulation methods.

6.4.1.1.1 Experiment 1

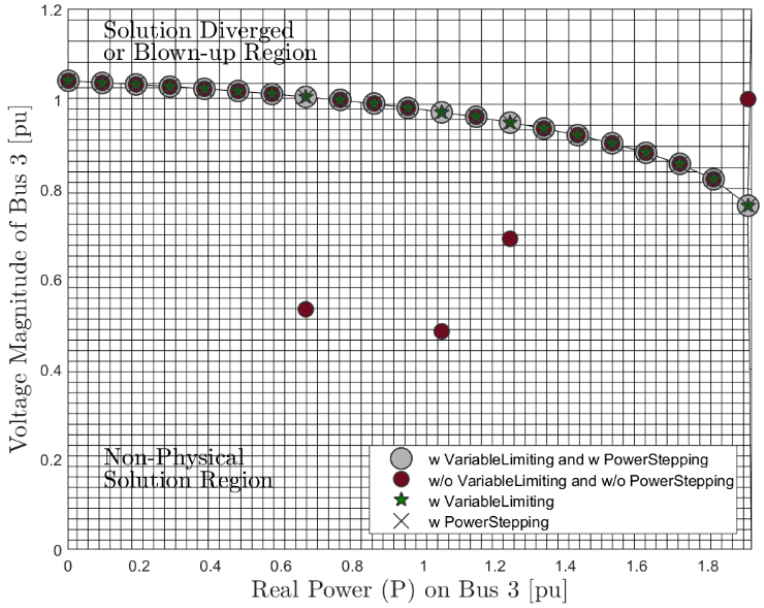

Figure 6-4: Solution of Bus 3 voltage for IEEE 14 bus test system with increasing loading factors with and without circuit simulation methods.

In this experiment, positive-sequence power flow simulations are run on the IEEE 14 bus test system (from flat start) in steps of increasing loading factors (up to 4x) for the following four scenarios: 1) both power stepping and variable limiting option disabled, 2) with power stepping option enabled and variable limiting disabled, 3) with variable limiting option enabled and power stepping disabled, and 4) both power stepping and variable limiting option enabled. The

solutions for the bus 3 voltage magnitude at the end of each simulation are then plotted in Figure 6-4. The plot shows that convergence to the correct physical solution is achieved for each simulation instance when either variable limiting, or power stepping option is enabled. However, without these options enabled in SUGAR, the solution in many simulation instances has either converged to the wrong solution or diverged altogether.

6.4.1.1.2 Experiment 2

In this experiment, power flow simulations are run on the 2869 PEGASE test system and 9241 PEGASE test system for 20 different initial guesses of $\boldsymbol{Q_G}$ values that are uniformly distributed in the range of -10 pu and 10 pu. All 20 simulations are run for each of these solver settings under the same four scenarios as were used in the case for Experiment 1. The convergence results plotted in Figure 6-5 show that without the use of circuit simulation techniques, most of the test case instances either diverge or converge to the wrong solution. Convergence to the correct physical solution is only observed when both variable limiting and power stepping are enabled.

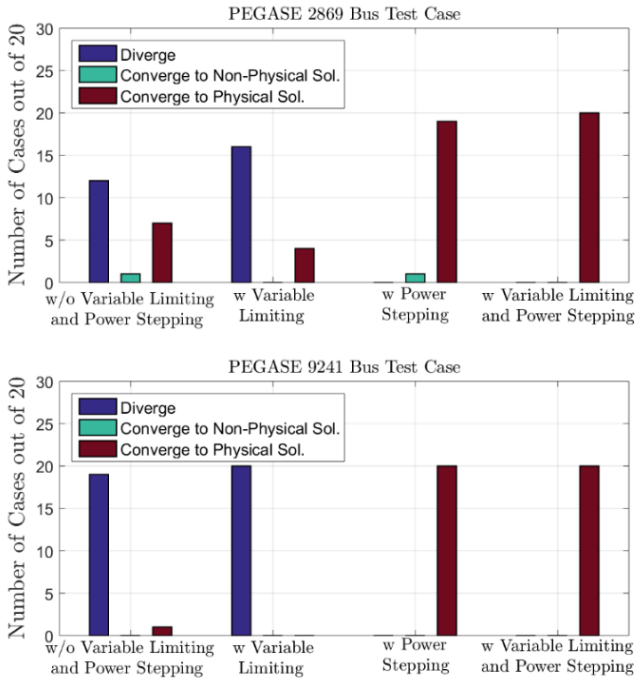

Figure 6-5: Power flow results for 2869 bus and 9241 bus test systems with and without circuit simulation techniques.

6.4.1.1.3 Experiment 3

To show the efficacy of circuit simulation methods in this experiment, contingencies were simulated on two hard to solve test-cases that represent different operating conditions for a real sub-network within the US power grid network models. The base cases for both test systems are first solved via the Tx-stepping method whose solutions are then used as initial conditions for the set of contingencies that were further run for two settings i) without the use of circuit simulation methods in SUGAR ii) with the use of circuit simulation methods in SUGAR. The contingencies in the contingency set include the loss of the largest 10% of the online generators and loss of 10% of the highest capacity lines and transformers taken off-line one at a time from the base case to create a single contingency instance within the contingency set.

The results in the Table 6-1 validate that the use of circuit simulation methods when applied to equivalent circuit formulation can significantly increase the robustness of the power flow solver as in the case when circuit simulation methods were disabled, we were able to ensure convergence to the correct physical solution for far fewer contingency instances.

TABLE 6-1: COMPARISON OF SUGAR WITH AND WITHOUT CIRCUIT SIMULATION TECHNIQUES

Case Id	# Bus	# Total Cases	SUGAR w/o Circuit Simulation Methods		SUGAR with Circuit Simulation Methods	
			Converge	Diverge /Infeasible	Converge	Diverge /Infeasible
Case 1	5944	754	735	19	750	4
Case 2	7029	801	706	95	793	8

6.4.1.2 Ill-Conditioned Test Cases

In this sub-section, we demonstrate results of our approach when applied to ill-conditioned test cases. A large condition number for a given matrix indicates that the matrix and the system corresponding to that matrix are ill-conditioned. In the power flow problem, the matrix of interest is the Jacobian that is used to calculate the updated system state variables at each NR step. If the condition number of the Jacobian matrix is large at the solution point, then the system is assumed to be ill-conditioned.

The following set of results are generated from SUGAR with circuit simulation methods enabled and are compared against those produced by the standard commercial tools used in the industry today.

6.4.1.2.1 Experiment 1: Ill-conditioned test cases in literature

The 11-bus, 13-bus, and 43-bus test cases from the power system literature [49] are considered to be ill-conditioned systems. However, it is systematically shown in [49] that out of these three systems, the 11-bus system is the only genuine ill-conditioned system with a maximum loading of 99.82 %. The 13-bus system is not an ill-conditioned system and can easily be solved via any power flow method, and the 43-bus test case has a maximum loading of 58%, for which there is no feasible solution for the base loading.

Table 6-2 shows the comparison of the results for a modified 11 bus ill-conditioned test case at 99.82% loading for different set of initial conditions. Using standard commercial tools, for most initial conditions the system is likely to converge to a low voltage solution or diverge. The commercial solver can only converge to the correct physical solution if the initial condition supplied is the solution itself. However, SUGAR can converge to the correct physical solution from arbitrary initial conditions when Tx Stepping is applied.

TABLE 6-2: COMPARISON OF RESULTS FOR MODIFIED 11 BUS TEST CASE

Initial Condition		Ill Conditioned 11 Bus Test Case	
V_{mag} (pu)	V_{ang} (°)	Standard Commercial Tool[2]	SUGAR[1]
1	0	Low Voltage	High Voltage
0.76	23	Low Voltage	High Voltage
0.71	45	Low Voltage	High Voltage
High Voltage	High Voltage	High Voltage	High Voltage

1. Tx Stepping was enabled while running simulations in SUGAR
2. Full Newton Raphson was the solver used in Standard Commercial Tool

6.4.1.2.2 Experiment 2: A large ill-condition system at operating point

Another notable case with a higher condition number at the operating point is the 13659-bus system from the PEGASE test cases. At the solution point, the approximate condition number of the system Jacobian is 1.7e8. Figure 6-6 shows convergence results for this test case from ten

arbitrary initial conditions for a standard commercial tool and SUGAR. The ten initial conditions were chosen uniformly from the set of:

$$V_R \in [0.6, 1.1\,], \qquad V_I = \{x \in \mathbb{R}^n \mid x = 1 - V_r\} \tag{99}$$

From the set of 10 initial conditions, the standard commercial tool converged to the correct physical solution once, diverged 8 times, and converged to the angular unstable solution one time. SUGAR, however, with variable limiting and voltage limiting enabled was able to converge to the correct physical solution for all ten initial guesses.

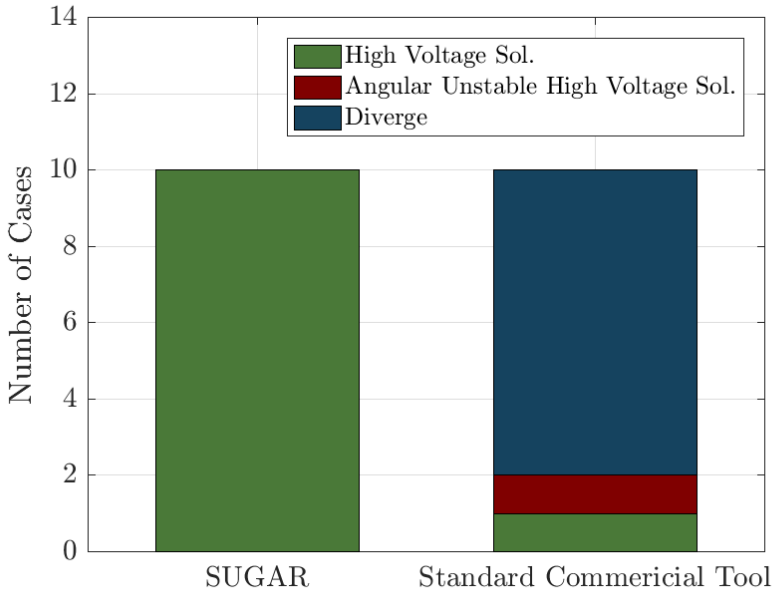

Figure 6-6: Results for 13659 buses PEGASE system.

6.4.1.3 Large Test Cases

In this experiment we demonstrate that SUGAR can robustly solve large test cases and that it ensures convergence to thecorrect physical solution from arbitrary initial conditions independent of the scale or conditioning of the system. Figure 6-7 shows the results for six distinct test systems that represent the eastern interconnection network of the US power grid under different loading conditions (Summer/Winter) and time periods (2017, 2018, 2021, 2026 etc.). The simulations were run on these systems from a set of different initial conditions that were uniformly chosen from the sets of:

$$V_{ang} \in [-50, 50], \qquad V_{mag} \in [0.6, 1] \tag{100}$$

The vertical and horizontal axes of the figure represent the set of initial conditions (V_{ang}, V_{mag}) for a given case, respectively and box within each sub-graph represent the numbers of nodes in the test system. If the case converged to a correct physical solution, it is marked via a green mark; whereas if the case diverged then it is marked via a red mark. The figure indicates that SUGAR was able to achieve convergence for all the six large eastern interconnection systems independent of the choice of initial conditions. The run-time per iteration for the eastern interconnection test cases in SUGAR is comparable to other available commercial tools (less than 0.4s per iteration). The total simulation time for the test cases is dependent on the choice of initial conditions.

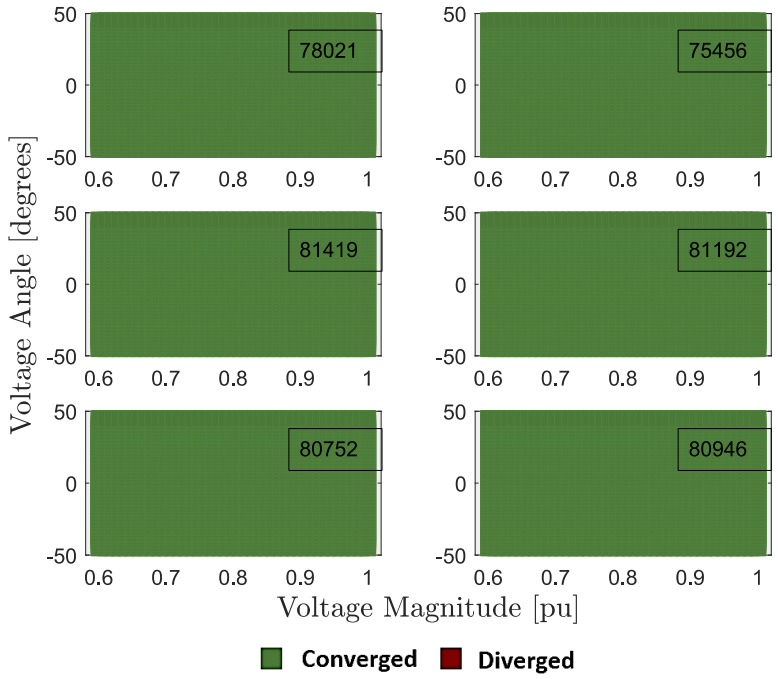

Figure 6-7: Convergence sweep of large cases that represent Eastern Interconnection from range of initial conditions (number of nodes for each test system given in the legend box)

We also repeated the same experiment on the publicly available SythenticUSA and ACTIVgs70k test cases [66] that demonstrated the same robust convergence as in the case of Eastern Interconnection test cases, as shown in Figure 6-8.

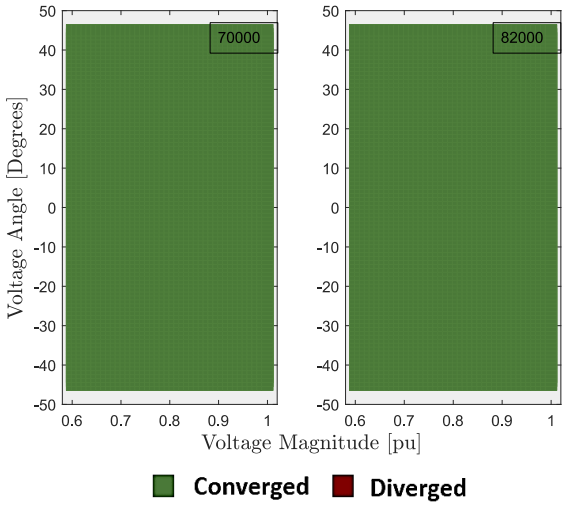

Figure 6-8: Convergence Plot for ACTIVgs70k (left) and SyntheticUSA (right) testcases.

We performed a similar experiment to compare the robustness of SUGAR tool against a standard commercial tool. To conduct the experiment, we ran three real and two synthetic [66] eastern interconnection sized systems for 15 different initial conditions in both the SUGAR tool and the standard commercial tool. The set of initial conditions for this experiment for all buses were identical and were uniformly sampled from:

$$V_{ang} \in [-40, 40], \; V_{mag} \in [0.9, 1.1]. \tag{101}$$

The results in Table 6-3 show that from any of the 15 different initial conditions, the standard commercial tool was unable to solve the system, whereas SUGAR with Tx stepping enabled was able to converge to the correct physical solution in all cases.

TABLE 6-3: CONVERGENCE PERFORMANCE FOR LARGE EASTERN INTERCONNECTION TEST CASES

Case Name	# Nodes	Standard Tool		SUGAR	
		# Converge	# Diverge	# Converge	# Diverge
Case 1	80778	0	15	15	0
Case 2	76228	0	15	15	0
Case 3	81904	0	15	15	0
SyntheticUSA	82000	0	15	15	0
ACTIVSg70k	70000	0	15	15	0

6.4.1.4 Contingency Analysis

To further demonstrate the robustness of our approach, we consider a set of scenarios wherein we plan a realistic contingency on large test cases and other hard to solve test cases. We compare the obtained results from SUGAR tool against those produced by the standard commercial tool.

6.4.1.4.1 Experiment 1: Contingency on Eastern Interconnection Test Cases

In this first experiment, we run contingency analysis on test cases that represent different operating and loading conditions for the U.S. eastern interconnection network. The contingencies in these cases are defined by loss of either two (N-2) or three (N-3) generators in the system. To obtain and further compare the results, we solve these contingency instances with both the standard commercial tool and the SUGAR tool. The initial conditions for all the cases are chosen to be the solution state prior to the contingency i.e. base case (thereby suggesting that the system is close to its operating state post-contingency).

TABLE 6-4: CONTINGENCY ANALYSIS FOR LARGE TEST CASES

Case	Contingency Type	No. of Buses	Standard Commercial Tool	SUGAR
Case 1	N-2	75456	Diverged	Converged
Case 2	N-2	78021	Diverged	Converged
Case 3	N-3	80293	Diverged	Converged
Case 4	N-3	81238	Diverged	Converged

The results in Table 6-4 demonstrate that while SUGAR was able to converge for all the contingency instances, whereas the standard commercial tool diverged for all thereby further strengthening the argument for robustness of our framework. Importantly, robustness of our tool toward solving contingencies can be extremely vital to grid operation and planning engineers who are required by NERC to evaluate each failed N-1 contingency [67].

6.4.1.4.2 Experiment 2: Contingency of hard-to-solve real life test cases

In this experiment, to demonstrate the robustness of SUGAR while performing contingency analysis, we consider a yet another real-life test grid that represents a sub-set of the US grid. This cases was known to be hard-to-solve. For this experiment, we perform N-1 contingency analysis on this test system. The set of contingencies includes loss of 10% of the highest capacity links

(transformers and branches) and 10% of the largest online generators taken off-lines one at a time from the base case run to create a single contingency instance. This results in total number of contingency instances within the contingency set to be 774. To run the contingency analysis, we first solve the base case with the use of the Tx-stepping method. With the solution of the base case as the initial condition, we run the contingency simulation instances in SUGAR. The standard commercial tool was unable to solve the base case, and therefore, we were not able to perform the contingency simulation instances on those. Table 6-5 documents the results from SUGAR contingency runs and it shows that SUGAR was able to solve the base case as well as all contingency instances robustly.

TABLE 6-5: N-1 CONTINGENCY ANALYSIS ON SET OF CRITICAL EQUIPMENT.

Solver	Number of Contingencies	System Convergence	
		Converged	Infeasible
SUGAR	774	774	0
Standard Commercial Tool	774	NA	NA

6.4.1.5 N-1+1 Analysis (Contingency Analysis + Corrective Action)

In this experiment we simulated an another real-life test case that represents an electric grid from Africa that it is pushed to its limits. For this experiment, we first perform N-1 contingency analysis on this system and based on the results we recommend a corrective action methodology that we refer to as N-1+1 analysis. In the set of contingencies for this analysis, we consider all the transformers, lines and generators dropped one at a time that resulted in a total of 717 contingency instances. Of these 717 contingency instances, 684 were found to be feasible whereas 33 instances were found to be infeasible. The 33 of them were confirmed to be infeasible based on the methodology documented in [63]. Furthermore, from the results gathered from the contingency analysis, it was found that akin to the base case, a significant number of simulation instances resulted in very high voltages as shown in Figure 6-9.

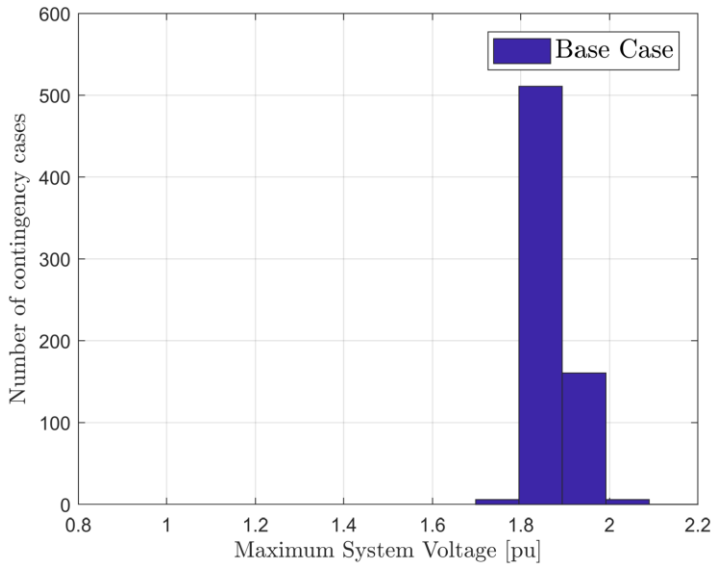

Figure 6-9: Maximum bus voltage range for contingency analysis.

Therefore, as a corrective action to improve the voltages in this system, we propose N-1+1 analysis. The algorithm for this analysis is as follows:

N-1+1 Algorithm

---

1. **procedure:**
2. **run** $N-1$ contingency
3. **identify** all regions (R_{inf}) with abnormal bus voltages in the system
4. for $\forall R_{inf}$:
    a. **add** reactive power compensating device to every bus in R_{inf} ($N+1$ scenario)
    b. **redo** $\rightarrow N-1$, find number of infeasible cases (N_{inf}) and range of voltages ($V_{max}-V_{min}$)
5. **choose,** $N+1$ scenario, with fewest infeasible cases (N_{inf}) and lowest spread of system voltages.

Based on the algorithm, we added a reactive power compensating device to the most sensitive bus in the system and were able to reduce the system voltages for the base case and the contingency cases while resulting in fewer infeasible cases. The maximum bus voltage range pre- and post- corrective action is shown in Figure 6-10.

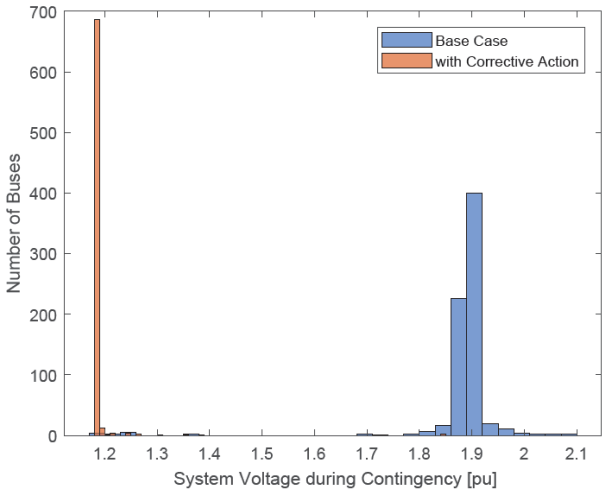

Figure 6-10: System bus voltage pre and post corrective action.

6.4.2 Three-Phase Power Flow Results

In the following section, we discuss results for three-phase power flow analysis. Akin to positive sequence power flow analysis, we first demonstrate the efficacy of circuit simulation methods toward robust convergence of distribution grid test cases.

6.4.2.1 Efficacy of Circuit Simulation Methods

In this experiment we demonstrate that the use of circuit simulation methods for three-phase power flow can ensure convergence for hard-to-solve three-phase test cases that were otherwise found unsolvable. To demonstrate one such example, we extended the standard 145 node transmission system model into a balanced three-phase network model. Figure 6-11 plots the convergence results for this test case with and without the use of the dynamic power stepping technique. It is shown that without the use of dynamic power stepping, the test system did not converge within the maximum number of allowable iterations; however, with the use of dynamic power stepping, the system robustly converged to the correct physical solution.

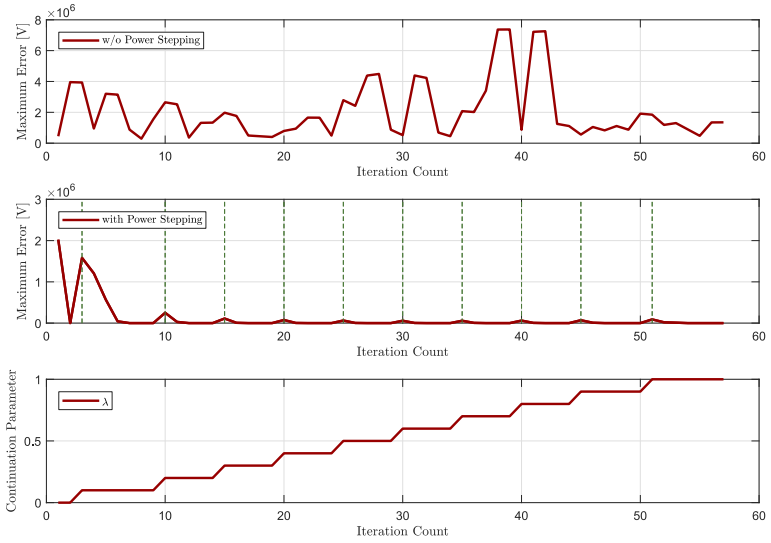

Figure 6-11: Convergence of 145 bus test case for three-phase power flow with (middle) and without (top) power stepping. For the power stepping case, the green dotted line represents the change in continuation factor λ whose evolution is shown in the bottom plot.

6.4.2.2 Taxonomical Test Cases and other Large Test Cases

Table 6-6 documents the results obtained from the SUGAR three-phase solver for standard taxonomical cases and three large meshed test cases. The standard taxonomical cases include both balanced and unbalanced three-phase test cases. The first two of the meshed test cases are the 342-Node Low Voltage Network Test Systems [68] that represent high density urban meshed low voltage networks. The third meshed test system is a high voltage 9241 node PEGASE transmission system that was extended to a balanced three-phase model from the positive sequence model. All these cases were simulated in SUGAR three-phase solver to validate the solver accuracy by comparing the obtained results against those produced from standard distribution power flow tool GridLAB-D. Slight differences (less than 1e-2) in the results were observed for cases between SUGAR and GridLAB-D and can be attributed to the default values used for unspecified parameters (e.g. neutral conductor resistance) in GridLAB-D.

TABLE 6-6: SUGAR THREE-PHASE RESULTS FOR TAXONOMICAL AND LARGE CASES

Cases	#Nodes	Iter. Count	Deviation from GridLAB-D	
			Max. ΔV_{mag} [pu]	Max. ΔV_{ang} [°]
GC-12.47-1	36	3	9.10E-06	6.6E-04
R1-12.47-1	2455	5	8.73E-04	9.94E-03
R2-12.47-3	2311	5	6.56E-04	1.32E-02

R3-12.47-3	7096	5	1.94E-03	3.89E-02
R4-12.47-1	2157	5	6.81E-04	9.61E-03
R5-12.47-5	2216	5	5.44E-05	4.20E-03
Network Model 1	1420	3	3.38E-03	2.14E-03
Network Model 2	1420	3	3.83E-03	6.00E-03
case9241pegase*	12528	5	NA#	NA#

** 9241 bus PEGASE transmission test case was extended to three-phase model*
#The following case did not run in GridLAB-D

7. Joint Transmission and Distribution Simulation

There is a growing adoption of variable and intermittent sources of generation especially wind and solar in the power systems across the globe. This high levels of penetration of renewables will result in much narrower operational margin than what's available today, thereby significantly affecting the reliability of the grid. To ensure that the reliability of the grid is not affected, interdependencies between the transmission grid and distribution grid (wherein a significant fraction of solar is likely to be installed) will have to be clearly understood while enabling control based on the knowledge of the operating state for both the transmission as well as the distribution grid. This was apparent when a transmission system operator in PJM coordinated with the Sturgis, Michigan distribution grid to avoid a blackout by utilizing 6 MW of distributed generation back in 2013 [69]. To securely and reliably enable control actions such as this, the operators and planners of the grid may require new simulation capabilities that will navigate through the invisible boundaries that exists today between the transmission and distribution grid analyses and solution methodologies. The existing simulation framework for power system analyses is incapable of capturing these interdependencies between the transmission and distribution grids. No standard tool exists in the industry today that can jointly model the transmission and distribution grids while ensuring robust steady-state solution for the same. This lack of simulation capability was highlighted in an ARPA-E workshop to identify paths to large-scale deployment of renewable energy resources, where one speaker noted that the "tools are not graceful in considering penetration levels at which much of the thermal fleet could get de-committed," and that "studies do not co-simulate impact of renewable injection into receiving AC systems" [6]. Another speaker noted that the tools for simulating increasingly coupled transmission and distribution systems "are not well integrated" [7].

In this chapter we demonstrate that our equivalent circuit framework can jointly model the transmission and distribution (T&D) grid without loss of generality and ensure robust

convergence for the same. Moreover, as shown in Section 6, the circuit simulation techniques developed within this thesis are directly applicable to both the power flow and the three-phase power flow problem, thereby allowing us to extend the same to be used in the case of joint transmission and distribution analyses for robust convergence.

7.1 Background

The existing research literature in the field of joint transmission and distribution simulation is limited primarily due to the use of disparate methods for the transmission and distribution formulation and algorithms [57]-[60]. Amongst these, the most common methodology for joint T&D simulation is to model the transmission network via positive sequence model and the distribution network via three-phase network and to couple the two. The assumption here is that the three-phases of the transmission network are balanced at the point of interconnection (POI). In general, most of these methods tend to couple the transmission and distribution systems via an interface and then solve the two via disparate methods [58]-[60]. For instance, [58] models the transmission grid via PowerWorld and the distribution grid via GridLab-D. The integrated simulation is then performed by running individual sub-circuits in their respective tools and then by exchanging variables via a communication port. Similar approaches are also used in [59]-[60]. Such approaches result in inheritance of legacy robustness issues from the positive sequence as well as the three-phase solvers, wherein a failure of either tool to solve a sub-circuit (transmission or distribution test case) results in complete breakdown of the framework. Moreover, due to the use of disparate tools/methods for solving the individual transmission and distribution test cases, it is difficult to develop methods that are generic and can guarantee convergence for both transmission and distribution systems. A more novel master-slave approach toward solving the joint simulation is proposed in [57], wherein the joint problem is solved in a distributed way. In this method, the problem is split into a transmission power flow and several distribution power flow sub-problems that are then solved via different power flow algorithms to capture the different features of transmission and distribution grids. However, the methodology has mostly been tested on unrealistically small sized systems with no claims of robust convergence for the individual sub-systems.

Another approach for joint simulation of transmission and distribution systems is to model the complete three-phase network for the transmission system and then coupling the same with three-phase networks of the distribution systems [61]. This approach does not require a balanced operation assumption of the transmission grid, and thus allows for modeling of unbalanced conditions. However, the primary limitations to this approach is the general lack of three-phase data for the transmission network, and the lack of research toward ensuring robustness for convergence of three-phase transmission networks.

7.2 General Methodology

To robustly solve for the joint transmission and distribution network, we make use of the equivalent circuit approach discussed in Section 5. In this approach, we represent the coupled transmission and distribution grid as an aggregated equivalent circuit and we use NR methods to solve for the set of non-linear equations defined by that aggregated circuit. The aggregated equivalent circuit for the transmission system is the positive sequence network of the same and assumes balanced operation of the grid, whereas the equivalent circuit of the distribution system models each phase of the distribution grid individually, thereby allowing for analysis of unbalanced operation of the grid. In the equivalent circuit approach, we can easily couple the two systems (transmission and distribution) to jointly simulate them and solve for the two. As the entire grid can be thought of as a circuit, coupling of the two circuits for joint simulation is fundamental to the circuit analysis domain. We model the positive sequence currents consumed by the distribution grid with current controlled current sources connected to the edge of the transmission system. Similarly, we model the three-phase voltages at the sub-station level of the distribution system by voltage-controlled voltage sources that are functions of the voltages at the transmission edge of the system.

7.3 Coupling port for transmission and distribution equivalent circuit

First, we develop the port that is used to couple the transmission and distribution sub-circuits for joint transmission and distribution simulations. The positive sequence transmission network

and three-phase distribution network are coupled at the POI to run joint simulation via the circuit shown in Figure 7-1.

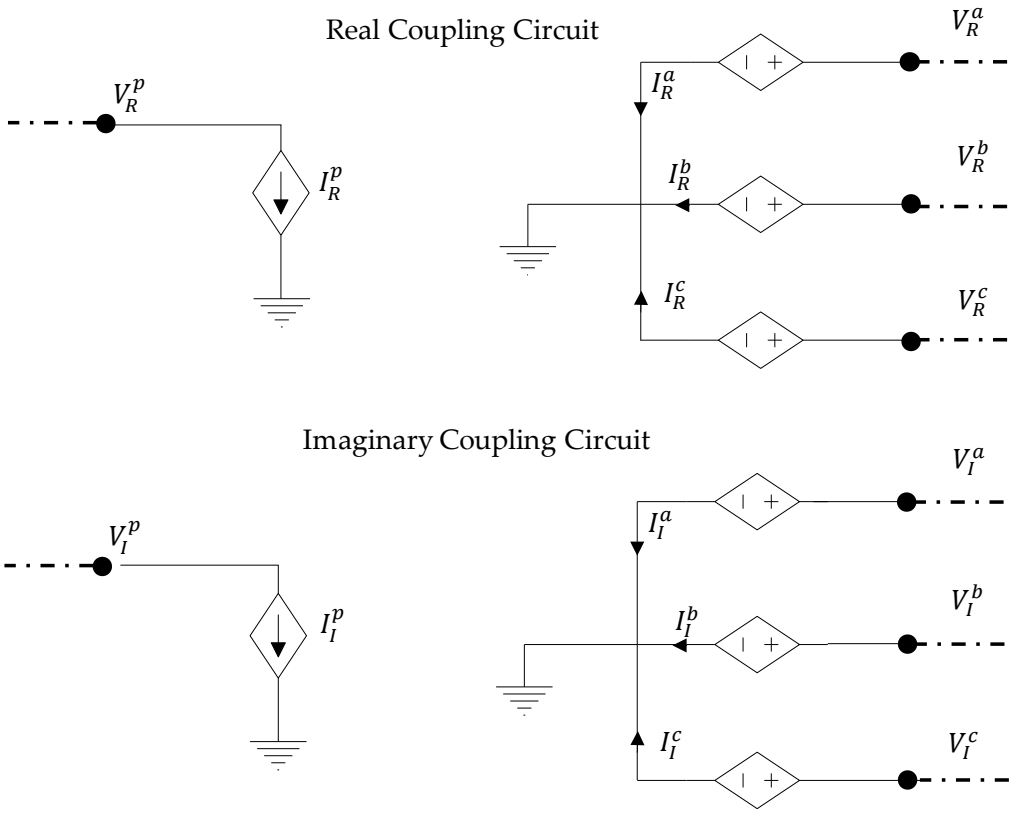

Figure 7-1: Coupling port for joint transmission and distribution analysis.

To derive the positive sequence currents $(I_R^p,\ I_I^p)$ and three-phase voltages $(V_R^a, V_I^a, V_R^b, V_I^b, V_R^c, V_I^c)$ required to model the port we make use of symmetrical components [54]. The positive sequence power flow problem for the transmission grid is assumed to have balanced operation, and therefore, the zero and negative sequence components of voltages and currents are ignored in the calculation of distribution grid currents consumed by the transmission grid. To calculate the transmission grid currents from three-phase distribution grid currents, (102) is used.

$$\begin{bmatrix} I_R^0 \\ I_I^0 \\ I_R^1 \\ I_I^1 \\ I_R^2 \\ I_I^2 \end{bmatrix} = \begin{bmatrix} 1 & 0 & 1 & 0 & 1 & 0 \\ 0 & 1 & 0 & 1 & 0 & 1 \\ 1 & 0 & \alpha^2 & 0 & \alpha & 0 \\ 0 & 1 & 0 & \alpha^2 & 0 & \alpha \\ 1 & 0 & \alpha & 0 & \alpha^2 & 0 \\ 0 & 1 & 0 & \alpha & 0 & \alpha^2 \end{bmatrix}^{-1} \begin{bmatrix} I_R^a \\ I_I^a \\ I_R^b \\ I_I^b \\ I_R^c \\ I_I^c \end{bmatrix} \tag{102}$$

Similarly, the distribution end voltages as a function of transmission POI voltages are calculated via:

$$\begin{bmatrix} V_R^a \\ V_I^a \\ V_R^b \\ V_I^b \\ I_R^c \\ I_I^c \end{bmatrix} = \begin{bmatrix} 1 & 0 & 1 & 0 & 1 & 0 \\ 0 & 1 & 0 & 1 & 0 & 1 \\ 1 & 0 & \alpha^2 & 0 & \alpha & 0 \\ 0 & 1 & 0 & \alpha^2 & 0 & \alpha \\ 1 & 0 & \alpha & 0 & \alpha^2 & 0 \\ 0 & 1 & 0 & \alpha & 0 & \alpha^2 \end{bmatrix} \begin{bmatrix} V_R^0 \\ V_I^0 \\ V_R^1 \\ V_I^1 \\ V_R^2 \\ V_I^2 \end{bmatrix} \tag{103}$$

Importantly, if unbalanced operation is expected at the high voltage transmission system level, then one must construct the three-phase equivalent circuit with of the transmission system and couple it directly with the three-phase equivalent circuit of the distribution system at the POI. This can be done via an equivalent circuit approach by following the formulation set forth in this thesis and in [31]-[35]. However, the analysis of an unbalanced three-phase transmission network is beyond the scope for this thesis work.

We explore two approaches for joint simulation of transmission and distribution (T&D) grids in this thesis:

i. Joint T&D simulation on a single machine.
ii. Joint T&D simulation on distributed cores with parallel computing.

7.4 Joint T&D simulation on a single machine

In this approach, we couple the transmission and distribution system using the coupling port network described in the previous section. We develop the aggregated equivalent circuit for the same and stamp the system matrix for each element in the coupled network. We then solve for the system matrix using NR. Figure 7-2 shows the coupled network for a single transmission and distribution network.

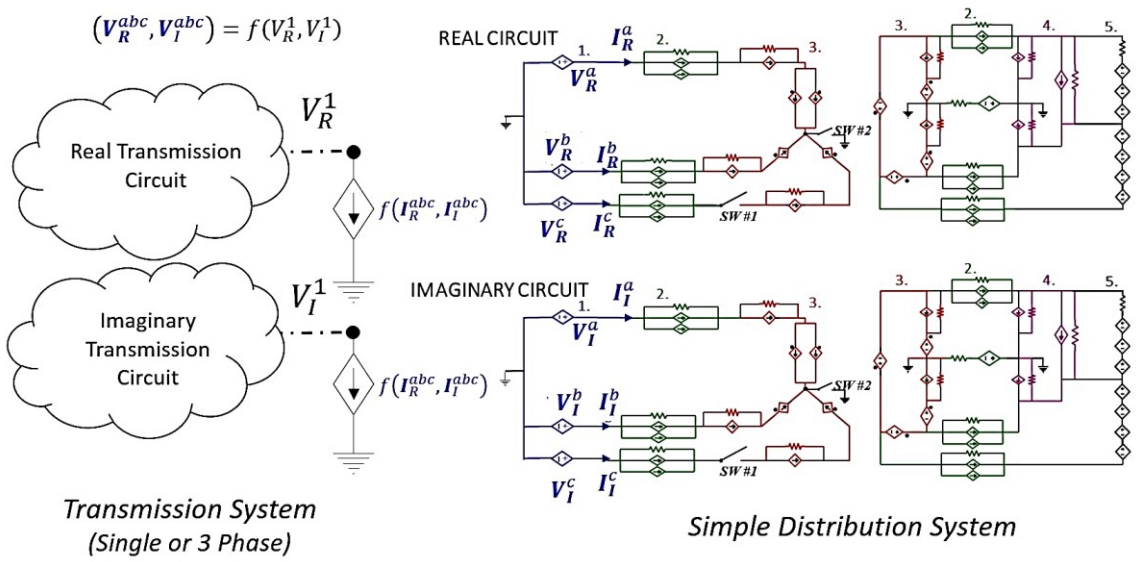

Figure 7-2: General framework for performing joint transmission and distribution simulation using equivalent circuit approach.

Here, we discuss some results from the simulations of joint T&D network on a single machine and demonstrate how our approach can overcome the challenges of the existing methods.

7.4.1.1 Experiment 1

In the first experiment, a 9241 node PEGASE test system is used to model the transmission grid, which is then coupled to a distribution grid modeled by a taxonomical feeder test case (R5-35.00-1) at the point of interconnection (POI). For the purposes of this experiment, the original distribution test case is modified to include distributed energy resources (DERs) in roughly 20 % of the system nodes that contain electrical loads. The net capacity of DERs at each node is kept variable and is modified throughout the experiment.

The goal of this experiment is two-fold:

i. To demonstrate that higher capacity of distribution loads can be supplied with higher penetration of DERs.

ii. To demonstrate that more resilient grid voltages can be obtained by higher penetration of DERs during both normal and contingency operation.

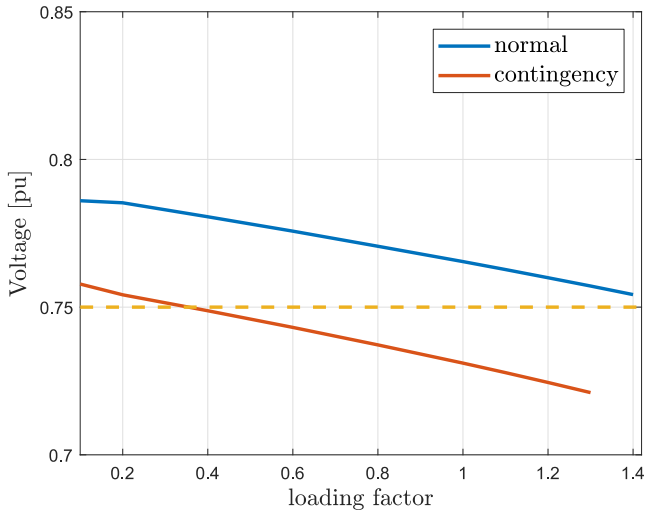

Figure 7-3: POI voltages under normal and contingency operation with changing distribution load.

To obtain the base maximum loading for the joint T&D system, we first develop the PV curve for the voltages at the POI by varying the loading factor of the distribution feeder, as shown in Figure 7-3. We repeat this analysis on the system with a loss of a generator on the transmission grid that is in close vicinity of the POI. As seen in the Figure 7-3, for the base case with no DERs, the voltages after the contingency has occurred are below 0.75 pu for majority of the loading factors and the likelihood of a system collapse is higher with increasing loading of the distribution feeder.

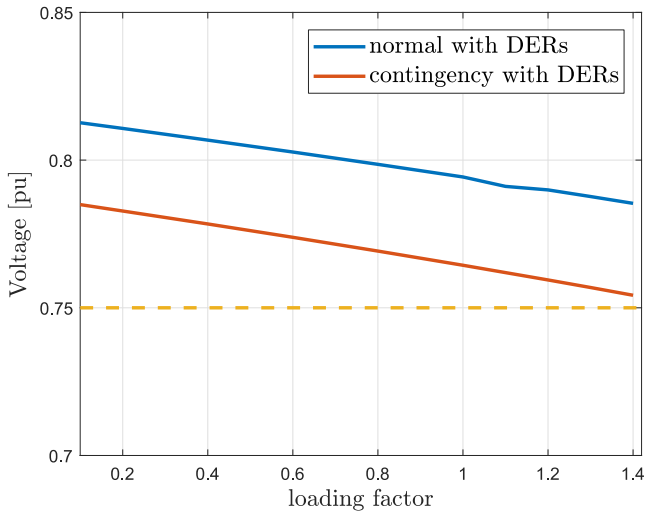

Figure 7-4: POI voltages under normal and contingency operation with changing distribution load and with DERs in the system.

To supply the full load in the distribution feeder such that the POI voltages remain above 0.75 pu, we scale up the penetration of DERs in the system. We simulate the contingency and normal cases again and show the results in Figure 7-4. With the penetration of DERs in the system, the voltages are above 0.75 pu under normal as well as contingency scenarios for all loading factors up to 1.4x while being able to supply greater than rated load of the distribution feeder without system collapse.

7.4.1.2 Experiment 2

A similar experiment is performed with a larger more realistic test case. In this experiment, the 78k+ nodes eastern interconnection of the U.S. is modeled via positive sequence transmission network. The 8000+ nodes taxonomical three-phase test system is then coupled to a weak point in the transmission grid for which voltages are highly sensitive to load currents. The primary goal of this experiment is to evaluate the minimum penetration of DERs needed to supply the full load of the distributed grid while ensuring that the sub-station voltage at the POI remains above 0.75 pu.

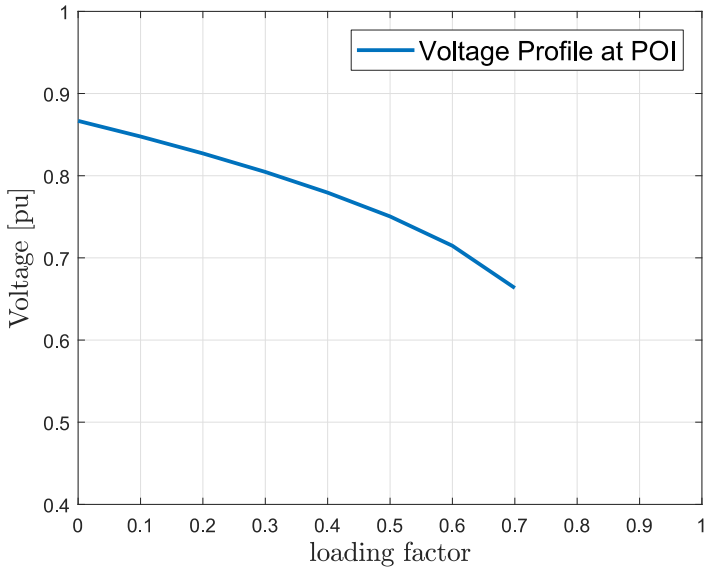

Figure 7-5: Voltage in pu at the point of interconnection with increasing loading factor of the distribution feeder.

To first evaluate the maximum transfer capacity at the POI prior to voltage collapse, we gradually increase the loading factor of the distribution feeder until the system collapses. As seen

in Figure 7-5, the system can only supply a fraction of the rated capacity (0.7 loading factor) prior to voltage collapse without any penetration of DERs.

As a remedial action, the penetration of DERs in the system is increased until the transmission grid can supply the full load of the distribution system while keeping the voltages at the POI above 0.75 pu. As in the prior experiment, the DERs in the system are added to roughly 20 % of the total system nodes that contain electric loads. A scaling factor is used to increase the penetration of DERs in the simulation. Figure 7-6 shows that with 20% penetration of distribution generation in the distribution grid, the transmission network can supply the full load while maintaining grid voltages above 0.75 at the interconnection sub-station.

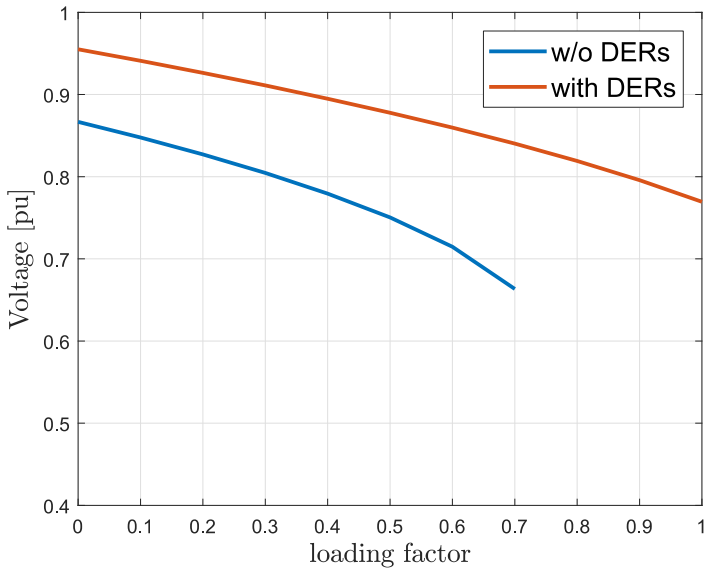

Figure 7-6: Voltage in pu at the point of interconnection with increasing loading factor of the distribution feeder i) with DERs and ii) without DERs.

7.4.1.3 Experiment 3

In this experiment the joint T&D framework is used to demonstrate the flow of power from the distribution network into the transmission network; i.e., reverse flow of power. This reverse flow of power is achieved by gradually increasing the penetration of DERs in the distribution feeder until the power flow direction is reversed. The results for the experiment are shown in Figure 7-7. The left vertical axis in the figure shows the active power transfer across the POI whereas the horizontal axis shows the penetration of DERs in the system as a function of its

scaling factor. It is shown that as the net penetration of DERs increase in the distributed feeder, the net active power transfer across the POI decreases. At around >1.2 times the rated capacity of DERs, the direction of flow of power is reversed with power flowing from the distribution feeder into the transmission network. On the right vertical axis of the figure, the voltage in pu for the POI is shown as a function of the variable DERs in the distribution feeder. As expected, the net increase in DERs result in a voltage magnitude increase at the POI. Akin to prior experiments, DERs are added to roughly 20 % of the distribution feeder nodes that carry electric load.

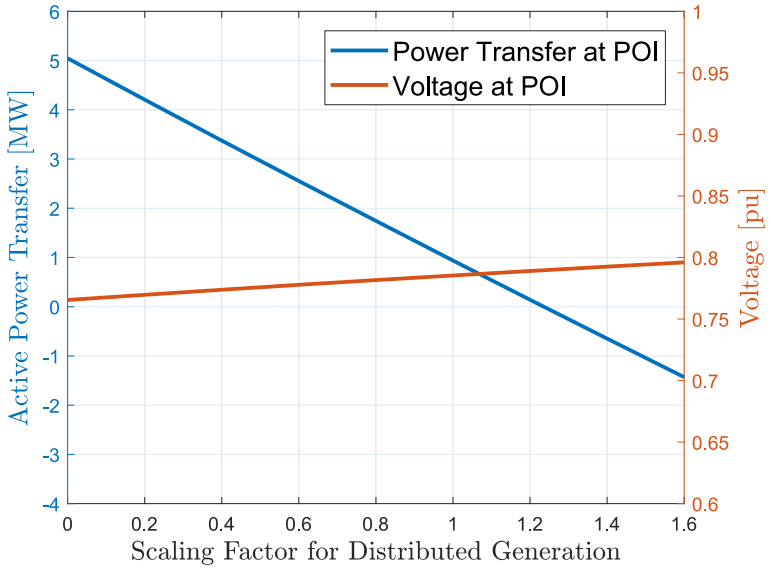

Figure 7-7: Reverse power flow observed during increasing DERs in the distribution feeder.

7.5 Joint T&D simulation on distributed cores with parallel computation

The experiments in the prior sub-section detail the equivalent circuit approach for joint T&D analysis on a single machine. However, while solving large joint T&D systems with hundreds of distribution networks connected to a single transmission network, the computational capacity and the system memory of a single machine may not be sufficient. Beyond a certain sized integrated system, the joint T&D simulation becomes computationally impractical on a single machine due to the large size of the solution matrix. Therefore, to address this limitation, we explore the use of a parallel simulation framework with the use of distributed cores or machines. In the proposed approach, the large integrated equivalent circuit with multiple transmission and distribution networks are "torn" into multiple sub-circuits using the theory of diakoptics [70],

first proposed by Kron. In the past, significant research has been carried out [71]-[73] for solving large circuits in parallel for solution matrices that have a special bordered block diagonal (BBD) structure. Interestingly, the solution matrix of the joint T&D simulation due to the hierarchical nature of the coupling between the various networks is inherently in BBD form, and therefore, the developed theory for parallel simulation in circuit simulation domain can be directly applied to our problem. One must note that the primary purpose of the following discussion within this section is not to develop parallel methods for power system simulation, but rather to introduce fundamental concepts and simple examples corresponding to the proposed equivalent circuit framework that in future may garner interest and further enable the available research in parallel circuit simulation to be applied directly to this problem [74], [78] and [81].

In the following sections, we discuss the "tearing" of large joint T&D system into multiple sub-circuits through domain-based decomposition [78]. We then briefly introduce the Gauss Seidel Newton (GSN) algorithm that can be used to solve a joint T&D problem in a parallel framework.

Importantly, one of the key prerequisites for a robust parallel simulation framework of a large T&D circuit is the ability to solve each individual sub-circuit robustly. In our case, this relates to solving the power flow and three-power flow equivalent circuits robustly. In a large simulation problem wherein, we may have hundreds, or even thousands of distribution networks connected to a single transmission network, it is of utmost importance that we can ensure robust convergence to a correct physical solution for each of the individual networks. Otherwise, it may cause severe bottlenecks in the overall problem convergence leading to divergence or even convergence to erroneous results. Our equivalent circuit framework with circuit simulation methods can ensure robust convergence for both the power flow and three power flow circuits, thereby extending the same robust properties to the parallel simulation framework.

7.5.1 Background

There has been extensive research towards the use of parallel simulation techniques for obtaining the DC and transient solution of very large integrated circuits [71]-[78]. The theory of diakoptics [70] and bordered block diagonal matrices [72] are integral to these solution methodologies and are developed within that work. We briefly discuss these key concepts in

following sub-sections and demonstrate how they can be extended to solve joint T&D problems in an equivalent circuit framework.

7.5.2 Diakoptics

Diakoptics, or the "methods for tearing" [70], involves taking a large problem and dividing it into the set of sub problems, which can then be solved independently prior to being coupled together again to provide an exact solution. The aim of this technique is to tear the network either through domain-based decomposition [78] prior to the construction of the solution matrix or through the direct partitioning of the solution matrix with no prior domain knowledge. In the joint T&D problem, the distribution feeders are known to be weakly coupled to the transmission network often at a single point of interconnection. This allows for the application of domain-based decomposition to "tear" the integrated T&D network into a set of sub-networks with POIs being the cut-set branches as shown in Figure 7-9. To numerically demonstrate the following, consider an aggregated T&D network with the following function form:

$$\mathcal{F}(\boldsymbol{V}_R, \boldsymbol{V}_I) = 0 \tag{104}$$

This large T&D network is torn into m independent sub-circuits that consist of the internal variables ($\boldsymbol{V}_R^{int}, \boldsymbol{V}_I^{int}$) that are only function of circuit elements within the sub-circuit and the external variables ($\boldsymbol{V}_R^{ext}, \boldsymbol{V}_I^{ext}$) that are functions of circuit element in the other sub-circuits [71]. The decomposed sub-circuits have the following function form:

$$\mathcal{F}_{int}\left(\boldsymbol{V}_R^{int}, \boldsymbol{V}_I^{int}, \boldsymbol{V}_R^{ext}, \boldsymbol{V}_I^{ext}\right) = 0 \tag{105}$$

$$\mathcal{F}_{ext}(\boldsymbol{V}_R^1, \boldsymbol{V}_I^1, \dots, \boldsymbol{V}_R^m, \boldsymbol{V}_I^m, \boldsymbol{V}_R^{ext}, \boldsymbol{V}_I^{ext}) = 0 \tag{106}$$

for $int = 1, \dots, m$, and $\{\boldsymbol{V}_R^{int}, \boldsymbol{V}_I^{int}\} \in \mathbb{R}^{n_i}$ are internal nodal voltages of sub-circuits, and $\{\boldsymbol{V}_R^{ext}, \boldsymbol{V}_I^{ext}\} \in \mathbb{R}^{n_e}$ are external nodal voltages.

7.5.3 Bordered Block Diagonal (BBD) Matrix Structure

In many fields of engineering and science, block bordered structured matrix-based problems arise. In the circuit simulation field, BBD matrix structure is common for representing the system

matrix for the VLSI circuits, wherein in the past partitioning (through node tearing or branch tearing) of the circuit is beneficial for parallel analyses. The ability to represent these large circuit's solution matrices in the BBD form allows for the use of vastly researched parallel sparse solver techniques [78] to obtain the system solution. The hierarchically structured joint T&D network, wherein a limited number of transmission networks supply bulk power to numerous local distribution feeders, is inherently representable in BBD form. For instance, consider Figure 7-8 in which three distribution networks are connected to a large transmission network. There exists a natural weak coupling between the different networks in the figure shown via the flow of current.

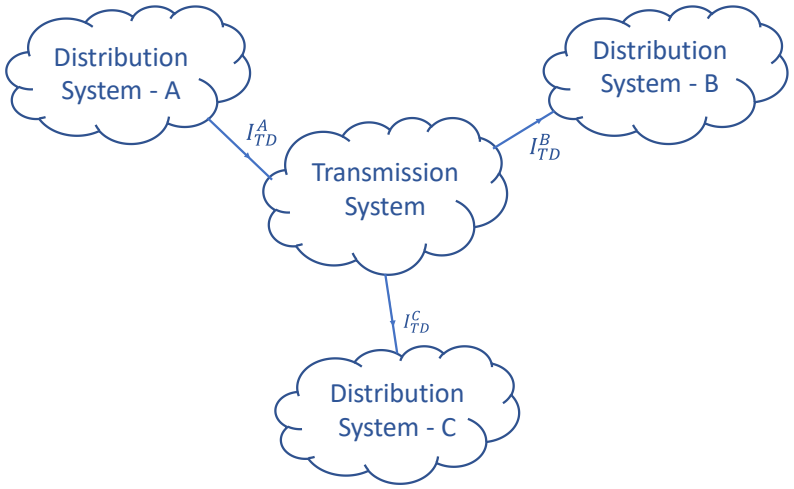

Figure 7-8: Weakly coupled transmission and distribution network.

This integrated network can be divided into a set of sub-systems (***S***) by the branch tearing technique at the coupling points between the transmission and distribution network, as shown in Figure 7-9.

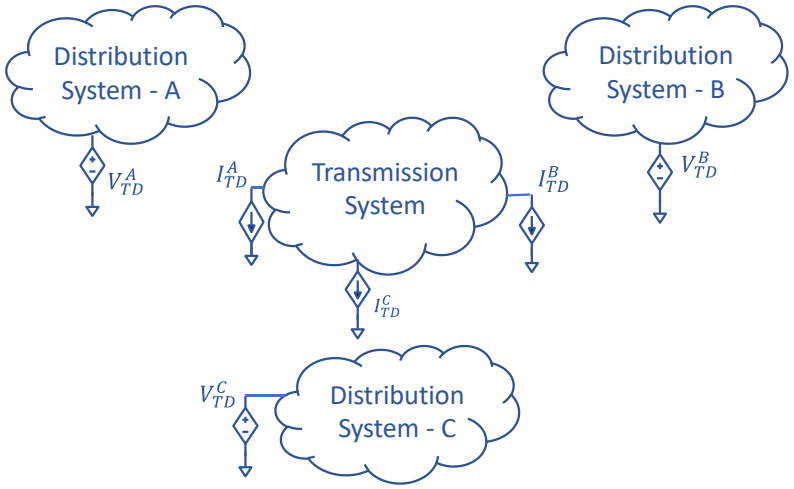

Figure 7-9: "Torn" transmission and distribution sub-systems.

The decomposed network is further representable in BBD form, as shown in Figure 7-10. The block diagonal terms in the matrix (T, D_A, D_B, D_C) represent the system Jacobian elements for the decomposed sub-circuits $(\boldsymbol{S} = \{\mathcal{F}_T, \mathcal{F}_{D_A}, \mathcal{F}_{D_B}, \mathcal{F}_{D_C}\})$ that are functions of sub-circuit's internal parameters $\{\boldsymbol{V}_R^{int}, \boldsymbol{V}_I^{int}\}$ whereas off-diagonal terms in the vertical right of the matrix i.e. (tt', td_a, td_b, td_c) are system Jacobian elements that are functions of sub-circuit's circuit external variables $\{\boldsymbol{V}_R^{ext}, \boldsymbol{V}_I^{ext}\}$. Remaining elements in the bottom of the matrix represent the Jacobian elements of the coupling sub-circuit (representing the port circuit equations) with respect to sub-circuits internal and external variables. Mathematically, these elements are given by:

$$T = \left\{\frac{\partial \mathcal{F}_T}{\partial \boldsymbol{V}_R^{i,int}}, \frac{\partial \mathcal{F}_T}{\partial \boldsymbol{V}_I^{i,int}}\right\}, i = 1, \dots, size(T) \tag{107}$$

$$tt' = \left\{\frac{\partial \mathcal{F}_T}{\partial \boldsymbol{V}_R^{i,ext}}, \frac{\partial \mathcal{F}_T}{\partial \boldsymbol{V}_I^{i,ext}}\right\}, i = 1, \dots, size(T) \tag{108}$$

$$TT' = \left\{\frac{\partial \mathcal{F}_C}{\partial \boldsymbol{V}_R^{i,ext}}, \frac{\partial \mathcal{F}_C}{\partial \boldsymbol{V}_I^{i,ext}}\right\}, i = 1, \dots, size(Y_C) \tag{109}$$

$$D_x = \left\{\frac{\partial \mathcal{F}_{D_x}}{\partial \boldsymbol{V}_R^{int}}, \frac{\partial \mathcal{F}_{D_x}}{\partial \boldsymbol{V}_I^{int}}\right\}, i = 1, \dots, size(D_x) \;\&\; x = \{A, B, C\} \tag{110}$$

$$td_x = \left\{\frac{\partial \mathcal{F}_{D_x}}{\partial \boldsymbol{V}_R^{ext}}, \frac{\partial \mathcal{F}_{D_x}}{\partial \boldsymbol{V}_I^{ext}}\right\}, i = 1, \dots, size(D_x) \;\&\; x = \{A, B, C\} \tag{111}$$

$$TD_x = \left\{ \frac{\partial \mathcal{F}_C}{\partial \boldsymbol{V}_R^{i,ext}}, \frac{\partial \mathcal{F}_C}{\partial \boldsymbol{V}_I^{i,ext}} \right\}, i = 1, \dots, size(Y_C) \;\&\; x = \{A, B, C\} \tag{112}$$

where set $\{A, B, C\}$ represents different sub-circuits for the distribution system. In the following section we discuss one of the techniques, i.e. Gauss Seidel Newton (GSN) method, for solving the BBD form joint T&D parallel problem.

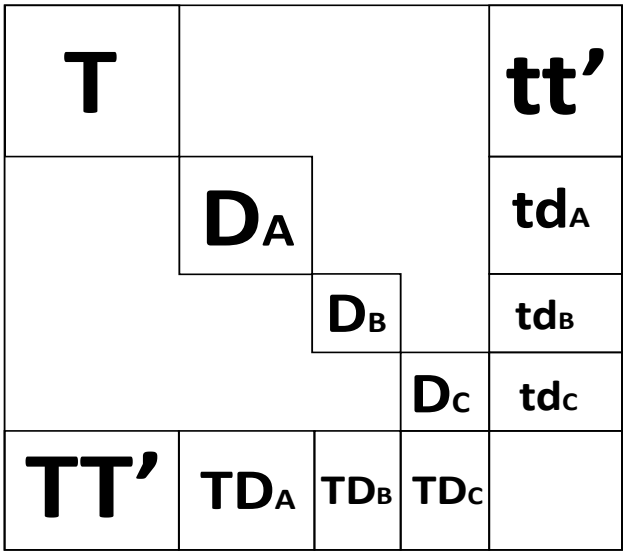

Figure 7-10: Bordered Block Diagonal structure for joint transmission and distribution system.

7.5.4 Gauss-Seidel-Newton Approach

We make use of the Gauss-Seidel-Newton (GSN) method [75], [80] to solve the set of sub-systems given by decomposed joint T&D sub-circuits. The subsystems are chosen such that the set of internal nodes ($\boldsymbol{x}^{int}$) for each sub system are far larger than the number of external coupling nodes ($\boldsymbol{x}^{ext}$). In this algorithm, within the inner loop, the set of independent sub-systems ($\boldsymbol{S}$) are solved in parallel using block NR algorithm until convergence or for a limited number of iterations. In this inner loop, the external coupling variables ($\boldsymbol{V}_R^{ext}$, $\boldsymbol{V}_I^{ext}$) are kept constant for each sub-circuit, whereas the internal variables ($\boldsymbol{V}_R^{int}$, $\boldsymbol{V}_I^{int}$) are solved for iteratively. In the outer loop, the external coupling variables from each sub-system are then fan out to other sub-systems via a Gauss step and the inner loop of NRs are performed again. This iterative algorithm is then repeated until the error of external coupling variables communicated between the consecutive

outer loops (*epochs*) are within a certain tolerance. This algorithm is graphically shown in Algorithm 7-1.

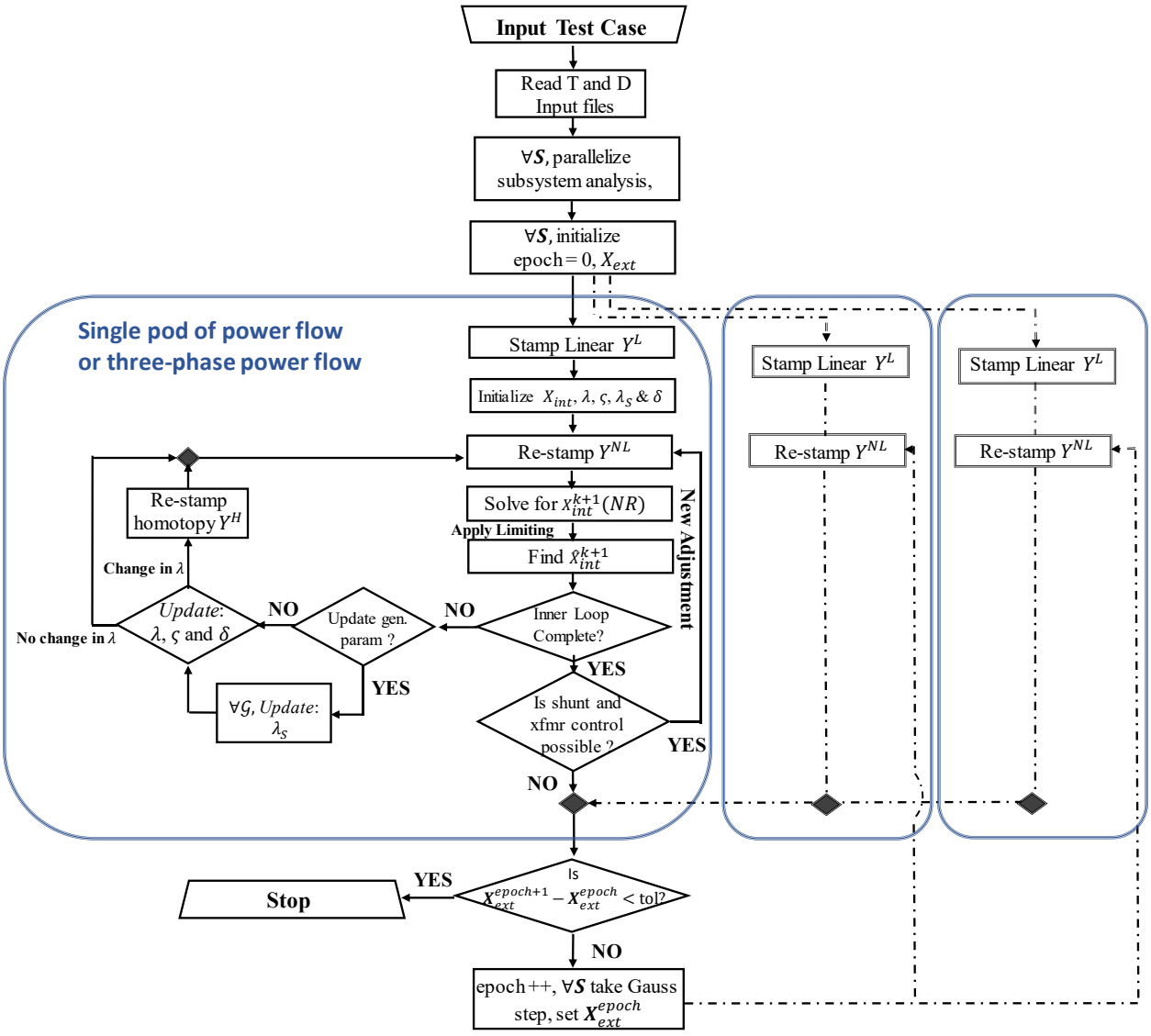

Algorithm 7-1: Parallel joint transmission and distribution using Gauss-Seidel-Newton method.

7.5.5 Validation

To validate the distributed parallel simulation framework for joint T&D problems, we compare the results obtained from the parallel algorithm using GSN on multiple cores against those produced by direct NR algorithm on a single core as described in Section 7.4. To setup the comparison, we couple an ~8000-node taxonomical distribution system [76] with a 9241 PEGASE

test case at the transmission node 2519. We then simulate the coupled system for different loading factors of the distribution network with the following algorithms:

i. The coupled network solved at once on a single core using direct NR algorithm

ii. The coupled network decomposed and solved in parallel on multiple cores using GSN algorithm

Figure 7-11 shows that the results obtained from the single core NR setup compare well with those obtained from the parallel simulation setup using GSN.

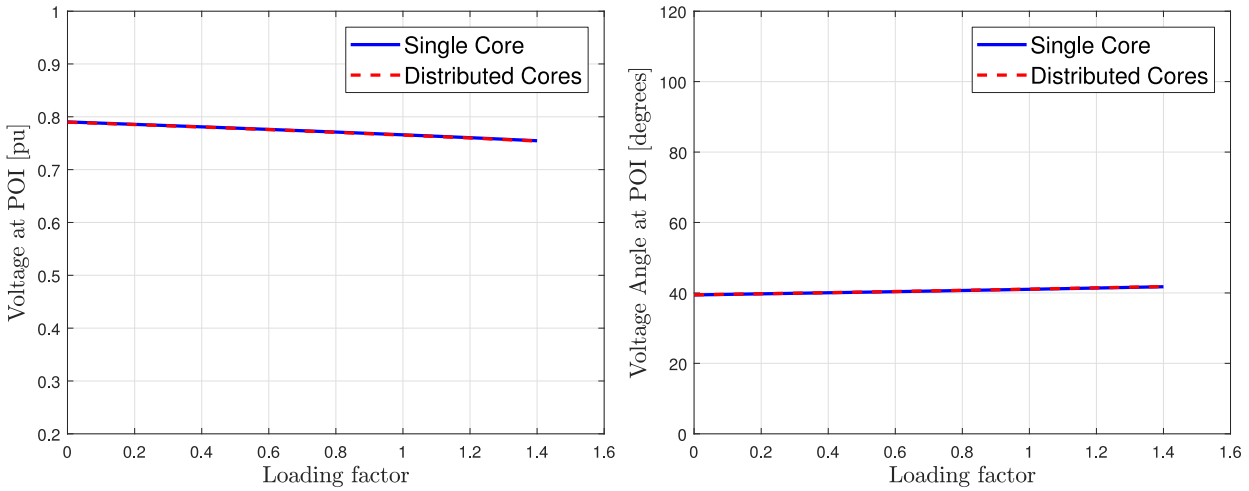

Figure 7-11: Comparison of joint T&D simulation algorithms: i) Single machine setup using NR (in blue), ii) Parallel simulation on distributed cores using GSN (in red).

7.5.6 Joint transmission and distribution analysis on a large system

To perform this experiment, 50 distribution feeders, each representing roughly 8000 nodes, were coupled to a large realistic transmission network at different locations. The eastern interconnection test case with roughly 85k+ nodes is used to represent the transmission network, and the set of distribution systems are represented via open-source taxonomical feeder test cases [76]. This problem represents a solution matrix size of roughly 3 million rank with a total of ~3x4,00,000 distribution nodes and ~85000 transmission nodes. We simulated the case using GSN until completion. In the final solution, the POI voltages were all found to be within the acceptable range of 0.8-1.2 pu and the complete simulation took less than a couple of minutes to converge

with Tx-stepping method enabled. The Figure 7-12 represents the evolution of the sub-station voltages at the POI during the Gauss-step in the outer loop of the parallel joint T&D simulation.

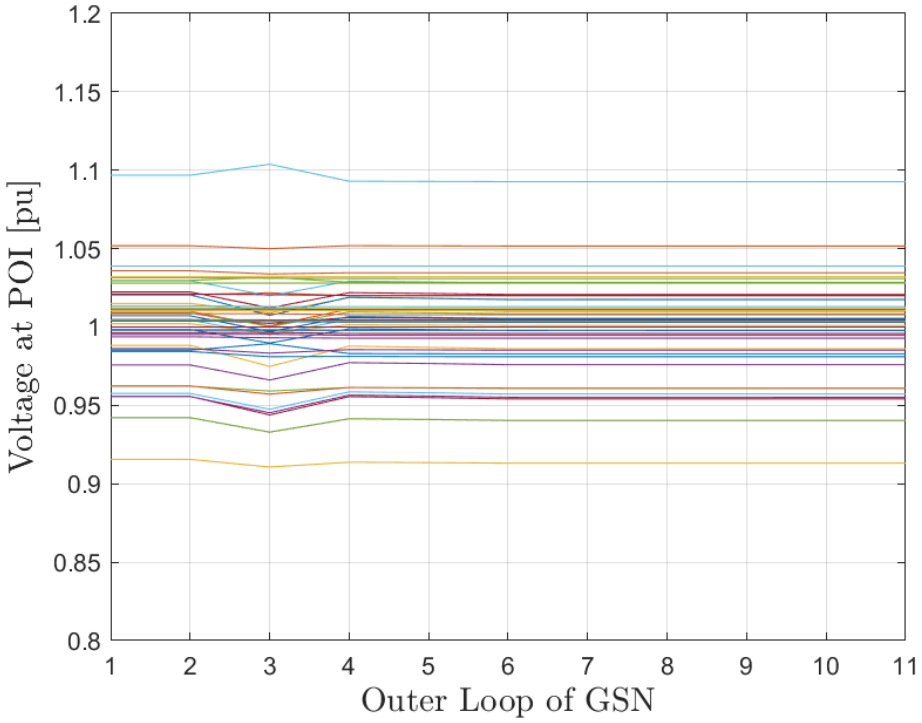

Figure 7-12: Voltages at the POI in the outer loop of GSN.

7.6 Notes on Convergence

Suppose that the system of non-linear equations that represents the large joint interconnected transmission and distribution network is given by:

$$JV = I \tag{113}$$

where matrix J has the form given in Figure 7-10. To further explore the convergence properties, this matrix J can be split into two components given by:

$$J = M - N \tag{114}$$

In general, for the Gauss-Seidal-Newton (GSN) algorithm to guarantee convergence for the decomposed matrix J the spectral radius of the iteration matrix ($\rho(M^{-1}N)$) needs to be less than

1. However, a less strict condition that requires the solution matrix to be point-wise strictly diagonal dominant is often sufficient i.e.

$$\sum_{i \neq j}^{n} |a_{ij}| \leq |a_{ii}|, \text{for all } i \tag{115}$$

where a_{ij} is a value in the matrix for i^{th} row and j^{th} column.

Due to the reason that the solution matrix J is representable in BBDF form, a much milder condition can guarantee convergence for the partitioned system. If the joint system is represented as an aggregated equivalent circuit and is partitioned into sub-circuits at multiple "tearing" nodes, then the existence of a capacitance at sub-set of these "tearing" nodes with a large enough value can guarantee convergence for the partitioned system via GSN algorithm [81]. This is a much milder sufficient condition for convergence when compared against the strict diagonal dominance condition for a general matrix that requires a large value capacitor from each node in the system to ground. However, modifications (adding a high value capacitance from the "tearing" node to ground) such as these are often unwarranted as they change the inherent structure of the problem, and therefore, other convergence techniques should be explored.

One such method is presented in [82] and ensures convergence for the power flow network-based problems via GSN by partitioning the matrix into BBDF such that the spectral radius of the iteration matrix corresponding to the partitioned system is ensured to be less than one. The work in [82] partitions the solution matrix J into M and N such that $J = M - N$, where M is a block diagonal matrix capturing the interactions between the internal variables of each block sub-circuit and N is the off-diagonal matrix that captures the communication between the variables of other sub-circuits. To ensure convergence by GSN, the method introduces a diagonal matrix $\bar{E}$, such that the matrices M and N are modified as follows:

$$M = D + \alpha\bar{E} \tag{116}$$

$$N = \alpha\bar{E} - E \tag{117}$$

where, $J = D + E$. It is shown in [82] that by choosing the value of $\alpha = \frac{1}{2}$, the algorithm can ensure convergence for the partitioned system.

Furthermore, it should be noted that other methods such as the use of distributed Schur's complement [85] can also be used to extract the exact solution of the linearized matrix J_l for $J_l V = I_L$ at each step of NR given that the linearized matrix J_l is in BBDF.

8. Conclusions and Future Work

The U.S. Department of Energy's Quadrennial Technology Review [79] underscores the need for "high-fidelity planning models, tools, and simulators and a common framework for modeling, including databases" for the future grid of tomorrow. Towards the direction of the common goal set forth in that report, this thesis developed a generic framework for modeling both the transmission as well as the distribution grid including novel methods that can solve robustly for the steady-state operating point of these network models. This is a significant advancement over state-of-art tools used today that use disparate tools and methods for transmission and distribution grid analysis and often require a good initial guess for obtaining the steady-state operating point of the grid. Within the scope of this thesis, to demonstrate the efficacy of the proposed framework while also validating the methodology, we developed a power system analyses tool SUGAR (Simulation with Unified Grid Analyses and Renewables) that can solve for the steady-state operating point of any transmission or distribution network from arbitrary initial conditions.

The different chapters of this thesis were devoted to different pieces of the complete puzzle; i.e., the robust steady-state analysis of the power grid. Chapter 5 introduced the concept of the equivalent circuit framework for power flow and three-phase power flow analyses. It developed models for some of the most common transmission as well as distribution network elements. Furthermore, it illustrated that any physics-based or measurement-based model derived in terms of current and voltage state variables can be directly incorporated into the equivalent circuit framework. Importantly, the developed framework treated the transmission grid positive-sequence models no differently than the distribution grid three-phase models, and as such allowed for methods to be developed in the Chapter 6 that can ensure convergence for these network models to correct physical solutions.

Chapter 6 extended and further developed new circuit simulation methods for the field of power system analyses, specifically for the power flow and the three-phase power flow analyses.

The first part of the chapter extended with modifications existing limiting methods used in the field of circuit simulation to power flow and three-phase power flow analyses. For hard-to-solve ill conditioned and large test cases, where these preliminary methods fail to ensure convergence to correct physical solutions, the chapter developed novel homotopy methods namely the Tx stepping method and dynamic power stepping method to ensure convergence to correct physical solutions. The results section of this chapter combined the equivalent circuit framework with developed circuit simulation methods to solve ill-conditioned as well as large networks for both power flow and three-phase power flow problems independent of the choice of initial conditions.

Chapter 7 addressed another key challenge within existing approaches for steady-state analysis of the power grid; i.e., a robust joint transmission and distribution (T&D) analysis framework. The existing use of disparate algorithms and solution methodologies for transmission power flow and distribution three-phase power flow problems has made it all but impossible to robustly solve the joint T&D system. As underscored previously, the proposed equivalent circuit approach in Chapter 5 treated the transmission grid equivalent circuits no different from the distribution grid equivalent circuits and as such can combine the two networks without loss of generality, while also broadly applying the developed circuit simulation methods to ensure robust convergence to correct physical solutions for the steady-state analysis of joint T&D system. Two approaches to solving the joint problem were proposed in this chapter. The first approach combined the transmission grid equivalent circuit with the distribution grid equivalent circuit at the point of interconnection and solved the combined system on a single machine as one problem using NR. For larger joint T&D systems with hundreds of distribution networks connected to a large realistic meshed transmission network, we proposed another approach. In this approach, a parallel distributed simulation framework for solving the joint T&D problem was briefly explored. The bordered block diagonal structure of the joint T&D problem is exploited to apply previously developed parallel simulation methods in the circuit simulation field directly to this problem. As an example, the Gauss-Seidel-Newton method was used to solve a large joint T&D system to ensure convergence to the correct physical solution.

Importantly circuit simulation techniques for power system analysis that were developed and discussed within this thesis are by no means exhaustive. Future work toward extending these techniques will include application of these methods or some modifications of it to other power system analysis such as in the case of optimal power flow and probabilistic power flow analysis. In general, these homotopy and limiting methods work by capturing the physics of the power grid network equations to simplify a complex problem and solve it. Therefore, in the future, any problem that requires to solve the power grid network equations within its framework can directly use these methods without loss of generality to ensure robust convergence.

Given that these methods were primarily designed to ensure robust convergence, much less rigor was spent within the scope of this thesis on optimizing these methods for computational speed. Even though it has been demonstrated that our tool SUGAR compares well in terms of speed against other state-of-art tools used in the industry today, we plan to adapt these methods to optimize for computational speed as well. This is pertinent to run computationally intensive simulations, such as the contingency analysis and probabilistic analysis, for time-critical operations of the power grid.

In Chapter 7, this thesis briefly explored the use of parallel simulation methods for solving the joint T&D problem. In the future, we plan to build on this fundamental concept by further probing into the theoretical guarantees for convergence of different parallel simulation algorithms that are available for the BBDF structured problems. This will necessitate the future exploration of other methods, such as the multi-level newton methods [71]-[77], within our framework for the parallel joint T&D simulation.

Appendix A. BIG Model: Linear Model for Aggregated Load in the Power Grid

A.1 Background

In traditional power flow and three-phase power flow analyses, non-linear models are used to characterize the aggregated electric load behavior. These models are often insensitive to system voltages (as in the case of PQ load model) and introduce strong non-linearities in the formulation (as in the case of ZIP load model). Interestingly, some of the challenges in terms of solution accuracy and convergence for both these analyses are often due to these models that are used to mimic the behavior of aggregated electric load in the system. For instance, consider the B.C. Hydro system wherein it was shown that decreasing the substation voltage by 1% decreased the active and reactive power demand by 1.5% and 3.4%, respectively [83]. PQ load models that make up the bulk of the aggregated load models used today are purely based on constant power variables and are independent of the complex voltage magnitude or angle at the connected node and therefore cannot replicate this behavior. Improvements to the PQ load models (e.g. ZIP model, exponential) can better characterize the voltage sensitive load behavior by incorporating the voltage magnitude dependency; however, like in the case of the PQ load model, they introduce significant non-linearities in the formulation. Furthermore, ZIP and exponential load models cannot characterize load characteristics on a constant voltage node in the system (e.g. load connected to a generator node) as the load magnitudes for these load models are independent of the voltage angle information at the connected node. To address these drawbacks, we developed a linear load model [44]-[47] that can capture the true voltage sensitivities for the aggregated load in the system.

To develop a load model to better characterize the true physics of the grid, we began with understanding the electric load behavior by observing the measurement data for a randomly chosen 48-hour period for the Carnegie Mellon University (CMU) campus as shown in Figure A-

1. We can infer from the figure that the load current variation (I_R and I_I) can be attributed to two factors: 1) system voltage variation and 2) variation in actual load demand (i.e. devices turning on and off).

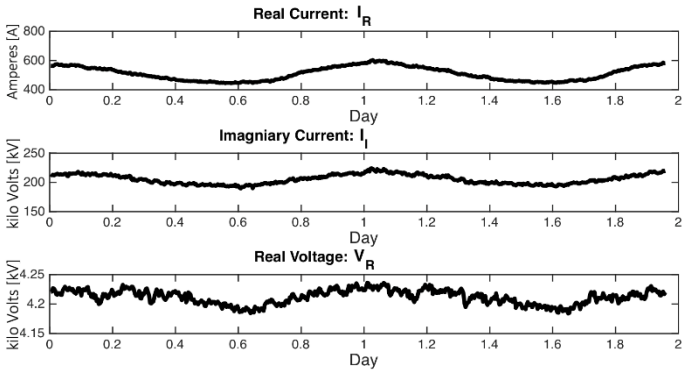

Figure A-1: CMU Dataset - current (real and imaginary), and voltage over time (2 days).

Therefore, to accurately capture the load behavior, the developed load model template needs to characterize the base load as well as the voltage sensitivities of the base load correctly. We developed a circuit theoretic model called *BIG* load model in [44]-[45] to achieve exactly that. Furthermore in [46]-[47], we explored the use of machine learning algorithms for fitting this *BIG* load model template. In the following sub-section, we will document and briefly discuss the development of this circuit theoretic load model, following which we explore the major contributions of the proposed *BIG* load model.

A.2 Circuit Theoretic *BIG* Load Model

A first-order impedance model can be used to represent any phase and magnitude relationship between current and voltage phasors at a single frequency as shown in Figure A-2. This first-order load impedance can be represented as an equivalent circuit model via a conductance (G) and susceptance (B) in series or parallel, and as such, would capture the load behavior wherein the current flowing into the load bus is directly proportional to the voltage across it. However, the aggregated loads can sometimes behave contrary to this behavior; for example, consider an aggregated load with a large percentage of induction motors that run to maintain a constant mechanical torque. Such loads are likely to exhibit a behavior wherein the current flowing into the load bus is inversely proportional to the applied voltage. This behavior is like that of a

constant PQ load model, where the increase in voltage has no influence on the constant power P and would conceptually correspond to a decrease in current.

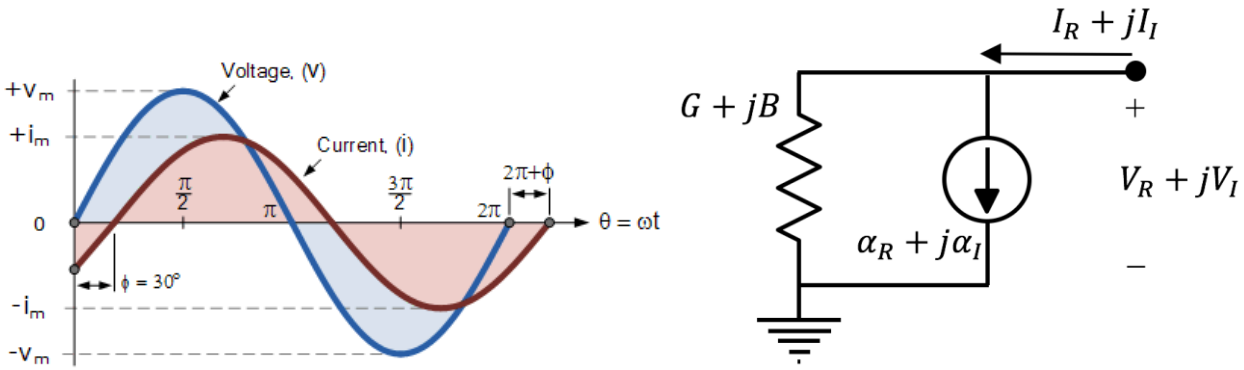

Figure A-2: First-Order Load Model.

To begin from a circuit modeling perspective, we consider a load model for a generalized aggregated load in the system that could capture both positive and negative voltage sensitivities for the load current.

First, we derive the circuit to capture negative sensitivities of load currents to system voltages. To do so let us consider the governing equation for the PQ load model:

$$I_R^{PQ} + jI_I^{PQ} = \frac{PV_R + QV_I}{V_R^2 + V_I^2} + j\frac{PV_I - QV_R}{V_R^2 + V_I^2} \tag{118}$$

We can split the complex current function in (118) and linearize it to obtain the real and imaginary terms:

$$I_R^{PQ\,k+1} = 2I_R^{PQ\,k} + \frac{\partial I_R^{PQ}}{\partial V_R}V_R^{k+1} + \frac{\partial I_R^{PQ}}{\partial V_I}V_I^{k+1} \tag{119}$$

$$I_I^{PQ\,k+1} = 2I_I^{PQ\,k} + \frac{\partial I_I^{PQ}}{\partial V_R}V_R^{k+1} + \frac{\partial I_I^{PQ}}{\partial V_I}V_I^{k+1} \tag{120}$$

where the constant terms represent the values of real and imaginary currents known from k^{th} iteration and are represented by a constant current source. Note that partial derivatives for which the real and imaginary currents are directly proportional to the voltages across the respective split circuit models, i.e. real and imaginary, are represented as a conductance (G), while the partial

derivatives for which real and imaginary currents are directly proportional to the voltages of other sub circuits are represented by a voltage controlled current source (B).

Furthermore, it can be shown that the respective partial derivatives defined in (119) and (120) have the following properties representing negative sensitivities:

$$\frac{\partial I_R^{PQ}}{\partial V_R} = \frac{\partial I_I^{PQ}}{\partial V_I} \equiv G < 0 \tag{121}$$

$$\left|\frac{\partial I_R^{PQ}}{\partial V_I}\right| = \left|\frac{\partial I_I^{PQ}}{\partial V_R}\right| \equiv B \tag{122}$$

From (119) and (120) we can observe that the governing equations of a PQ load model, i.e. (118), can be translated to an equivalent circuit corresponding to a constant current source in parallel with the susceptance and a negative conductance that compensates for the inverse relationship between the current and voltage of the load. With this model, as the voltage across the load increases, the current will decrease and vice versa. This model is now extended to even capture positive sensitivities of the load current to voltage sensitivities.

To capture both load type sensitivities with respect to voltage, we consider the complex governing equation of the generalized load current that is given by:

$$I_R + jI_I = \alpha_R + j\alpha_I + (V_R + jV_I)(G + jB) \tag{123}$$

where the complex admittance $(G + jB)$ with positive G captures the constant impedance load behavior and is directly proportional to the voltage across the load, and the combined impedances capture the voltage sensitivities. Specifically, a negative conductance in conjunction with complex current $(\alpha_R + j\alpha_I)$ will mimic the inverse current/voltage sensitivity relationship and positive conductance will represent the other. Both the positive and negative impedances capture the change in load with voltage with respect to the portion of the load that is modeled by the current source.

The complex equivalent circuit and the split-circuit of the proposed susceptance (B), current source (I), and conductance (G) load model, *BIG*, defined by equations (124)-(125), is shown in Figure A-3.

$$I_R = \alpha_R + V_R G - V_I B \tag{124}$$

$$I_I = \alpha_I + V_I G + V_R B \tag{125}$$

It is worth noting that the *BIG* model is equivalent to the ZIP load model with the real power coefficient set to zero and a different "fixed complex current" term. Most importantly, the *BIG* load model is linear in a current/voltage formulation, while the ZIP model is nonlinear in both current/voltage and traditional PQV formulations. In addition, the *BIG* model can capture dependency of load with respect to the voltage angle.

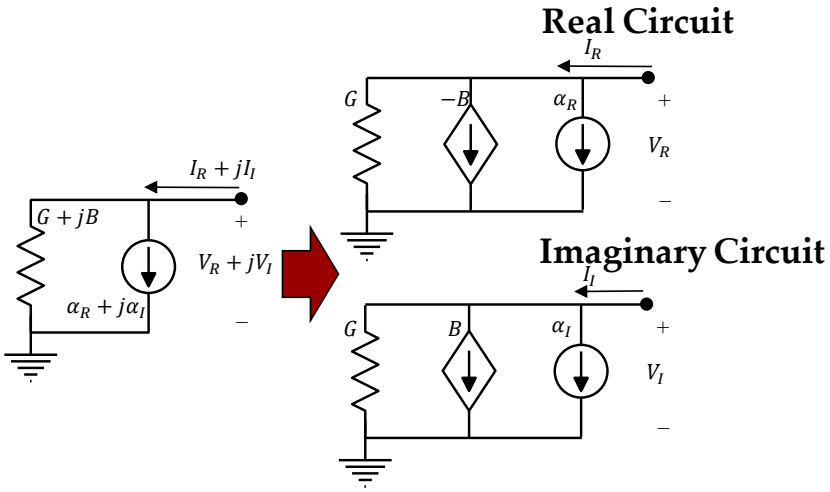

Figure A-3: *BIG* Load Model.

A.3 Contributions of *BIG* Load Models

The *BIG* load model has many benefits over existing aggregated load models. Among these, the four that are most important are as follows:

A.3.1 Linearity

The *BIG* load model is a linear load model as shown in [44] and results in linear network constraints for the network in the equivalent circuit approach. This contrasts with non-linear PQ

and ZIP load models. The use of the *BIG* load model significantly reduces the non-linearities in our equivalent circuit framework thereby significantly reducing the probability of the solver to result in divergence or convergence to an erroneous solution. Importantly the *BIG* load model still results in non-linear network constraints with the use of the 'PQV' formulation and therefore does not extend the same benefits as it does in the case of the equivalent circuit framework.

A.3.2 Captures voltage sensitivities

The *BIG* load model when parameterized using real measurement data captures the true sensitivities of the load currents (as a function of system voltage) at the given operating point. This further enables the use of linearized equivalent circuits for any further analysis around the operating point. Accurate analysis with a linearized system requires the system sensitivities to be accurately defined as is done via the *BIG* load model. Figure A-4 shows the measured real and imaginary currents for the Carnegie Mellon campus and the constructed currents using the *BIG* load model segments [47]. In the figure, the *BIG* model load model is shown to capture the true sensitivity of the measured load currents in the system. This contrasts with all existing aggregated load models in the literature.

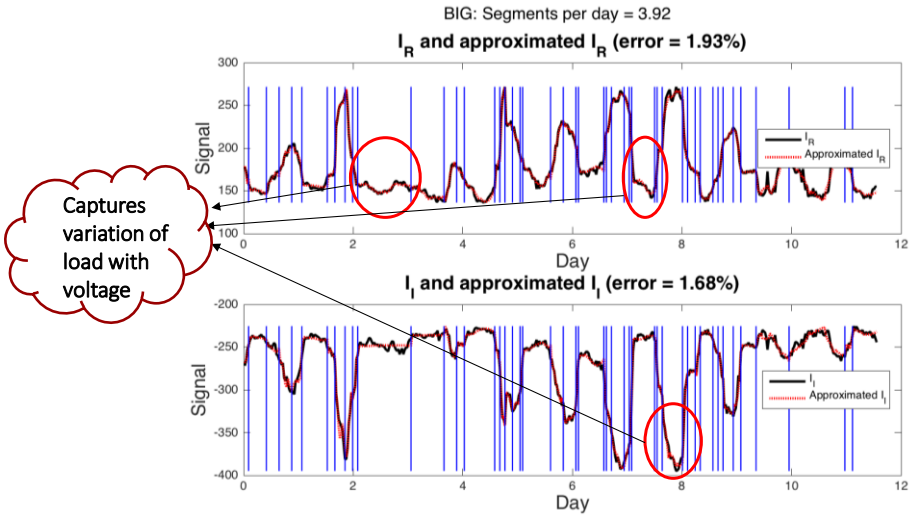

Figure A-4: *BIG* load model is shown to capture the voltage sensitivities if the measured CMU system load [84].

Another experiment that demonstrates the ability of the *BIG* load model to capture true voltage sensitivities is performed. In this experiment, a synthetic test grid is setup with incorporation of

physics-based load models for IMs, resistive heater load, and capacitors banks. Synthetic measurement data is then generated for days for a range of voltage inputs. The *BIG* load model and *PQ* load model parameters are then fitted based on the synthetic measurement data using the same methods as described in [46]-[47]. Now to evaluate and further validate the sensitivity of the fitted load model to the system voltages, the source voltages are decreased and increased by 5 % respectively, and new synthetic measurements are produced from the test grid. As it is seen in Figure A-5, the previously fitted *BIG* load models can still capture the load characteristics accurately with perturbed voltages whereas the PQ load model results in erroneous currents.

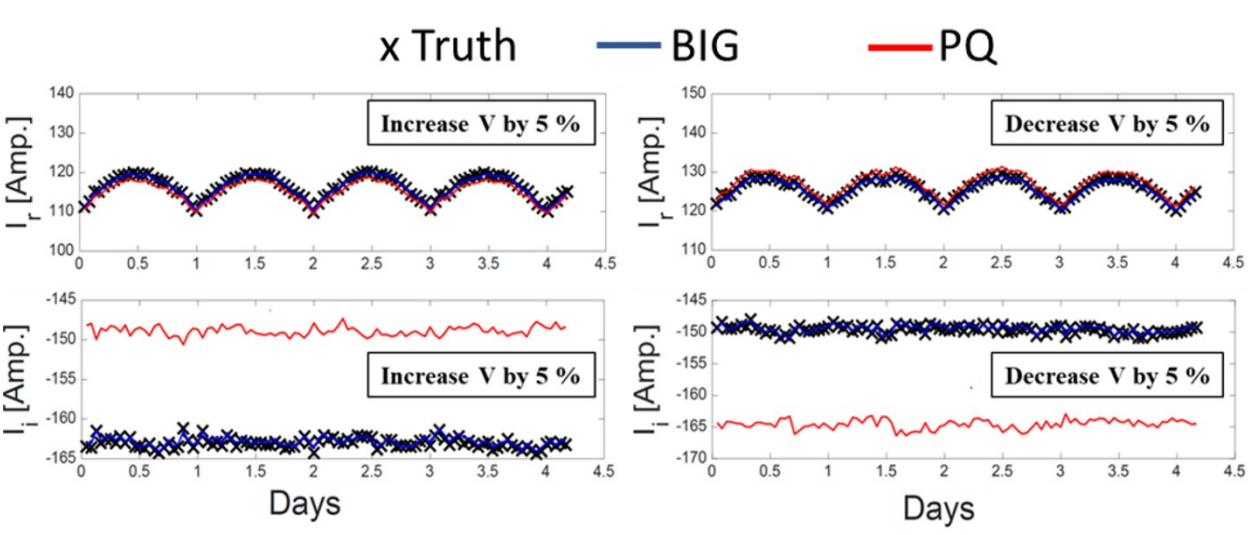

Figure A-5: Fitted *BIG* versus PQ load model with perturbed system voltages [84].

A.3.3 Captures voltage angle information

Unlike PQ and ZIP load models that are either fixed in magnitude or voltage magnitude dependent only, the *BIG* load models consider sensitivity to both the voltage magnitude and voltage angle. This allows for modeling of complex voltage sensitive aggregated load that is connected to constant voltage magnitude (PV buses) nodes in the system whose behavior would be like the one represented in Figure A-6. The figure illustrates complex voltage characteristics of a PV node in a power flow case study where the real power load connected to the PV node is varied from 100 MW to 650 MW. The graph shows that the real power absorbed by the PV node is independent of the voltage magnitude at that node and can be represented as a function of voltage angle (with respect to the reference) only. Therefore, existing load models such constant

PQ and voltage magnitude dependent ZIP model will fail to model this behavior, whereas the proposed *BIG* load model can capture it.

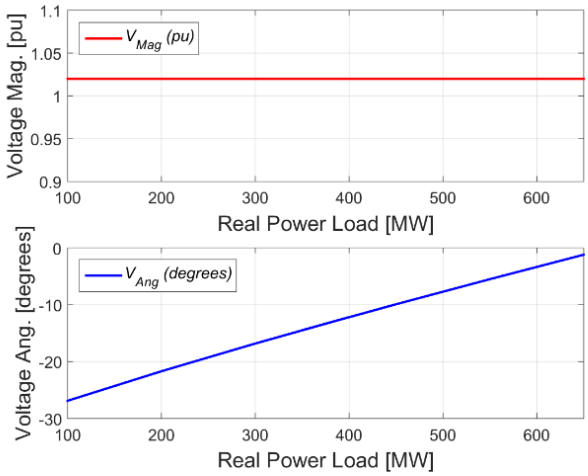

Figure A-6: Complex voltage profile on PV node with variable real power injection.

A.3.4 Generic Model for both power flow and transient analysis

Importantly, BIG load model unlike ZIP and PQ load model can be used for both transient analysis as well as power flow and three-phase power flow analysis without any modification; hence enabling the unification of the two analysis as discussed in Appendix B. PQ and ZIP load models cannot be directly used for time-domain transient analysis due to the existence of time-average power terms.

Appendix B. Unified Power System Analyses and Models

B.1 Introduction

One of the key underlying challenges in the existing power system analyses is the lack of consistent solutions between the steady-state analysis (power flow and three-phase power flow) and the steady state obtained from time-domain transient analysis. In general, the expectation is for the final steady state of the transient response to match exactly the balanced power flow solution or the three-phase power flow solution. However, this is generally not the case in the existing framework for power system analysis where the nonuse of standardized modeling and solution methods between the steady-state and the transient analyses result in inconsistent and often erroneous results. This contrasts with what's observed in the field of circuit simulation [43], wherein standardization of models and algorithms guarantees consistent solutions between the steady state and time-domain transient analyses for electronic circuits with billion plus nodes.

The most notable cause for inconsistent solutions between the steady-state and the transient analyses is the use of disparate models for aggregated loads and generators in the two analyses. In steady-state power flow and three-phase power flow analyses, power variables with time average magnitudes and phasor relationship are used to model the aggregated loads as well as the generators (PV/PQ models). These models are inherently incompatible with time domain analysis, where instead physics-based models or some form of approximation of the constant power models (e.g. constant impedance) are used to represent the same resulting in inconsistent solutions between the two analyses. To enable consistent solutions between the two analyses requires that either the network models are derived from the true physics of the equipment or are aggregated such that they can be represented in terms of voltages and currents in both time-domain and frequency-domain without loss of generality.

In the past, the use of real and reactive power variables to model the aggregated load and generation for positive sequence and three-phase power flow was necessary due to the inability of the exiting frameworks to include physics-based models directly and due to the lack of real synchronized measurement data for the power grid that could characterize the load behavior in terms of currents and voltages. However, the advent of phasor measurement units (PMUs) with time stamped voltage and current measurements has allowed for aggregated load characterization using real measurement data with voltage and current as unknown variables as shown in the case of the *BIG* load model in the previous Appendix A. In this appendix as an alternative approach, we explore the use of physics-based models that can be generically used in both the power flow as well as the time-domain transient analyses. Importantly, both these approaches: i) measurement-based empirical modeling (in Appendix A) and physics-based modeling (discussed within this appendix) are generically applicable to both the steady-state as well as time-domain transient analyses and hence result in consistent solutions between the two.

To demonstrate the use of physics-based models in the equivalent circuit approach for both the time-domain analysis and power flow analysis we consider a simple model of a three-phase squirrel cage induction motor (IM) developed in Section 5.5. This model is used to create a simple example test network and is used to demonstrate consistent solution between the transient and steady-state analyses. The trivial network used for the following results includes an IM model connected to a independent voltage source through a transmission line.

B.2 Validation of IM model

To first validate the physics-based model of the IM that is developed in Section 5.5, we run a time-domain analysis on the test network, which simulates IM's starting characteristics from stand still to rated speed. We simulate this in our prototype SUGAR transient analysis tool and compare the produced results against those produced by the same IM model in MATLAB SimscapePowerSystems (SPS). Figure B-1 shows the response of IM's critical parameters during motor start-up and past that into the steady-state region for both the simulation tools. The evolution of motor state variables over time exhibit similar form and shape when simulated with

both the SimscapePowerSystems and the SUGAR thus validating the developed model for IM for both transient and stead-state operating region.

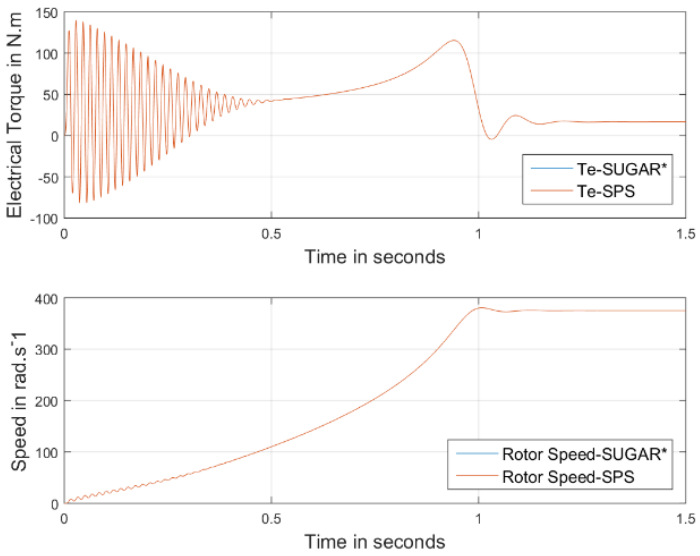

Figure B-1: Electrical Torque and Rotor Speed comparison between SimscapePowerSystems (SPS) and SUGAR with SUGAR restricted to maximum of one N-R iteration.

B.3 Solution consistency between the steady-state and transient analysis

Next, we demonstrate that the derived IM model results in consistent solutions for both the steady-state from the transient analysis as well as the steady-state from the power flow analysis. For this experiment, the power flow model of IM developed in Section 5.5 is used. To run power flow analysis, the source frequency of the IM steady-state model is set to system frequency. The results from the steady state solver are then compared against the one obtained from the transient solver for the same IM. The time-domain transient analysis is run from t=0 to an approximate steady state condition at t=1.5 seconds as shown in Figure B-1. The comparison of results is documented in Table B-1 and are a perfect match between the two analyses to at least three significant digits.

TABLE B-1: IM RESULTS IN EQUIVALENT CIRCUIT FRAMEWORK FOR STEADY-STATE (POWER FLOW) AND TIME-DOMAIN TRANSIENT ANALYSIS

Parameter	Unit	Steady State	Transient @ t=1.5 sec
Rotor Speed	$rad.s^{-1}$	375.01	375.01
Electric Torque	N.m	16.64	16.64
Stator direct-axis current	Amps	-11.36	-11.36
Stator quadrature-axis current	Amps	13.09	13.09
Rotor direct-axis current	Amps	11.56	11.56
Rotor quadrature-axis current	Amps	-0.49	-0.49

9. References

[1] Quadrennial Energy Review: Energy Transmission, Storage, and Distribution Infrastructure, April 2015.

[2] "The disaster that could follow from a flash in the sky", Economist, July 13th, 2017.

[3] W. F. Tinney and C. E. Hart, "Power flow solutions by Newton's method," IEEE Transactions on PAS, Vol. 86, No. 11, pp. 1449-1460, Nov. 1967.

[4] D. Shiromohammadi, H. W. Hong, A. Semlyen, G. X. Luo, "A compensation-based power flow method for weakly meshed distribution and transmission networks", *IEEE Transactions on Power Systems*, Vol. 3, No. 2, May 1988.

[5] P. A. N. Garcia, J. L. R. Pereria, S. Carneiro Jr., M. P. Vinagre, F. V. Gomes, "Improvements in the Representation of PV Buses on Three-Phase Distribution Power Flow", *IEEE Transactions on Power Systems*, Vol. 19, No. 2, April 2004.

[6] J. Bebic, "Power Systems Operation and Planning Practices and Challenges," *ARPA-E Interconnected- Highly Utilized Grid Workshop*, Sept. 2016.

[7] S. Grijalva, "Planning and Operational Challenges in Interconnected DER-based Grids," *ARPA-E Interconnected- Highly Utilized Grid Workshop*, Sept. 2016.

[8] H.W. Dommel, W.F. Tinney, and W.L. Powell, "Further developments in Newton's method for power system applications," *IEEE Winter Power Meeting, Conference Paper No. 70 CP 161-PWR New York,* January 1970.

[9] W. Murray, T. T. De Rubira, and A. Wigington, "Improving the robustness of Newton-based power flow methods to cope with poor initial conditions", North American Power Symposium (NAPS), 2013.

[10] A. G. Exposito, E. R. Ramos, "Reliable Load Flow Technique for Radial Distribution Networks", *IEEE Transactions on Power Systems*, Vol. 14, No. 3, August 1999.

[11] J. Liu, M. M. A. Salama, R. R. Mansour, "An efficient power flow algorithm for distribution systems with polynomial load", *International Journal of Electrical Engineering Education*, 39/4.

[12] Whei-Min Lin, Tung-Sheng Zhan, Ming-Tong Tsay, "Multiple –Frequency Three-Phase Load Flow for Harmonic Analysis," *IEEE Transactions on Power Systems*, Vol. 19, No. 2, May 2004.

[13] Mary B. Cain et al.,"History of Optimal Power Flow and Formulations," Federal Energy Regulatory Commission, December 2012.

[14] A. Trias, "The holomorphic embedding load flow method", *IEEE PES General Meeting*, 2012.

[15] S. S. Baghsorkhi and S. P. Suetin. (Mar. 2015). ''Embedding AC power flow with voltage control in the complex plane: The case of analytic continuation via Padé approximants.''

[16] M. K. Subramanian, Y. Feng, and D. Tylavsky, ''PV bus modeling in a holomorphically embedded power-flow formulation,'' in Proc. North Amer. Power Symp. (NAPS), Manhattan, KS, USA, Sep. 2013, pp. 1–6.

[17] I. Wallace, D. Roberts, A. Grothey, and K. I. M. McKinnon. (Jul. 2016). ''Alternative PV bus modelling with the holomorphic embedding load flow method.''

[18] M. S. Srinivas, 'Distribution load flows: a brief review', in *Proc. IEEE PES Winter Meeting*, Singapore, 2000.

[19] V. Ajjarapu, C. Christy, "The Continuation Power Flow: The Tool for Steady-State Voltage Stability Analysis", *IEEE Transactions on Power Systems*, Vol. 7, No. 1, February 1992.

[20] C. Liu, C. Chang, J. A. Jiang and G. H. Yeh, "Toward a CPFLOW-based algorithm to compute all the type-1 load-flow solutions in electric power systems," in *IEEE Transactions on Circuits and Systems I*: Regular Papers, vol. 52, no. 3, pp. 625-630, March 2005.

[21] Ken Kundert, "Simulation of Analog and Mixed Simulation Circuit", Cadence Design Systems, Inc.

[22] Jan Ogrodzki, Circuit Simulation Methods and Algorithms, CRC Press, May 2018.

[23] L.W. Nagel and D.O. Pederson, "SPICE: Simulation Program with Integrated Circuit Emphasis", Memorandum No. ERL-M382, Electronics Research Laboratory, University of California Berkeley, 12 April 1973.

[24] Laurence W. Nagel., "SPICE2: A Computer Program to Simulate Semiconductor Circuits," Memorandum No. ERL-M520, University of California, Berkeley, May 1975.

[25] McCalla, William J., Fundamentals of Computer-Aided Circuit Simulation, Kluwer Academic Publishers, Boston (1988).

[26] Kundert, Kenneth S., "Sparse Matrix Techniques and their Application to Circuit Simulation," in *Circuit Analysis, Simulation and Design,* ed. Albert E. Ruehli, North-Holland Publishing Co. (1985).

[27] Saleh, Resve, "Nonlinear Relaxation Algorithms for Circuit Simulation," *Electronics Res. Lab.,* University of California, Berkeley, (April 1987).

[28] Thomas Linwood Quarles, "Analysis of Performance and Convergence Issues with Circuit Simulation," Memorandum No. ERL-M89/42, University of California, Berkeley, April 1989.

[29] "IEEE 4-Node Test Feeder," IEEE PES Power System Analysis, Computing, and Economics Committee, Distribution System Analysis Subcommittee.

[30] L. DeMarco, T. J. Overbye, "Low voltage power flow solutions and their role in exit time -based security measures for voltage collapse", 27th Conference of Decision and Control, Austin, Texas, Dec. 1988.

[31] D. Bromberg, M. Jereminov, L. Xin, G. Hug, L. Pileggi, "An Equivalent Circuit Formulation of the Power Flow Problem with Current and Voltage State Variables", PowerTech Eindhoven, June 2015.

[32] M. Jereminov, D. M. Bromberg, A. Pandey, L. Xin, G. Hug, L. Pileggi, "An equivalent circuit formulation for three-phase power flow analysis of distribution systems" T&D Conference, 2016 IEEE PES.

[33] M. Jereminov, D. M. Bromberg, L. Xin, G. Hug, L. Pileggi, "Improving Robustness and Modeling Generality for Power Flow Analysis," T&D Conference and Exposition, 2016 IEEE PES.

[34] A. Pandey, M. Jereminov, G. Hug, L. Pileggi, "Improving Power Flow Robustness via Circuit Simulation Methods," IEEE PES General Meeting, Chicago, 2017.

[35] A. Pandey, M. Jereminov, G. Hug, L. Pileggi, "Robust Convergence of Power Flow using Tx Stepping Method with Equivalent Circuit Formulation," Power Systems Computation Conference, 2018.

[36] A. Agarwal, A. Pandey, L. Pileggi, "Continuous Analytical Models for Implicit Control in Power Flow Analysis.", *IEEE Transaction in Power Systems*. (In Preparation)

[37] Russell Kao, "Piecewise Linear Models for Switch-level Simulation" Technical Report: CSL-TR-92-532, Computer Systems Laboratory, Stanford University, June 1992.

[38] J. Katzenelson, "An algorithm for solving nonlinear resistor networks," in *The Bell System Technical Journal*, vol. 44, no. 8, pp. 1605-1620, Oct. 1965.

[39] Private communication between Larry Pileggi, Amritanshu Pandey, Barry Rawn from Electrical and Computer Engineering Department in Carnegie Mellon University and Tochi Nwachuku from Nigeria Infrastructure Advisory Facility.

[40] S. Cvijic, P. Feldmann, M. Ilic, "Applications of homotopy for solving AC power flow and AC optimal power flow", IEEE PES General Meeting, San Diego, July 2012.

[41] Mehta, H. D. Nguyen, K. Turitsyn, "Numerical Polynomial Homotopy Continuation Method to Locate All the Power Flow Solutions", IET Generation, Transmission and Distribution, Vol. 10, No. 12, August 16.

[42] A. Pandey, M. Jereminov, X. Li, G. Hug, L. Pileggi, "Unified Power System Analyses and Models using Equivalent Circuit Formulation," IEEE PES Innovative Smart Grid Technologies, Minneapolis, USA, 2016.

[43] L. Pillage (Pileggi), R. Rohrer, C. Visweswariah, Electronic Circuit & System Simulation Methods, McGraw-Hill, Inc., New York, NY, USA, 1995.

[44] M. Jereminov, A. Pandey, H. A. Song, B. Hooi, C. Faloutsos, L. Pileggi "Linear load model for robust power system analysis", IEEE PES Innovative Smart Grid Technologies, Torino Italy, September 2017.

[45] A. Pandey, M. Jereminov, X. Li, G. Hug, L. Pileggi, "Aggregated Load and Generation Equivalent Circuit Models with Semi-Empirical Data Fitting," *IEEE Green Energy and Systems Conference (IGESC 2016)* November 2016.

[46] H. A. Song, B. Hooi, M. Jereminov, A. Pandey, L. Pileggi, C. Faloutsos," PowerCast: Mining and forecasting power grid sequences" Joint European Conference on Machine Learning and Knowledge Discovery in Databases, Springer 2017.

[47] B. Hooi, H. A. Song, A. Pandey, M. Jereminov, L. Pileggi, and C. Faloutsos. StreamCast: Fast and Online Mining of Power Grid Time Sequences. Submitted to Proceedings of the 2018 SIAM International Conference on Data Mining. Society for Industrial and Applied Mathematics.

[48] L. B. Goldgeisser and M. M. Green, "Using Continuation Methods to Improve Convergence of Circuits with High Impedance Nodes," in IEEE International Symposium on Circuits and Systems, 2000, Geneva Switzerland.

[49] Y. Wang, L.C.P. DaSilva, W. Xu., Y. Zhang, "Analysis of ill-conditioned power flow problems using voltage stability methodology", IEEE Proceedings in Generation, Transmission, and Distribution, Vol. 148, No. 5, September 2001.

[50] P.C. Krause and C.H. Thomas, "Simulation of Symmetrical Induction Machinery" in *IEEE Transactions on Power Apparatus and Systems* Vol. PAS-84, No.11, November 1965.

[51] "Electric Motors use 45% of Global Electricity, Europe Responding", cleantechnica.com, June 16th, 2011.

[52] W. H. Kersting, Distribution System Modeling and Analysis, CRC Press, Boca Raton, Florida, USA, 2002.

[53] R.J. Lee, P. Pillay, and R. G. Harley, "DQ Reference Frames for the Simulation of Induction Motors." at Electric Power Systems Research, 8(1984-1985) 15-26.

[54] Charles L. Fortescue, "Method of Symmetrical Co-Ordinates Applied to the Solution of Polyphase Networks". Presented at the 34th annual convention of the AIEE (American Institute of Electrical Engineers) in Atlantic City, N.J. on 28 June 1918. Published in: *AIEE Transactions*, vol. 37, part II, pages 1027–1140 (1918).

[55] K. Iba, H. Suzuli, M. Egawa, and T. Watanabe, "Calculation of the critical loading with nose curve using homotopy continuation method," *IEEE Trans. Power Syst.*, vol. 6, no. 2, pp. 584–59, May 1991.

[56] H. D. Chiang and T. Wang, "Novel Homotopy Theory for Nonlinear Networks and Systems and Its Applications to Electrical Grids," in *IEEE Transactions on Control of Network Systems*.

[57] H. Sun, Q. Guo, B. Zhang, Y. Guo, Z. Li, and J. Wang, "Master–slave splitting based distributed global power flow method for integrated transmission and distribution analysis," IEEE Trans. Smart Grid, vol. 6, no. 3, pp. 1484–1492, May 2015.

[58] K. Kalsi et al., "Integrated transmission and distribution control," Pacific Northwest Nat. Lab., Richland, WA, USA, PNNL22157. [Online]. Available from: http://www.pnnl.gov/main/publications/ external/technical_reports/PNNL-22157.pdf.

[59] K. Anderson, J. Du, A. Narayan, and A. El Gamal, "GridSpice: A distributed simulation platform for the smart grid," in Proc. 2013 Workshop Modeling Simulation Cyber-Phys. Energy Syst., 2013, pp. 1–5.

[60] B. Palmintier et al., "Integrated distribution-transmission analysis for very high penetration solar PV (final technical report)," Nat. Renew. Energy Lab., Golden, CO, USA, NREL Tech. Rep. NREL/TP-5D00-65550, Jan. 2016.

[61] Q. Huang, V. Vittal. "Integrated Transmission and Distribution System Power Flow and Dynamic Simulation Using Mixed Three-Sequence/ Three-Phase Modeling," IEEE Trans. on Power Systems, vol. 32, no. 5, pp. 3704-3714, Sept. 2017.

[62] E. L. Allgower and K. Georg, Numerical continuation methods: an introduction, Vol. 13, Springer Science & Business Media, 2012.

[63] M. Jereminov, D. M. Bromberg, A. Pandey, M. R. Wagner, L. Pileggi, "Adjoint Power Flow Analysis for Evaluating Feasibility" in *IEEE Transactions on Power Systems,* 2018.

[64] C. Y. Ku, Y. H. Tsai, "Solving Nonlinear Problems with Singular Initial Conditions Using a Perturbed Scalar Homotopy Methods", *International Journal of Nonlinear Sciences and Numerical Simulation, Vol. 14, Issue. 6,* Aug. 2018.

[65] A. Pandey, M. Jereminov, M. R. Wagner, D. Bromberg, G. Hug, L. Pileggi, "Robust Powerflow and Three-Phase Power Flow Analyses," in *IEEE Transactions on Power Systems*, 2018.

[66] A. B. Birchfield, E. Schweitzer, H. Athari, T. Xu, T. J. Overbye, A. Scaglione, and Z. Wang, "Validation metrics to assess the realism of synthetic power grids," Energies, vol. 10, no. 8, p. 1233, Aug. 2017.

[67] NERC Standard TOP-001-3 — Transmission Operations.

[68] K. Schneider, P. Phanivong, J. Lacroix, "IEEE 342-Node Low Voltage Network Test System", *IEEE PES General Meeting Conference*, July 2014.

[69] "Technical Analysis of Operational Events and Market Impacts During the September 2013 Heat Wave," PJM Interconnection, Dec. 23 2013.

[70] Kron G. (1963) Diakoptics: The Piecewise Solution of Large Scale Systems, MacDonald Publishing.

[71] N. Rabbat, A. Sangiovanni-Vincentelli AND H. Hsieh, "A multilevel Newton algorithm with macro modeling and latency for the analysis of large-scale nonlinear circuits in the time domain", *IEEE Trans. Circuits and Systems*, CAS-26, pp. 733-741.

[72] M. Vlach, "LU decomposition and forward-backward substitution of recursive bordered block diagonal matrices," IEEE Proceedings G, Electronic Circuits and Systems, vol. 132, no. 1, pp. 24–31, February 1985.

[73] Chai, J., Zhu, N., Bose, A., & Tylavsky, D. "Parallel newton type methods for power system stability analysis using local and shared memory multiprocessors," *IEEE Trans. Power Syst*., 6(4), 1539–1545.

[74] A. R. Newton and A. L. Sangiovanni-Vincentelli, "Relaxation-based electrical simulation," IEEE Transactions on Electron Devices, vol. 30, no. 9, pp. 1184– 1207, September 1983.

[75] J. M. Ortega and W. C. Rheinboldt, Iterative Solution of Nonlinear Equations in Several Variables. Academic Press, 2000.

[76] Modern Grid Initiative: Distribution Taxonomy Final Report, *Pacific Northwest National Laboratory*, November 15th, 2008.

[77] M. Honkula, K. Karanko, and J. Roos, "Improving the convergence of combined newton Raphson and gauss-newton multi-level iteration method," *2002 IEEE International Symposium on Circuits and Systems. Proceedings (Cat. No.02CH37353)*, May 2002.

[78] P. Li, Parallel Circuit Simulation: A Historical Perspective and Recent Developments, Now Publishers.

[79] Quadrennial Technology Review: An Assessment of Energy Technologies and Research Opportunities, Department of Energy, U.S., September 2015.

[80] M. LaScala, M. Brucoli, F. Torelli and M. Trovato, "A Gauss-Seidel-block-Newton Method for Parallel Transient Stability Analysis," IEEE PES Winter Meeting, Atlanta, February 1990.

[81] M. P. Desai, I. N. Hajj, "On the Convergence of Block Time-Point Relaxation Methods for Circuit Simulation," Coordinated Science Laboratory, University of Illinois, Urbana Champaign, Jan. 1988.

[82] A. Minot, Y. M. Lu and N. Li, "A Distributed Gauss-Newton Method for Power System State Estimation," in *IEEE Transactions on Power Systems*, vol. 31, no. 5, pp. 3804-3815, Sept. 2016.

[83] J. R. Marti, H. Ahmadi, and L. Bashualdo, "Linear Power Flow Formulation Based on a Voltage-Dependent Load Model," *IEEE Trans. Power Delivery*, vol. 28, issue: 3, April 2013.

[84] Private communication between Bryan Hooi, Machine Learning Department, Carnegie Mellon University and Amritanshu Pandey, Electrical and Computer Engineering Department, Carnegie Mellon University.

[85] Yousef Saad and Maria Sosonkina, "Distributed Schur Complement Techniques for General Sparse Linear Systems," SIAM Journal on Scientific Computing 1999 21:4, 1337-1356.